Investigating the role of the clathrin light chain *in vivo*

Author: Jessica McNeill

Supervisors: Dr Natalia Bulgakova, Professor Elizabeth Smythe

Department of Biomedical Science

Abstract (238 words)

Clathrin-mediated endocytosis (CME) is the process by which proteins are transported into cells from their surfaces. This process is fundamental for organism development and adult tissue homeostasis, and occurs via the invagination of the plasma membrane which pinches off to form cargo-containing vesicles. The clathrin light chain (CLC) is a component of the molecular lattice that facilitates membrane bending on the inner surface of the cell. Based on the evidence from *in vitro* and cellular work, we hypothesise that CLCs are required when membrane properties are refractory to bending i.e. high tension, and/or for the uptake of specific cargos such as large receptors. This project investigates the role of CLCs in the developing tissues of *Drosophila melanogaster* – in an environment containing native biomechanical cues. Together, the data from this project suggests that there is a differential requirement for CLC at the tissue, cellular and protein level in *Drosophila melanogaster*. Knockdown of CLC in the developing retina interfered with the morphogenesis of some tissues but not others, and perturbed the morphology of some cell types within the retina, while other cell types remained unaffected. Additionally, an enhancer suppressor screen has identified candidates that genetically interact with CLC and has potentially highlighted signalling pathways/proteins that are dependent on CLC during development. This context-dependent requirement for CLC aligns with the current literature and demonstrates that investigating endocytic dynamics in a living organism is key to building a holistic understanding of this process.

Contents

Table of Abbreviations

AAK1	AP-2-associated kinase 1
act	*Actin*
AP-2	Adaptor protein 2
CCP	Clathrin-coated pit
CCV	Clathrin-coated vesicle
CLC	Clathrin light chain
CME	Clathrin-mediated endocytosis
EGFR	Epidermal growth factor receptor
ey	*eyeless*
fmi	*flamingo*
GFP	Green fluorescent protein
GMR	*Glass multiple reporter*
GPCR	G-protein coupled receptor
GRK2	GPCR-related kinase 2
hbs	*hibris*
HCC	Hepatocellular carcinoma
Hip1R	Huntingtin-interacting protein 1–related protein
IOC	Interommatidial cell
MDCK (cells)	Madin-Darby Canine Kidney (cells)
NEKL	Group of NIMA-related kinases in *C. elegans*
NGS	Normal goat serum
NSCLC	Non-small cell lung carcinoma
p.d.	Pupal development
PBS	Phosphate buffer saline

PBST	Phosphate buffer saline with Triton X-100
PEDV	Porcine epidemic diarrhoea virus
PRC	Photoreceptor cell
RNAi	RNA interference
shg	*Shotgun*
TfR	Transferrin receptor
TGF-β	Transforming growth factor beta
twi	*Twist*
UAS	Upstream activating sequence
ubi	*Ubiquitin-63E*
YFP	Yellow fluorescent protein
zip	*Zipper*

1. Introduction

1.1   Clathrin-mediated endocytosis

Clathrin-mediated endocytosis (CME) is the process that traffics cargo, such as transmembrane receptors, from the cell surface into the cell through invagination of the plasma membrane (Figure 1.1). CME is highly evolutionarily conserved and vital for numerous cellular processes such as modulating cell signalling by altering surface levels of receptors, recycling of synaptic vesicles, and regulating immune responses (Kaksonen and Roux, 2018). CME is indispensable for fundamental cellular processes and is vital for key developmental processes such as neuronal migration (Shieh et al., 2011) and regulating endocytosis of proteins key to cell fate decision-making (Gaiano and Fishell, 2002).
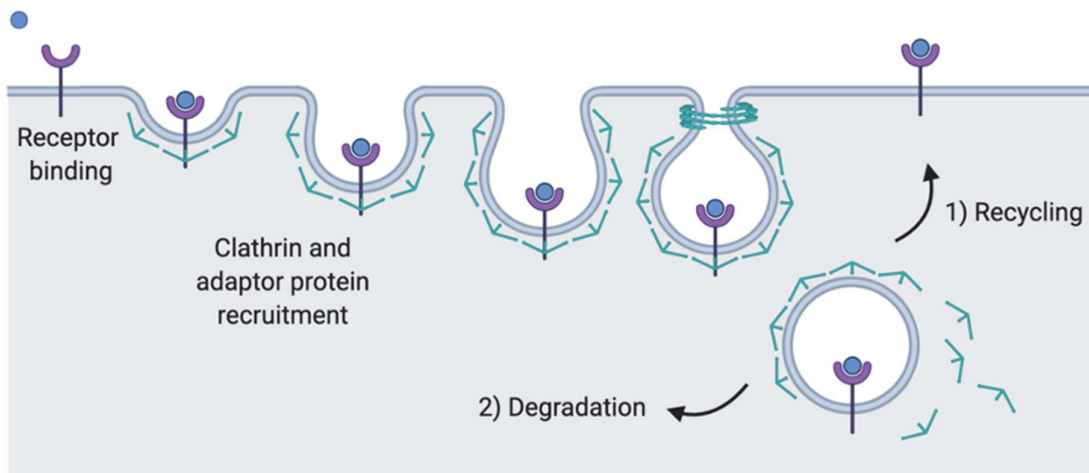
Figure 1.1: Schematic to illustrate the initial steps of endocytosis. Upon receptor binding, the clathrin lattice polymerises at the plasma membrane and key endocytic proteins are recruited to the forming clathrin-coated pit (CCP). The CCP invaginates further and undergoes dynamin-mediated scission to release a clathrin-coated vesicle (CCV) into the cytoplasm. The CCV is uncoated and, depending on its function, the internalised cargo is sorted e.g. to be recycled or degraded.

The clathrin protein assembles into trimeric unit (a "triskelion") consisting of three heavy chain proteins (190 kDa) and three light chains (~23-26 kDa) (Ferreira et al., 2012) (Figure 1.2). Individual endocytic events occur through the recruitment and polymerization of clathrin triskelia on the inner surface of the plasma membrane. Over 50 components of the endocytic machinery facilitate cargo recruitment, membrane bending and the formation of a clathrin-coated vesicle that pinches off the membrane and enters the endosomal pathway. Adaptor protein 2 (AP-2) is one of the components of this machinery that is required for CCP and CCV formation. It is a heterotetrameric protein that binds to cargo proteins, lipids within the plasma membrane and clathrin and through its role as a scaffolding protein, AP-2 has a key role in cargo recognition and clustering (Kaksonen and Roux, 2018).
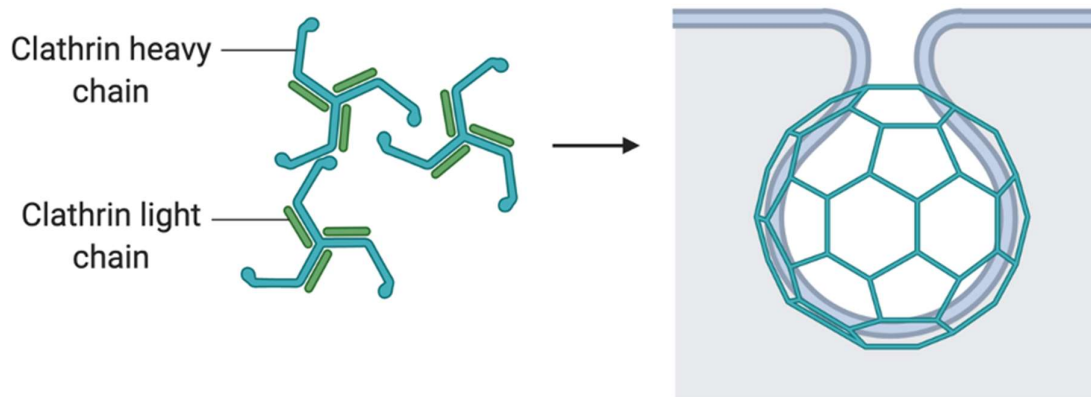
Figure 1.2: Schematic to illustrate how clathrin triskelia, each molecule made up of three clathrin heavy chains (blue) and their associated light chains (green), polymerize into a lattice structure around the invaginating plasma membrane during endocytosis.

1.2 Mechanisms of clathrin-mediated endocytosis

1.2.1 Generation of membrane curvature

For CME to occur the membrane must acquire sufficient curvature to invaginate and ultimately form a spherical CCV. The generation of inward curvature therefore must involve a mechanism that can overcome the intrinsic resistance of the plasma membrane to bending. The plasma membrane bends inwards approximately 150 nm before it pinches off to form a vesicle (Kaksonen and Roux, 2018). The underlying actin cytoskeleton polymerises to form a network of actin filaments under the membrane to facilitate the later stages of invagination of the membrane, however, the early stages of curvature acquisition primarily involve the polymerisation of the clathrin coat itself, associated with a range of accessory proteins. In the early stages of CME research, it was proposed that the driving force behind curvature acquisition comes from the formation of the clathrin coat itself: the polymerization of the lattice has the capacity to shape the underlying membrane (Kirchhausen and Harrison, 1981). The exact nature of how this happens is still under debate. Already from pioneering electron microscopy it was evident that clathrin lattices exist with variable degrees of curvature in the cell ranging from flat arrays predominantly consisting of hexagonal clathrin units to curved arrays containing pentagonal clathrin structures (Heuser, 1980).

Further investigations into the mechanisms behind curvature acquisition led to two opposing models, each supported by different experimental approaches. One of the hypotheses postulated that the formation of CCVs involved structural rearrangements that resulted in the steady acquisition of curvature. According this hypothesis, clathrin exchange within a flat, hexagonal lattice, results in the production of pentagons and subsequently drives formation of a curved lattice (den Otter and Briels, 2011). This became known as the "constant area model", given that the surface area remains constant during lattice reorganization. This model is supported by cellular data that revealed extensive clathrin exchange during CME while the surface area of the CCP was relatively constant (Avinoam et al., 2015). However, biochemical data suggested the high energetic cost of this extensive coat reorganization - the conversion of multiple hexagonal units of clathrin

into pentagons – which deems the model energetically unfavourable (Kirchhausen, 1993). Such *in vitro* data instead favoured another mode of curvature acquisition, known as the "constant curvature model" (Dannhauser and Ungewickell, 2012). In this case, the clathrin triskelia directly assemble into a curved lattice, driving invagination of the membrane during clathrin polymerization.

Although different approaches tended to favour one of the models over the other, emerging evidence suggests that there is more to membrane bending during CME than just two opposing modes of curvature. A combination of several microscopy techniques (pol-TIRF, atomic force microscopy and electron microscopy) enabled visualisation of individual endocytic events in the same cell (Scott et al., 2018). This revealed that the timing of membrane invagination and clathrin polymerization was not consistent between endocytic events suggesting that there was more than one mode of membrane bending in a given cell (Scott et al., 2018). This finding supports the idea that factors other than a universal intrinsic property of the cell type may influence the mode of curvature within a local region of the plasma membrane. In contrast, combining mathematical modelling with correlative electron and light microscopy actually challenged both of the existing models and produced data that supported neither (Bucher et al., 2018). Instead, the authors put forward a new model that involves initial polymerization of clathrin into a flat lattice, followed by reorganization of the coat into a curved structure when the coat has not yet reached its final size. The transition from a flat to curved clathrin array is associated with a shift in the ratio between clathrin itself and adaptor protein 2, AP-2, when the coat has reached approximately 70% clathrin content. Additionally, the authors highlighted the limitations of the indirect measurements of CCP formation that provided evidence for the constant area model (Avinoam et al., 2015), indicating that the need for accurate understanding of the coat rearrangement dynamics remained. Although their multidisciplinary approach provides intriguing new insight into CCP assembly, it comes with its own limitation, i.e. utilising *in vitro* cultured cells which do not recapitulate the native biomechanical cues of a living organism.

1.2.2 The effect of membrane properties on clathrin-mediated endocytosis and membrane bending

Clathrin-mediated endocytosis is not just regulated by a wide variety of mechanisms such as posttranslational modifications and conformational changes of CME machinery (Mettlen et al., 2018), but it is also highly sensitive to fluctuations in the biophysical environment. There has been extensive research in cells and *in vitro* into how mechanical factors influence CME. The two major mechanical properties of the membrane found to be refractory to membrane bending/endocytic dynamics are the lateral tension of the membrane and its rigidity. These factors are inversely related to the rate of endocytosis (Dai et al., 1997; Raucher and Sheetz, 1999; Sheetz and Dai, 1996), and during CME, the plasma membrane and associated endocytic machinery must overcome them. In circumstances where the plasma membrane is not under increased mechanical stress, e.g. when lateral tension is low, the energy of clathrin polymerization is sufficient to drive membrane curvature (Boulant et al., 2011; Dannhauser et al., 2015). In contrast, increased membrane tension hinders clathrin polymerization *in vitro* by altering the energy required for membrane budding (Saleem et al., 2015). In such conditions, early stages of membrane curvature are achieved, but

later stages of membrane invagination are hindered. Mathematical modelling demonstrated that while a shift in the clathrin–AP-2 ratio drives membrane curvature, the increased tension of the plasma membrane stalls reorganization of the clathrin lattice (Bucher et al., 2018) at a stage prior to budding (before the membrane invaginates against outward pressure). To overcome this, cells often adapt to these refractory conditions and counteract the tension, e.g. by using actin dynamics to facilitate formation of clathrin-coated structures. Cells with naturally high membrane tension due to increased turgor pressure, such as yeasts, display aberrations in CME if the actin dynamics to overcome this increased tension is abolished (Aghamohammadzadeh and Ayscough, 2009). This dependence on actin to counteract increased tension in the plasma membrane during CME has also been reported in MDCK cells (Boulant et al., 2011). MDCK cells are polarized: in contrast to the basolateral membrane, the apical surface consists of numerous microvilli and is dependent on actin for the complete formation of clathrin-coated pits. The reduced membrane tension in the basolateral membrane relative to the apical membrane renders this surface independent of actin dynamics during clathrin-coated pit formation. However, when the membrane tension is increased in these cells by either hypotonic treatment or lateral stretching, both the apical and basolateral membranes become reliant on actin dynamics for CME.

How does actin interact with the budding vesicle/clathrin coat? Actin indirectly interacts with the light chains (CLC) within the clathrin coat via Huntington interacting protein 1 (Hip1R, Chen and Brodsky, 2005). Hip1R acts as a scaffolding protein between the CLCs in the clathrin coat and actin filaments. This interaction promotes actin polymerisation at the neck of the budding vesicle to 'push' the vesicle inwards and facilitate invagination of the plasma membrane. Disruption of this interaction in polarized mammalian cells with high membrane tension impedes CCP assembly at late stages (Boulant et al., 2011). Similarly, artificially raising membrane tension in the same cells in the absence of functional actin brings about the same outcome (Boulant et al., 2011). Depletion of Hip1R or CLC, thus abolishing the interaction of actin with the budding CCP, results in the accumulation of actin at endocytic sites (Poupon et al., 2008). This ties together the requirement for actin dynamics for completion of CME when the membrane properties oppose bending.

Another biophysical factor contributing to the rate of endocytosis is the membrane fluidity with evidence that it is important for the maturation of oocytes in humans. Treating oocytes with antioxidative melatonin shows that it can facilitate CME by increasing the fluidity of the plasma membrane through its effects against free radical-induced peroxidation of fatty acids (Li et al., 2019). Melatonin increases the number of clathrin-coated structures and upregulates the expression of clathrin itself and adaptor protein 2. Treatment with dynasore hinders the maturation of oocytes, however, melatonin is able to significantly elevate the expression of these endocytic components and partly rescue oocyte maturation in the presence of this endocytic inhibitor (Li et al., 2019). The clinical approach of altering the membrane rigidity in order to enhance clathrin-mediated endocytosis during development highlights the importance of considering mechanical factors in the regulation of this process.

1.3 Clathrin light chain

The clathrin light chain connects the clathrin coat to the cytoskeleton, but is its role restricted to regulating actin dynamics during CME? *In vitro* data on artificial membranes in the absence of actin

show that the CLC increases the stiffness of clathrin lattice and enhances the bending capacity of membranes, providing evidence that the properties of clathrin lattices are dependent on the presence of CLC (Dannhauser et al., 2015). This study artificially manipulated the rigidity/flexibility of liposomal membranes by exposing them to a range of temperatures. Clathrin polymerization was able to deform membranes at physiological (permissive) temperatures in the absence of light chains, but not rigid membranes at 15℃ (Dannhauser et al., 2015). Given the lack of actin in this system, this data suggests that actin dynamics alone is not the sole driving force of membrane deformation under non-permissive conditions. It also indicates that the CLC, by increasing rigidity and bending capacity of clathrin, has a significant role in facilitating endocytosis by altering the properties of the clathrin lattice itself. The importance of CLC is also apparent in immune responses: CLC is crucial for the uptake of large bacterial particles (Bonazzi et al., 2011) and the endocytosis of a subset of receptors in lymphocytes (Wu et al., 2016). These data highlight the physiological significance of the CLC, not just in actin dynamics, but also in some aspects of cell signalling.

Given the ability of the CLC to the enhance the biophysical properties of the clathrin lattice in membranes with higher tension, as well as other roles in cell signalling, it is surprising that a significant volume of earlier work concluded that CLC knockdown did not impede CME (Hinrichsen et al., 2003; Huang et al., 2004). CME dynamics was commonly examined by tracking the uptake of the transferrin receptor (TfR) – a single pass transmembrane protein that relies on clathrin to be transported into the cell (Harding et al., 1983) – and knockdown of CLC does not affect TfR endocytosis. In contrast, recent work has shown that CLCs are essential for regulated endocytosis of a subset of G-protein coupled receptors (GPCRs) (Ferreira et al., 2012). Specifically, the phosphorylation of a serine residue of CLCb by G protein-coupled receptor kinase 2 (GRK2) in HEK293T cells is required for endocytosis of these GCPRs. Additionally, although TfR endocytosis does not typically require CLCs, TfR uptake is affected when the composition of the cargo within a CCP is altered (Maib et al., 2018). Stimulation of receptor endocytosis with GPCR agonists in cells expressing dominant-negative CLC disrupted uptake of GPCRs, but also TfR due to the stochastic colocalization of these transmembrane proteins (Maib et al., 2018). Therefore, the requirement of the CLC is at least partially dependent on the composition of the invaginating CCP. It raises the possibility that clustering of large cargo such as GPCRs in CCPs could alter the rigidity of the plasma membrane (Maib et al., 2018), increasing the energy required to deform it.

To summarise, mechanical properties of the membrane such as lateral tension and rigidity are refractory to the acquisition of membrane curvature. When membrane tension/rigidity is low, the energy of clathrin polymerization is likely to be sufficient to drive CME. Conversely, when mechanical properties oppose membrane bending, for example in polarized cells or in GPCR-rich CCPs, CLCs seem to promote CME by recruiting actin and enhancing the capacity of the clathrin lattice itself to deform the membrane. These properties are not necessarily an intrinsic property of a given cell and likely differ across regions of the plasma membrane.

Altogether, future work is required to investigate CLC function *in vivo*, in a system with native biomechanical cues, to fully understand the dynamics of CME. Given the multitude of processes during the development of *Drosophila* when cells are exposed to a range of physical forces, it is

ideally suited to investigate CME dynamics. Additionally, CLCs seem to play a part in regulating cell signalling, which is another important avenue to explore.

1.4 Clathrin-mediated endocytosis *in vivo*

1.4.1 Clathrin-mediated endocytosis during development

Clathrin-mediated endocytosis (CME) is indispensable not just for adult cell physiology but for the regulation of fundamental signalling events during development. CME is essential for the trafficking of receptors, which signal to determine key cell fate and developmental decisions. This process is highly modulated during development in order to avoid hypo- and hyperactivation of signalling pathways that could evoke severe physiological defects as a result of stalled or prolonged endocytosis. For example, Delta/Serrate/LAG-2 ligands must be endocytosed via the clathrin pathway in order for Notch signalling to occur and correctly specify cell fate (Gaiano and Fishell, 2002; Overstreet et al., 2004; Parks et al., 2000; Seugnet et al., 1997). However, the internalisation of the cargo itself is not the only factor to consider: spatial and temporal regulation of endocytosis is also essential. Indeed, both sustained and curtailed endocytosis of a signalling receptor, e.g. as a result of stalling CCP formation, can result in severe aberration in downstream signalling (Baschieri et al., 2020; Mitsunari et al., 2005).

Wnt signalling regulates many aspects of development, and both activation and downregulation of this pathway rely on clathrin-mediated endocytosis. Modulation of Wnt signalling to evade hyperactivation of the pathway requires the internalisation and subsequent degradation of the LRP6 receptor. Without appropriate regulation, Wnt signalling can lead to developmental defects, cancer and neurodegeneration (Nusse and Clevers, 2017). Recently, evidence has emerged that clathrin-mediated endocytosis of the LRP6 receptor is enhanced by the AP2 associated kinase 1 (AAK1) following prolonged Wnt signalling (Agajanian et al., 2019). This negative feedback loop limits activation of this pathway through clathrin-mediated endocytosis, highlighting the significance of regulating endocytosis in key developmental signalling pathways.

Another family of kinases, the NIMA-related kinases (NEKLs) have also been recently implicated in the regulation of clathrin-mediated endocytosis during development in *C. elegans*. Downregulating these kinases in C. elegans larvae results in molting defects and mislocalisation of trafficking components (Joseph et al., 2020). Additionally, in adults NEKL depletion causes abnormal localisation of clathrin itself and its mobility is perturbed. A genetic screen identified a strong association between NEKLs and AP-2 as they mutually rescue defects in one another, strengthening the link between this defect and endocytosis (Joseph et al., 2020). These data support the idea that it is vital to regulate CME for normal morphogenesis during development.

1.4.2 Clathrin-mediated endocytosis in disease

Clathrin-mediated endocytosis is not just vital for development, but also for fundamental cellular processes throughout life e.g. synaptic vesicle recycling, signal transduction and nutrient uptake.

When this process is dysregulated during tissue homeostasis, it can lead to a wide range of pathologies. Therefore, effective regulation of clathrin-mediated endocytosis in adult tissues is also of substantial importance.

Many viruses invade host cells through clathrin-mediated endocytosis by hijacking the host cell's endocytic machinery (Cossart and Helenius, 2014). One way cells can counteract this is to purposefully downregulate endocytosis to impede entry of viruses. There is an interaction between a protein called Mortalin and the clathrin heavy chain that hinders entry of porcine epidemic diarrhoea virus (PEDV) (Fan et al., 2019). The protective mechanism is also utilised by several other viruses including vesicular stomatitis virus and rotavirus (Fan et al., 2019).

While the internalisation of pathogens through CME is one mechanism of pathogenesis, disease can also occur when CME is perturbed and a signalling pathway is misregulated. Signalling proteins and their receptors can be recruited to clathrin-coated pits to form a clustering platform where membrane signalling is amplified (Ichinose et al., 2004). This level of regulation has recently been shown to be significant in invasive hepatocellular carcinoma (HCC) where a novel role for clathrin in liver tumorigenesis has been described. Transforming growth factor (TGF)-β signalling can induce both pro- and anti-apoptotic signals. Many HCC patients have increased TGF-β signalling, which results in the transactivation of the EGFR signalling pathway. The EGFR pathway mediates anti-apoptotic signalling, a hallmark of tumorigenesis. Many HCC patients with increased TGF-β expression also exhibit increased expression of clathrin, which is required for EGFR transactivation. Clathrin knockdown attenuates the anti-apoptotic signals in liver tumour cells and sensitizes them to cell death, highlighting a novel role of clathrin in tumorigenesis. Patients with increased expression of both clathrin and TGF-β have a significantly lower rate of survival, which may identify patients that would be suitable for treatments that target TGF-β signalling. Another example of the impact CME misregulation in tumorigenesis is in non-small cell lung cancer (NSCLC). NSCLC is a malignant disease often caused by alterations in EGFR signalling. There is evidence that treating NSCLC with a CME inhibitor in conjunction with established anti-cancer drugs improves the prognosis of patients with this disease (Kim et al., 2020). These studies support the idea that understanding how CME is regulated in disease can shed light on potential therapeutic avenues.

1.5 *Drosophila melanogaster*: model organism

1.5.1 Introduction to Drosophila

Drosophila melanogaster, the model organism used in this project, has been widely used as a system to study developmental biology for over 100 years. Famously used in Thomas Hunt Morgan's experiments that confirmed chromosome theory and how genetic traits are inherited, *Drosophila* has become a powerful tool to study genetics and development. Firstly, this model organism is well suited to laboratory use due to its short life cycle, cheap maintenance costs and ease of handling. Due to advances in imaging technology, *Drosophila* is an incredibly useful developmental system because whole tissues can be dissected and imaged at various stages of development, and they are also well suited to live imaging. They are also highly amenable to gene

expression manipulation using tools such as CRISPR/Cas9 and the UAS-GAL4 system, making this organism a very powerful tool for developmental biology. Although the *Drosophila* genome is much smaller compared to mammalian systems (approximately 14,000 *Drosophila* genes and 23,000 human genes), it is of low redundancy and it shares significant homology of roughly 75% (Reiter et al., 2001) with vertebrate systems in key developmental and disease-associated genes.

1.5.2 Development of Drosophila

The *Drosophila* life cycle is approximately 10 days at 25°C, however, the duration is subject to temperature (Roote and Prokop, 2013). For the purpose of this introduction, all times stated refer to 25°C conditions. The initial stage of embryonic development lasts for approximately 21 hours. Once embryogenesis is complete, 1st instar larvae hatch and, two days later, develop into 2nd and 3rd instar larvae. During these feeding and foraging stages, the imaginal discs mature. Imaginal discs are epithelial structures that will later form structures in the adult such as the eyes, wings, antennae and legs during pupal stages (Roote and Prokop, 2013). 3rd instar larvae then enter the wandering stage where they migrate from their food source and then pupariate. During the pupal stages the organs are broken down in a process called histolysis and are remodelled to form the adult structures (metamorphosis). Adults then emerge from the pupal case (eclosure) and become sexually mature 5-8 hours later, after approximately 10 days from egg lay.

1.5.3 Structure of the Drosophila eye

The main model system used in this project is the *Drosophila* eye, a compound structure consisting of 800 hexagonal ommatidia. The ommatidia in the *Drosophila* eye are assembled into a lattice with a highly stereotypical arrangement (Treisman, 2013). Each ommatidium is a functional unit comprised of an array of cell types: light-sensitive photoreceptor cells (PRC), pigment cells and cone cells (Figure 1.3). The geometry, patterning and packing of cells in the *Drosophila* eye is highly stereotypic and reproducible.

PRCs are specialised epithelial cells that are elongated along the apical-basal axis. They comprise the light-sensing component of the retina and contain rhodopsin, a photosensitive molecule (Yamaguchi et al., 2010). Each ommatidium contains 8 PRCs, which are stereotypically arranged together, and surrounded by pigment cells. Pigment cells collectively provide a layer of insulation around each cluster of PRCs, to ensure the light that enters each ommatidium is contained within it (Carthew, 2007). Primary pigment cells are crescent-shaped cells that enclose the PRC clusters and contain ommochromes, a brown pigment. Secondary and tertiary pigment cells surround each ommatidium and contain pteridines, a red pigment. In each ommatidium, four glial-like cone cells that contain ommochromes are situated above the PRCs (Tomlinson, 2012). Lastly, each ommatidium contains three tertiary cells and three mechanosensory bristle cells.
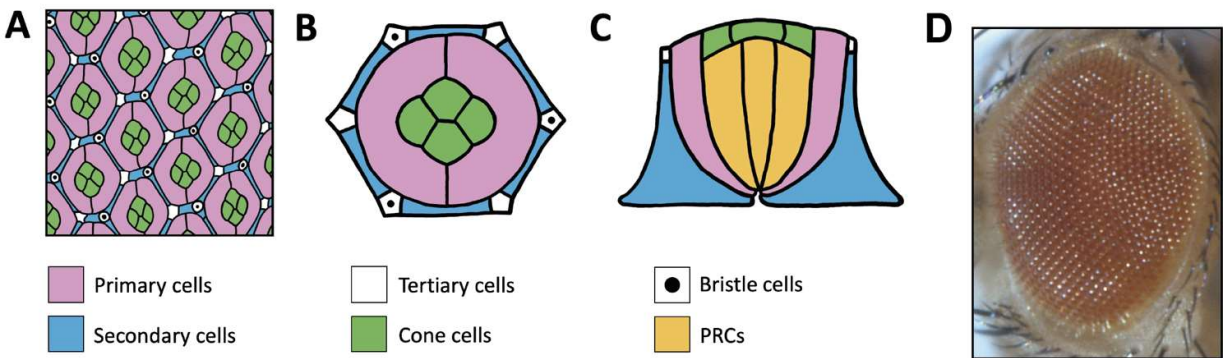
Figure 1.3: A schematic to illustrate the structure of the *Drosophila* eye at pupal and adult stages. (A) Illustration of the pupal retina that exhibits the highly stereotyped lattice structure made up of hexagonally shaped ommatidia at 42% p.d. (B-C) Schematic of cells in an individual ommatidium: primary cells (pink), secondary cells (blue), tertiary cells (white), cone cells (green), bristle cells (white with black dot) and photoreceptor cells (orange). Top (apical, B) and transversal (C) views are shown. (D) Fully developed compound eye of an adult. Figure adapted from Hayashi and Carthew, 2004.

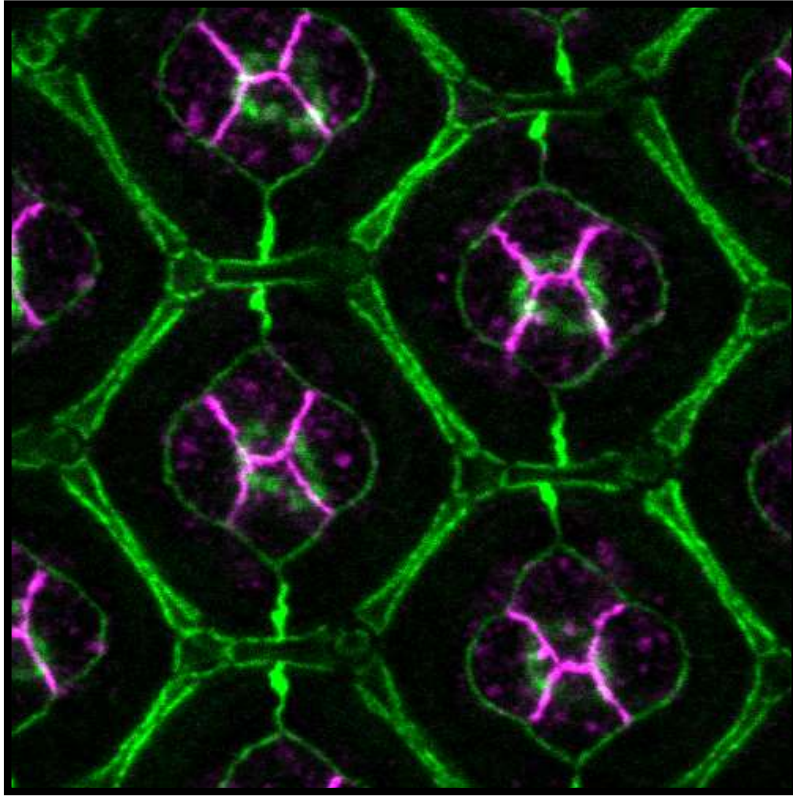### 1.5.4 Development of the Drosophila eye

The *Drosophila* eye is an ordered structure that originates from an imaginal disc – an epithelial monolayer which grows during larval stages. Differentiation of the retinal cells in the developing eye disc occurs as a wave, sweeping across the tissue during the third instar larval stage in a posterior to anterior direction. A transient structure driven by Hedgehog signalling – the morphogenetic furrow – progresses anteriorly across the disc and the disorganised array of dividing cells becomes a regularly patterned lattice (Greenwood and Struhl, 1999). As the morphogenetic furrow moves across the tissue, it sequentially triggers differentiation in each row of cells it passes. The Hedgehog signalling also triggers a signalling pathway involving Dpp, Atonal and Wingless, that stimulates neurogenesis. In the field of cells behind the morphogenetic furrow, clusters of proneural cells are formed. Within each cluster a single cell begins to differentiate into the PRC R8, this is followed by the sequential specification of the remaining PRCs. Retinal pigment cells are also specified at this stage. Primary pigment cells and cone cells differentiate first, followed by the secondary and tertiary cells, or interommatidial cells (IOCs). Notch signalling is vital in the differentiation of the cells in the eye field (Cagan and Ready, 1989; Nagaraj and Banerjee, 2007; Parody and Muskavitch, 1993). Excess IOCs are eliminated via apoptosis after a period of cell sorting between 16% and 21% pupal development. The end result is that each ommatidium has a total of 20 cells (Reiter et al., 1996). Notch and EGFR signalling act antagonistically in the cells of the retina to induce and inhibit apoptosis, respectively (Cagan and Ready, 1989; Kurada and White, 1998; Miller and Cagan, 1998). At 42% pupal development (p.d.), all cells in the retina have been recruited, differentiated, and are arranged in the highly stereotyped lattice pattern.

The development of the *Drosophila* eye is dependent on highly regulated signalling pathways and proteins that ensure correct cell fate specification, maintain appropriate cell contacts and patterning across the retina. Notch is indispensable for regulating proneural enhancement and

lateral inhibition: Notch enhances the expression of Atonal and prevents the neighbours of proneural cells from adopting the same fate (Baker and Yu, 1997). The specification of the photoreceptor cells and neighbouring non-neural cells is dependent on Notch signalling (Cagan, 2003; Carthew, 2007; Doroquez and Rebay, 2006). A key regulator of the Notch signalling pathway is the protein, Numb. Numb negatively regulates Notch by promoting its internalisation and the subsequent degradation of the receptor (Guo et al., 1996; Santolini et al., 2000).

Another protein that plays a vital role in *Drosophila* eye morphogenesis is the epidermal growth factor receptor, EGFR. EGFR is a transmembrane receptor tyrosine kinase and it is involved in regulating progression of the cell cycle, driving ommatidial rotation, adherens junctions remodelling and cell survival (Freeman, 1996; Shilo, 2003). Like Notch, EGFR has a key role in the determination of photoreceptor cell fate (Frankfort and Mardon, 2002; Hsiung and Moses, 2002). Additionally, Notch has been shown to fine-tune EGFR signalling in the R4 photoreceptor by upregulating the expression of the inhibitory EGFR ligand, *argos* (Koca et al., 2019), highlighting the complex interplay between developmental signalling pathways during development. The precise regulation of the Notch and EGFR signalling pathways by endocytosis during development highlights just two examples of the vital role this process plays during the development of the *Drosophila* eye. There are many other signalling pathways that are crucial during eye morphogenesis and adult tissue homeostasis that depend on the precise spatiotemporal regulation of endocytosis.

As well as signalling, highly regulated cell-cell adhesion is crucial for eye patterning during development. E-cadherin is expressed in all cells of the *Drosophila* eye and is indispensable for adult tissue homeostasis. N-cadherin is another cadherin expressed in the *Drosophila* eye and it is only expressed at the junctions that connect each of the four cone cells to one another. N-cadherin is a major determinant of their shape (Figure 1.4, Hayashi and Carthew, 2004). In addition to cadherins connecting epithelial cells, Roughest and Hibris are adhesion molecules that are essential for determining the patterning of cells in the retina. During the development of the eye, epithelial cell contacts are remodelled and there is a highly coordinated interplay between adhesion molecules that results in each cell type exhibiting a stereotyped morphology. During development, differential expression of Roughest and Hibris must be tightly coordinated during development in order for the cone cells to adopt their mature conformation through a process called cell intercalation (Figure 1.5, Blackie et al., 2019). There is also an interplay between signalling pathways, adhesion molecules and tissue remodelling during the development of the eye: Notch differentially controls the expression of Roughest and Hibris, as well as two other proteins, Sticks-and-Stones and Kin of Irre (Bao, 2014).

Figure 1.4: Confocal image to show localisation of E-cadherin (green) and N-cadherin (magenta) at cell junctions in the *Drosophila* retina at 42% pupal development. Image taken from Figure 3.8.
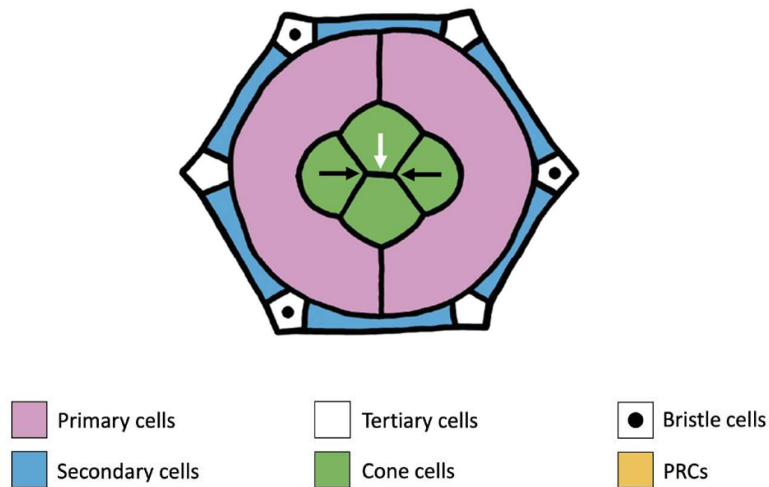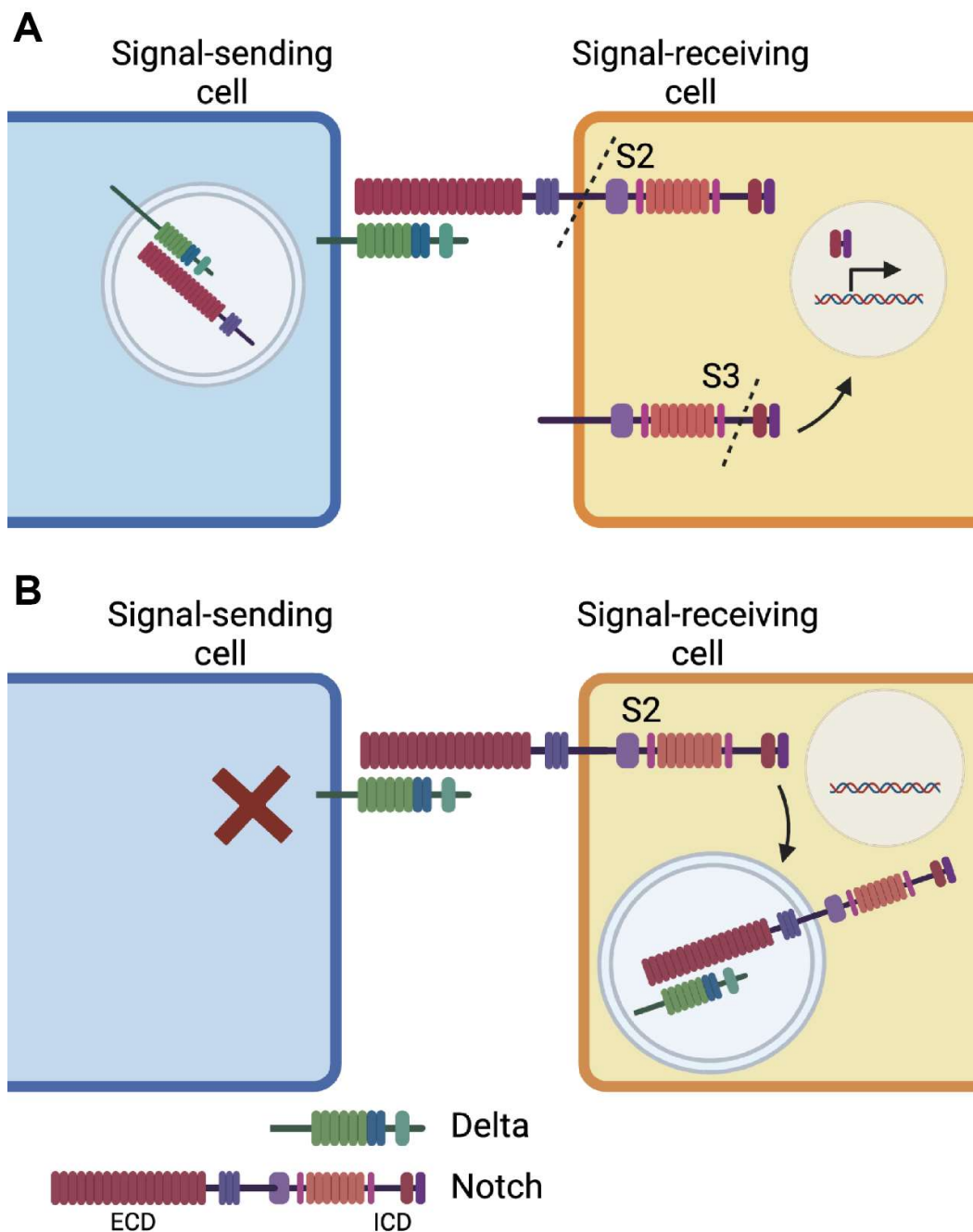

Figure 1.5: Schematic to illustrate the mature conformation of cone cells at 42% p.d. White arrow indicates the single junctional interface between the polar and equatorial cone cells that forms following intercalation. Black arrow indicates the two intersection points that each connect three cone cells.

1.5.5 Endocytosis in the Drosophila eye

From early stages of eye morphogenesis such as progression of the morphogenetic furrow to later stages of tissue remodelling, a vast number of signalling pathways are required to ensure development proceeds correctly. Endocytosis is vital for eye development and pattern formation because it modulates the surface expression of key signalling molecules and adhesion proteins that morphogenesis relies on. For example, the release of vital secreted ligands such as Hedgehog and Wingless, and the subsequent activation of signalling pathways after binding to their counterpart receptors, is dependent on intracellular trafficking machinery (Chan et al., 2011).

The Notch signalling pathway is just one example of a receptor in the *Drosophila* eye that relies on endocytosis to function correctly. The endocytosis of the Notch ligand is required for active signalling, which is indispensable for correct specification and patterning in the eye. For active Notch signalling to occur, endocytosis of the intracellular domain of the receptor, and its subsequent entry into the nucleus of the signal-receiving cell, is essential. Upon ligand binding, a pulling force must be exerted onto the ligand-receptor bridge in order to expose a cleavage site (Figure 1.6, Langridge and Struhl, 2017). Once this cleavage site has been severed, the receptor undergoes a second cleavage step that releases the intracellular domain into the signal-receiving cell where it enters the nucleus and regulates gene expression. The remaining portion of the ligand-receptor bridge that is situated on the membrane of the signal-sending cell is then endocytosed in an epsin-dependent manner. Notch endocytosis is unique because not only are both the ligand and receptor membrane-bound, but if a pulling force is not exerted on them after binding, active signalling does not occur (Langridge and Struhl, 2017). If no such force is generated the cleavage site is not exposed, and the entire ligand receptor bridge is endocytosed into the signal-receiving cell. As a result, the intracellular domain is not released into the cytoplasm and active Notch signalling does not take place. Finely-tuned Notch signalling is vital in several stages of eye development e.g. regulating the number of IOCs in pupal stages. CME is responsible for downregulating pro-apoptotic Notch signalling in excess IOCs (Peralta et al., 2009). In the context of eye development, Notch signalling must be precisely regulated by endocytosis so that vital developmental milestones are met, such as neural cell fate determination and programmed cell death.

Figure 1.6: A schematic to illustrate the process of Notch endocytosis. (A) Productive signalling occurs when a pulling force that is exerted onto the ligand-receptor bridge exposes a site in the receptor that undergoes S2 cleavage. After a second cleavage step (S3), the intracellular domain of the Notch receptor is released into the cytoplasm of the signal-receiving cell where it then enters the nucleus and regulates gene expression. (B) When no pulling force is exerted onto the ligand-receptor bridge, it is endocytosed into the signal-receiving cell. In this case, the intracellular domain is not released into the cytoplasm of the and as a result, no active Notch signalling takes place.

EGFR, the receptor tyrosine kinase that is vital in *Drosophila* eye development as described above, is also dependent on endocytosis to regulate the level of signalling, alongside other mechanisms

such as controlling ligand processing. Endocytosis of the receptor after ligand binding does not halt signalling, rather it continues throughout the endosomal pathway (Burke et al., 2001). For example, EGFR signalling is promoted in endosomal compartments by the tyrosine phosphatase Myopic (Miura et al., 2008). This emphasises that the intracellular trafficking of EGFR must be highly regulated to ensure appropriate levels of signalling.

As well as being essential for the regulation of specific signalling pathways, endocytosis in the *Drosophila* eye is implicated in being vital for maintaining the structure and function of the tissue e.g. the positioning and function of photoreceptor cells. The maintenance of the apical localisation of photoreceptor nuclei depends on a functional relationship between the RabGAP RN-Tre and the endosomal GTPases Rab5 and Rab11 (Houalla et al., 2010). Without this regulation by the intracellular trafficking machinery, the nuclei become mis-localised. Intracellular trafficking is also essential for maintenance of the light-sensing membrane of photoreceptors. The transport and maturation of Rhodopsin, a light-sensitive molecule in the photoreceptors, between the Golgi and endoplasmic reticulum depends on Rab1 and Rab6 (Shetty et al., 1998). Furthermore, endocytosis regulates the turnover of Rhodopsin: aberrant accumulation of Rhodopsin in late endosomes as a result of perturbed intracellular trafficking leads to retinal degeneration (Midorikawa et al., 2010).

1.5.6 Tissue mechanics in the Drosophila eye

Cell geometry is governed by mechanical properties, which in epithelial cells are a product of the interplay between intercellular adhesion and the intracellular actin cytoskeleton (Lecuit and Lenne, 2007). In the *Drosophila* eye, the differential expression of both adhesion molecules and actin give rise to neighbouring cells with intrinsically different mechanical properties. For example, myosin-II is enriched in secondary pigment cells during mid pupal development (Baumann, 2004; Blackie et al., 2020) which suggests that these cells have a higher cortical tension relative to their neighbours. Blackie et al., 2020 revealed that these cells are more prone to deformation in response to ablated neighbouring cells compared to cone cells. While all ommatidial cells express E-cadherin, the interface between cone cells also expresses N-cadherin. As a result, these cells are packed together in a way that minimises their surface, similar to soap bubbles, a property not shared with neighbouring retinal cells (Hayashi and Carthew, 2004). Together this highlights that differential expression of adhesion molecules and actomyosin machinery determines the topology and mechanical properties of epithelial cells in the *Drosophila* eye.

In addition to the intrinsic differences in the shapes and mechanics of individual cells within an ommatidium, the whole eye might display tissue-level mechanical differences. According to Euler's theorem, curved structures made up of hexagonal units are not energetically favourable and so the retina may be under increased mechanical stress across the whole tissue. Therefore, the cells in the *Drosophila* eye are exposed to both external forces during development (e.g. from ommatidial rotation) and have intrinsically different geometries and mechanical properties. Additionally, endocytosis has recently emerged as an important factor which regulates how adhesion contributes to cell shape and mechanical properties (Greig and Bulgakova, 2019).

1.6 Project aims

The principal aim of this project was to investigate the role of the clathrin light chain (CLC) *in vivo* using *Drosophila melanogaster* as a model organism. In particular, the role of CLC in the developing epithelial tissue of the eye, a robust *in vivo* system for studying clathrin-mediated endocytosis, was explored.

The first objective was to take a loss of function approach using the UAS-GAL4 system to determine whether CLC is required for the morphogenesis of different tissues in *Drosophila*. Following CLC knockdown, adult tissues were screened for any resulting phenotypes. The adult eye produced a phenotype and became the primary model system of this project.

The second aim of the work was to investigate the role of CLC in individual cell types in the adult eye. A cell classification algorithm was used to assess the requirement for CLC in different cell types.

The third aim of was project was to identify specific proteins and signalling pathways that rely on CLC during endocytosis.

Together, this project aimed to identify and characterise a phenotype resulting from CLC knockdown *in vivo*, in order to build on the findings of previous *in vitro* and cell culture studies. Investigating the function of CLC *in vivo*, where cells are exposed to the dynamic environment of a living tissue, has begun to shed light on the mechanism of action of this protein during development and adult tissue homeostasis.

2. Materials and methods

2.1 Materials

2.1.1 General laboratory equipment

Microscopes: Olympus FV1000 confocal microscope BX61 TRF (imaging of pupal eyes), Nikon SMZ Extended Focus Stereomicroscope (imaging of adult eyes), fluorescent microscope: Zeiss AX10 Zoom.V16 and Zeiss Upright Light Microscope.

2.1.2 Buffers/solutions/media

PBS	0.01 M phosphate buffer, 0.0027 M potassium chloride, 0.137 M sodium chloride, pH not adjusted for this project
0.1% PBST	0.1% (v/v) Triton X-100 in PBS
4% formaldehyde	37% formaldehyde solution diluted to 4% with PBS (made fresh each use from stock stored at room temperature)
100% Normal Goat Serum (NGS)	

2.1.3 Antibodies for immunohistochemistry

2.1.3.1 Primary antibodies

Antibodies	Description	Dilution for immunohistochemistry (pupal eye discs)	Reference/source
DCAD2 (ECD)	Monoclonal rat antibody	1:200	DSHB
anti-Notch (C458.2H)	Monoclonal mouse antibody	1:50	DSHB

anti-Sdt-PDZ	Polyclonal rabbit antibody	1:200	E. Knust
anti-N-cadherin	Monoclonal rat antibody	1:20	DSHB

2.1.3.2 Secondary antibodies

Antibodies	Description	Dilution for immunohistochemistry (pupal eye discs)	Reference/source
Cy™3 AffiniPure Donkey Anti-Mouse IgG (H+L)	Polyclonal	1:200	https://www.jacksonimmuno.com/
Cy™3 AffiniPure Donkey Anti-Rabbit IgG (H+L)	Polyclonal	1:200	https://www.jacksonimmuno.com/
Alexa Fluor® 488 AffiniPure Donkey Anti-Rat IgG (H+L)	Polyclonal	1:200	https://www.jacksonimmuno.com/
Alexa Fluor® 647 AffiniPure Donkey Anti-Rat IgG (H+L)	Polyclonal	1:200	https://www.jacksonimmuno.com/

2.1.4 Fly stocks

2.1.4.1 Balancer chromosomes

Stock	Description	Reference
FM7c	1st chromosome balancer	Lindsley and Zimm, 1992
CyO	2nd chromosome balancer	Lindsley and Zimm, 1992
CyO actGFP	2nd chromosome balancer	Bloomington 3499
CyO twiGFP	2nd chromosome balancer	Bloomington 24900

2.1.4.2 Driver lines

Stock	Description	Reference/source
w; *ey*GAL4	Expressed in the developing eye from early embryonic stages until mid-pupal development	Bloomington 5535
w; *GMR*GAL4	Expressed from 3rd instar larvae, in all eye cells behind the morphogenetic furrow	Bloomington 1104
w; *MS1096*GAL4	Expressed in dorsal wing pouch of third instar larvae	Bloomington 8860
w; *54*GAL4	Expressed in specified pigment cells	R. Cagan

2.1.4.3 CLC knockdown

For clathrin light chain knockdown, two VDRC UAS-RNAi stocks were used:

- V103362: P{KK107357}VIE-260B
- V22318: w^{1118}; P{GD12083}v22318 / CyO

These two RNAi lines target overlapping sequences in the CLC, however, all available/known CLC RNAi lines and reagents shown on FlyBase target the same region. Additionally, these two lines each have the same off-target effect, Aurora A (see section 4.7).

2.1.4.4 Candidates for enhancer suppressor screen

For this screen, CLC knockdown flies were crossed with flies carrying recessive mutations. These candidates were selected because each of these proteins/signalling pathways plays a vital role in eye structure/development. The progeny of each cross were screened for an enhancement or suppression of the CLC knockdown rough eye phenotype, in order to identify a novel genetic interaction.

Stock	Description	Reference/source
cn^1 shg^2 bw^1 sp^1 / CyO *twi*GFP	Shotgun (*Drosophila* E-cadherin) mutant	Bloomington 3085

zip² *ubi*::E-cad-GFP / CyO *twi*GFP	Myosin-II mutant	Bloomington 8739 Recombined by N. Bulgakova
numb¹ *ubi*::E-cad-GFP / CyO *twi*GFP	Numb mutant	Bloomington 4096 Recombined by N. Bulgakova
w¹¹¹⁸; *hbs⁶⁶*/ CyO	Hibris mutant	Bloomington 27618
EGFR^{F2} / CyO	EGFR mutant	Bloomington 2768
fmi^{E59}/ CyO *act*GFP	Flamingo mutant	D. Strutt
N^{55e11} FRT19A / FM7c	Notch mutant	Bloomington 28813

Enhancer/suppressor screen fly husbandry

10 virgin *ey*GAL4 UAS-Clc-RNAi (v22318) / CyO *act*GFP, *ey*GAL4 UAS-Clc-RNAi (v103362) / CyO *act*GFP and *ey*GAL4 / CyO *twi*GFP (control) females were each crossed to three males of the stocks highlighted in green.

10 virgin females from the stocks highlighted in orange were each crossed to three of the following males: *ey*GAL4 UAS-Clc-RNAi (v22318) / CyO *act*GFP, *ey*GAL4 UAS-Clc-RNAi (v103362) / CyO *act*GFP and *ey*GAL4 / CyO *twi*GFP.

Crosses were carried out in experimental vials at 25 °C and flipped every three days.

The size of the eye and a score for necrotic tissue were analysed in flies carrying both UAS-Clc-RNAi and the recessive mutation, as well as in external and internal controls. For external control, the driver *ey*GAL4 was crossed with the candidates to ensure expression of the GAL4 protein alone did not produce a phenotype. Internal controls were the following:

eyGAL4 UAS-Clc-RNAi (v106632 or v22318) / balancer	This control produces a rough eye phenotype from the CLC knockdown alone. This will provide a 'baseline' rough eye.
'n' / balancer	This control, the candidate mutation over a balancer chromosome, determines whether recessive expression of this mutation has any effect on eye morphology, in the absence of UAS-Clc-RNAi.

Controls for this experiment were kept at the same density in the vial as well as the same food composition. This ensured that any changes in the rough eye phenotype were not likely to be as a result of food/reproductive competition.

2.1.4.5 Other stocks

Stock	Description	Reference/source
NRE::EGFP	Notch signalling reporter	A. Saj. 2010
Notch-YFP / FM7	Insertion of YFP into Notch at aa residue 2388	L. Couturier, N. Vodovar, F. Schweisguth. 2012
ubi::E-cad-GFP	E-cadherin-GFP expressed under the ubiquitin (*ubi*) promoter	H. Oda, S. Tsukita. 2001
shg::E-cad-GFP	E-cadherin-GFP expressed under shotgun (*shg*) regulatory sequences	Bloomington 60584

2.1.5 Fly food

Ingredient	Amount	Manufacturer	Supplier
Cold tap water	1 Litre		
Medium Cornmeal	80g	Triple Lion	Lembas/Easton Enterprises
Dried Yeast	18g	Kerry Ingredients	BTP Drewitt
Soya Flour	10g	Lembas Wholefoods	Lembas
Malt Extract	80g	Rayner's Essentials	Lembas
Molasses	40g	Rayner's Essentials	Lembas
Agar	8g		BTP Drewitt
10% Nipagin in Absolute Ethanol	25ml	Clariant UK Ltd; Fisher	Chemolink Specialities Ltd; Fisher
Propionic Acid	4ml	Fisher	Fisher

All nutrient-rich fly culture media is prepared in a specialist media maker in batches by the Fly Food Facility at the University of Sheffield.

2.2 Methods

2.2.1 Histological methods

2.2.1.1 Immunohistochemistry on pupal eye discs

Pupae were staged until 42% pupal development (p.d.) (100% p.d is 103 hours at 25 °C):

1. At regular time intervals (~1 hour) newly pupated white pupae were collected from bottles and transferred to a labelled (genotype, date, time collected) petri dish.
2. To maintain humidity in the dish, a soaked paper towel was placed in the dish and the lid placed on top.
3. The dishes were incubated at 25 °C until 42% p.d. (43 hours after pupation at 25 °C).
4. Using the fluorescent microscope, pupae were selected and dissected, i.e. pupae without the fluorescent CyO *act*GFP balancer were collected.

The retina-brain complexes were dissected in PBS and fixed for 20 minutes in 4% formaldehyde (Figure 2.1). The dissected retina-brain complexes were washed three times in 0.1% PBST for 15 minutes. Primary antibodies diluted in 1% NGS/0.1% PBST were incubated with the retinas overnight at 4°C in a wet chamber, followed by three 15 minute 0.1% PBST washes. Secondary antibodies diluted in 1% NGS/0.1% PBST were incubated with the retinas for two hours at room temperature in a wet chamber (dark) and then washed three times with 0.1% PBST for 15 minutes. The retina-brain complexes were then transferred into PBS and eye discs were dissected from the tissue. Discs were mounted face up on a SuperFrost® Plus microscope slide with VectaShield® antifade mounting medium. The coverslips were sealed with clear nail varnish and the slides were stored in the dark at 4°C until imaging.
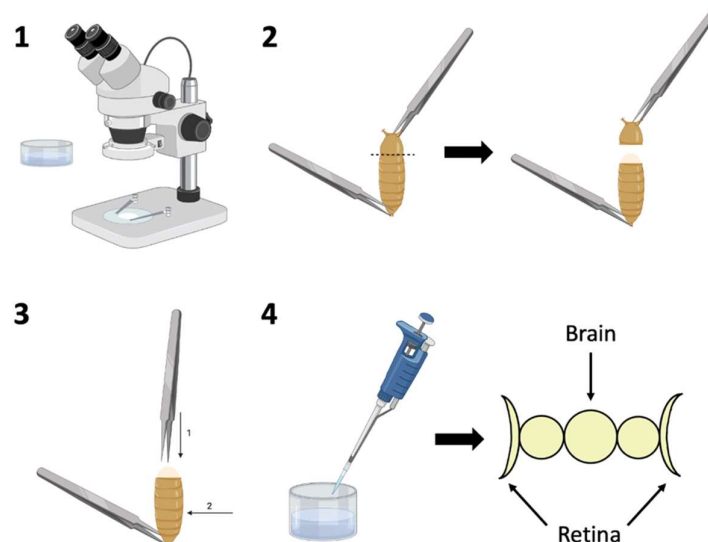
Figure 2.1: Step-by-step illustration of pupal eye disc dissection. 1) Staged pupae were dissected in glass wells containing PBS under a dissecting microscope. 2) The anterior portion of the pupal casing was removed using forceps, by gripping the posterior end of the casing to keep the pupa in place. 3) One tip of the forceps was used to pierce the head of the pupa (arrow labelled 1). The anterior content of the pupa was removed by pinching the

middle area of the pupal casing (arrow labelled 2). 4) In the dish, a P1000 Gilson pipette with the end of the tip cut off (to widen the hole) was used to gently pipette up and down in PBS in order to wash the retina-brain complex out. The remaining fat/tissue was gently dissected off with forceps to reveal a clean, whole retina-brain complex, ready to be fixed, stained and mounted.

2.2.1.2 Adult wing dissection

Adult female flies were collected approximately 24 hours after eclosion. Flies were dehydrated in various concentrations of ethanol in order to minimise bubble formation when mounting wings, as follows:

70% ethanol	2 x 10 minute washes
96% ethanol	x2 10 minute washes
100% acetone	10 minute wash
Fresh 100% acetone	Overnight with rotation

The following day, the flies were removed from the acetone and dried on tissue. A strip of Canada balsam (Benz) was placed onto a microscope slide (Menzel). One at a time, each fly was placed onto the balsam and the wings were carefully removed and embedded within (bodies removed from resin and discarded). Once all the wings were embedded, a cover slip was placed on top and the Canada balsam was left for five days to solidify (Figure 2.2).
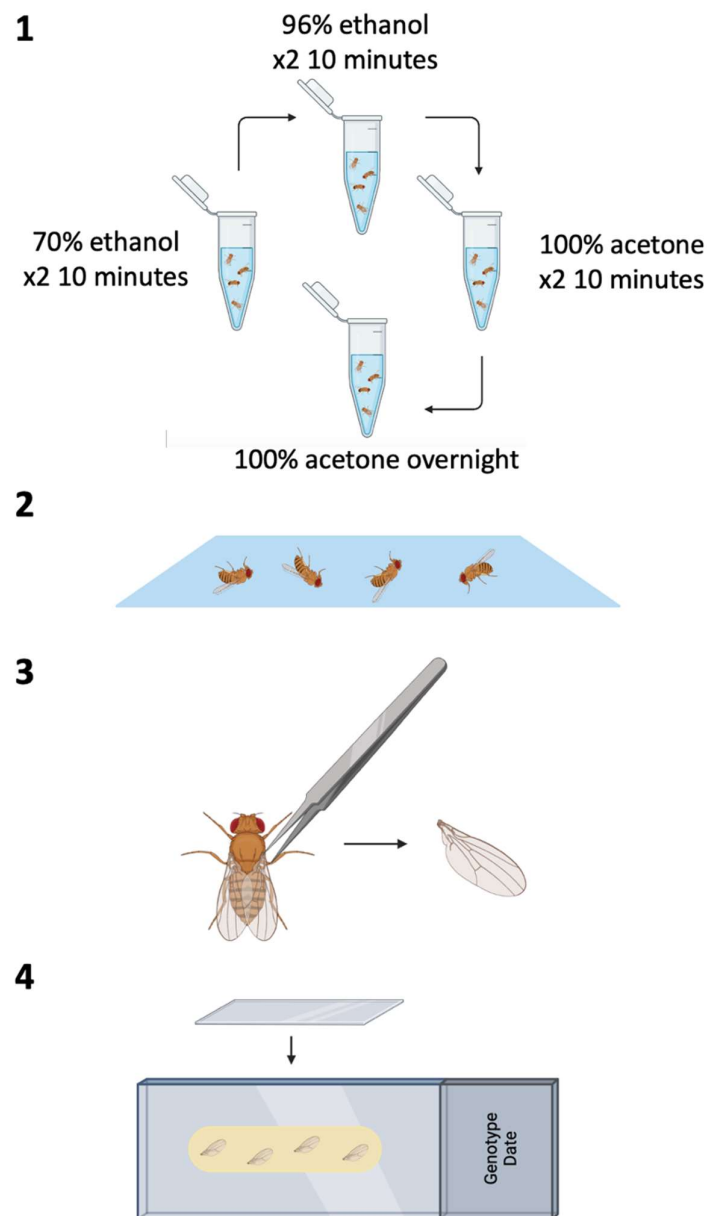
Figure 2.2: Step-by-step illustration of adult wing dissection. 1) Adult flies were dehydrated in series of ethanol and acetone solutions. 2) Flies were dried by placing on tissue paper. 3) (Carried out on a strip of Canada Balsam on Menzel slide) Wings were removed using forceps and embedded in Canada Balsam. 4) Once all wings were embedded, a coverslip was placed on top, sealed and left to dry for 5 days.

2.2.2 Genetic methods

The UAS-GAL4 system was used to express UAS constructs in a tissue-specific manner at the desired developmental stages (Brand and Perrimon, 1993). The driver line, containing the yeast transcription factor GAL4 downstream of a regulatory element, crossed with an effector line,

containing an upstream activation sequence (UAS) upstream of the gene of interest, results in the expression of the UAS construct in all cells expressing the GAL4 regulatory element (Figure 2.3).
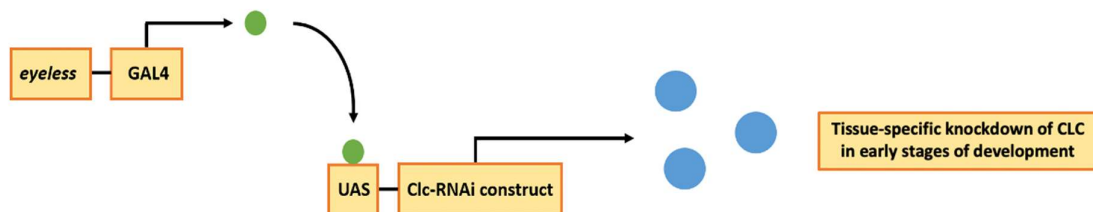
Figure 2.3: A schematic to illustrate the tissue-specific knockdown of clathrin light chain in early development. The eyeless promoter drives expression of the UAS-Clc-RNAi constructs from early embryonic stages in the *Drosophila* eye (Beronja et al., 2005).

2.2.3 Image acquisition

2.2.3.1 Confocal microscope imaging

Confocal images were taken using the Olympus FV1000 Confocal microscope with the 60x/1.4 Oil PlanApoN objective. Eye discs were imaged at 42% pupal development, from the top of the cone cells down to the top of the photoreceptors. For image acquisition, FV10-ASW software was used.

Imaging properties/microscope settings:

Bit depth	16-bit
Image dimension	1024x1024 (70.66 μM x 70.66 μM)
Resolution	14.5 pixels/μM
Laser power	3.0%
Step size	0.3 μM
Scan speed	4.0 frames/s
Observation mode	LSM
Offset	6
Gain	2.0

2.2.3.2 Stereomicroscope imaging

Adult eyes

Images of female adult eyes were taken using the Nikon SMZ Extended Focus Stereomicroscope (camera name: DS-Fi1-U2). Z stacks that span the depth of the entire eye were taken and saved as .oib files. An average intensity projection of the Z stack was made using Fiji and the projection was saved as a .tif file. NIS Elements software was used for image acquisition.

Image properties/microscope settings:

Image type	RGB
Image dimension	2560 x 1920
Resolution	1.0 pixels/μM
Step size	1.0 μM
Offset	0
Gain	3.40x
Exposure time	400 ms
White balance	Auto
Manual zoom	10.0x

<u>Adult wings</u>

Adult wings were imaged at 5x objective on the Zeiss Upright Light Microscope and images were saved as .tif files.

Image properties/microscope settings:

Bit depth	16-bit
Image dimension	1280 x 960
Resolution	0.2 pixels/μM
Magnification	5.0x

2.2.4 Image analysis

All images were processed and analysed using Fiji software (http://fiji.sc) and in-house MATLAB scripts (https://github/nbul/Intensity).

2.2.4.1 Border intensity

The level of E-cadherin at cell borders in average intensity projections (spanned from the top of the cone cells down to the top of photoreceptor cells) of pupal eye discs at 42% p.d. was determined by measuring the fluorescence intensity of E-cadherin-GFP expressed under either its endogenous promoter, *shg*, or an independent promoter, *ubi*. Fluorescence intensity of E-cadherin-GFP was measured in *ey*GAL4 UAS-Clc-RNAi (v106632 or v22318)/ *ubi*::E-cad-GFP and *ey*GAL4 UAS-Clc-RNAi (v106632 or v22318)/ *shg*::E-cad-GFP. For the control, *ey*GAL4 / *ubi*::E-cad-GFP and *ey*GAL4 / *shg*::E-cad-GFP were used because there is no expression of the UAS construct.

Images were processed and analysed as follows:

1. An average intensity projection of Z-stacks was produced in Fiji and saved as a .tif image: Image → Stacks → Z projection
2. Number of stacks per projection must be the same.
3. Average intensity projections were segmented using the Tissue Analyzer plugin in Fiji to trace cell borders: Plugins → Tissue Analyzer
    a. Selected "Segmenting" tab: Detect bonds (preview only) → Removed cells smaller than 20 pixels and used two blurs for better cell outlines (strong blur = 12, weak blur = 1.7).
    b. Once cell borders were traced, the save icon was clicked to store progress.
    c. Selected "Correction" tab → Removed false bonds.
    d. Manual correction: used drawing tool to manually correct borders detected by Tissue Analyzer.
    e. Selected "PostProcess" tab: Finish all
    f. Selected "Tracking" tab: Track cells (static tissue), used displacement exclusion criterion and did not exclude biggest cell
4. Instructions for analysing images were found at https://github.com/nbul/Intensity
    a. Two subfolders for input files were created:
        i. tifs_original: contained average intensity projections of original images. Files must be named 1, 2, 3….
        ii. borders: contained segmented images in subfolders, name must correspond to original file (1, 2, 3…). Subfolders must contain "handCorrection.tif" and "vertices.tif" files.
    b. Ran the script according to instructions – for eye discs, selected "wing disc" option.
5. The "Intensity-wing.csv" output folder contained the average fluorescence intensity at cell borders for each image.

2.2.4.2 Puncta analysis

The volume and intensity of Notch-YFP puncta were quantitatively analysed using the 3D Object Counter plugin in Fiji. An average threshold value determined what would be detected as an object (individual puncta). This was obtained by manually determining the optimal threshold of control images (*ey*GAL4 / N-YFP) and calculating an average value. This optimal threshold value was applied to stacks of *ey*GAL4 UAS-Clc-RNAi (v106632 and v22318) / N-YFP pupal eye discs (42% p.d.). 3D

Object Counter measured the number, volume and intensity of puncta. All stacks contained the same number of z-sections and spanned the same depth of the eye disc (from the top of the cone cells to the top of the photoreceptor cells).

2.2.4.3 Cell morphology analysis

Cell morphology in pupal eye discs was measured using an in-house interactive cell classification algorithm. Maximum intensity projections of eye discs were segmented using the Tissue Analyzer plugin in Fiji (see Steps 1-2 under Border Intensity). Cell outlines in pupa eye discs were visualised by *ubi*::E-cad-GFP in *ey*GAL4 UAS-Clc-RNAi (v106632 or v22318)/ *ubi*::E-cad-GFP, and in the control, *ey*GAL4 / *ubi*::E-cad-GFP. Cell properties of each cell type were obtained in each image as follows:

1. The input files were "handCorrection.tif" and the original unmodified maximum intensity projections "*.tif".
   Original unmodified projections were saved into a folder named "tifs original" and named sequentially: "1.tif", "2.tif" etc and the "handCorrection.tif" images produced by image segmentation were saved into subfolders numbered according to the name of the original tif image.
2. Ran the script.
3. When prompted to select individual cells from an image in order to extract their properties, approximately 15 cells per image were clicked (Figure 2.4A).
4. The output folder produced the following data (see chapter 3.2 for further explanation) and output images of the selected cells (Figure 2.4B):
   a. Area: Number of pixels in the region.
   b. Eccentricity: Eccentricity of the ellipse that has the same second-moments as the region.
   c. Circularity: Roundness of objects.
   d. Equivalent Diameter: Diameter of the circle that has the same area as the region.
   e. Solidity: Proportion of the pixels in the convex hull that are also in the region.
   f. Perimeter: Distance around the boundary of the region.
   g. Mean Intensity: Mean of all the intensity values in the region (cytoplasmic region).
   h. Border intensity: Average intensity of pixels within the border of the region (cell membranes).
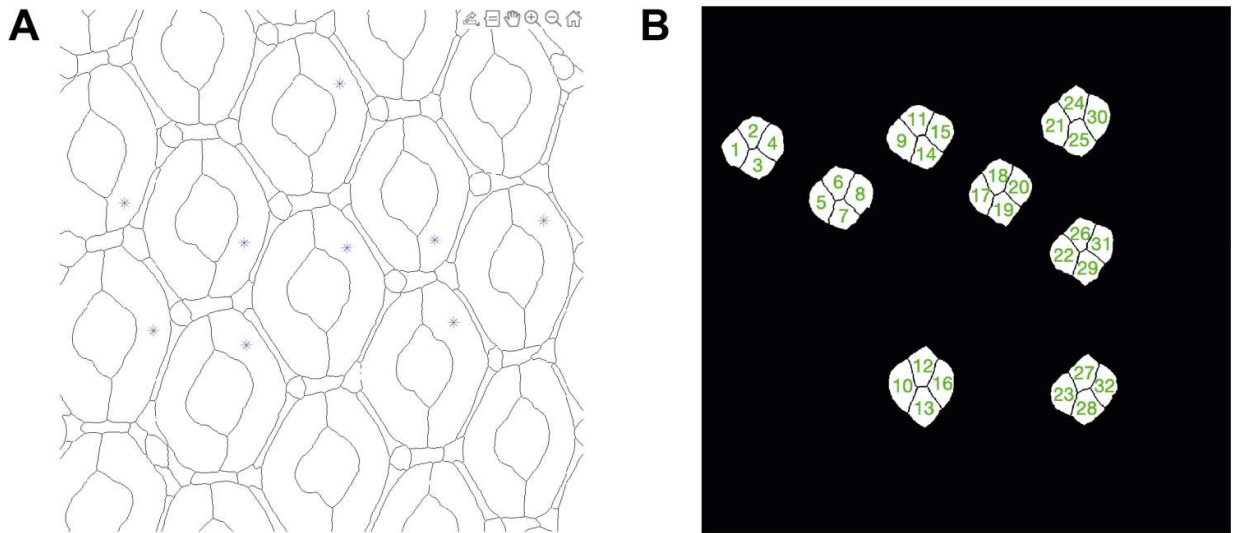
Figure 2.4: Image to demonstrate cell selection in Interactive Cell Classification algorithm. (A) Image shows 9 selected primary cells. To select a cell, left click, to finish selecting cells, double click/right click. (B) Example of an output image of a selection of cone cells. This will be saved alongside the data for each labelled cell.

### 2.2.4.4 Quantification of the disorganisation of the pupal retina

The disorganisation of the pupal retina at 42% p.d. was quantified by manually measuring the distance between the centre of each photoreceptor cluster in the ommatidia of *ey*GAL4 UAS-Clc-RNAi (v106632 or v22318)/ *ub*i::E-cad-GFP pupal eye discs, and in *ey*GAL4/ *ub*i::E-cad-GFP for the control (Figure 2.5).

1. Maximum intensity projections of Z-stacks through apical areas of pupal eyes were produced in Fiji so that the photoreceptors at the centre of each ommatidium were visible. Here, number of stacks per projection is not crucial because this measure is not measuring pixel intensity, but the morphology of the eye.
2. The distance between the centre of the photoreceptor clusters in neighbouring ommatidia was obtained using the Measure tool in Fiji (see above) (Figure 2.5A). At least 10 measurements were made per image.
   a. For fused ommatidia, the clusters were treated as one object if the photoreceptors were directly in contact, and treated as two if they were not (Figure 2.5B).
3. The standard deviation and the mean of the distance measurements were calculated for each image.
4. To give a measure of disorganisation, the coefficient of variation per image was calculated:

$$CV = \sigma / \mu$$

σ = population standard deviation
μ = population mean
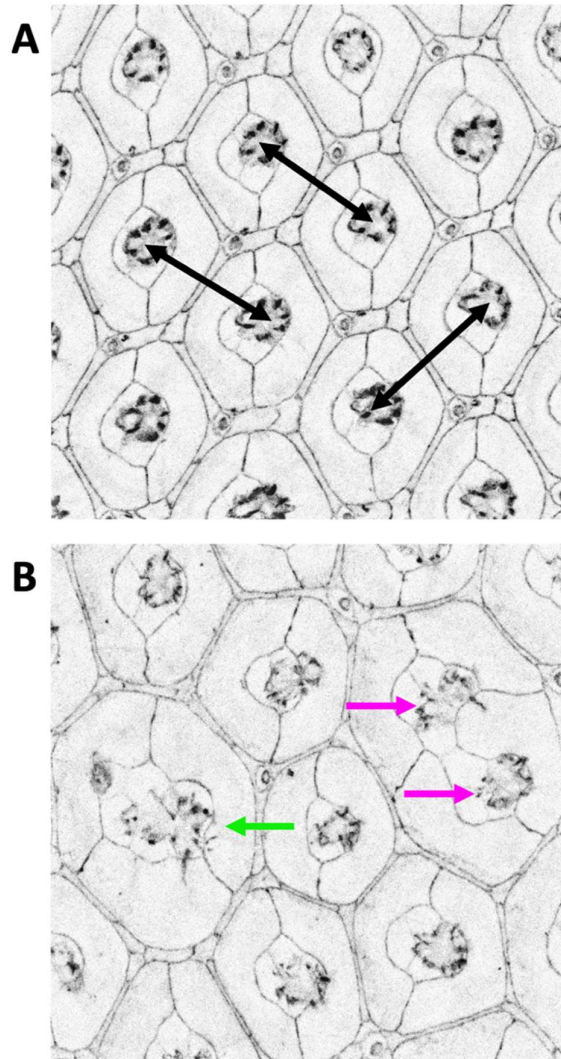
Figure 2.5: Illustration of how to manually measure the distance between photoreceptor clusters in neighbouring ommatidia to assess the severity of disorganisation in the pupal retina. A) Arrows illustrate how the length between the centre of photoreceptors in neighbouring ommatidia was measured using the selection tool in Fiji. B) Two clusters of photoreceptors in fused ommatidia that were directly in contact were treated as a single object/cluster (green arrow). Two clusters of photoreceptors in fused ommatidia that are not directly in contact were treated as two separate objects/clusters (magenta arrow).

2.2.4.5 Enhancer/suppressor screen analysis

The area of adult eyes in CLC knockdown eyes was measured using the selection tool in Fiji. The tool was used to draw around the edge of the eye and the number of pixels in each region was measured. Approximately 10 images for each genotype were analysed. The area of adult eyes of the internal controls and flies carrying both UAS-Clc-RNAi and the candidate mutation were

normalised to the average area of the adult eyes in the external control for each cross (*ey*GAL4 / *balancer*).

2.2.5 Statistical analysis

Statistical analysis was carried out using Microsoft Excel and GraphPad Prism 8 (https://www.graphpad.com/scientific-software/prism). Each data set was tested for normal distribution and outliers using D'Agostino-Pearson and ROUT tests, respectively. Normal distribution was tested to ensure the data was taken from a normally distributed population, which is essential for ordinary one-way ANOVA. A ROUT test was used rather than a Grubb's test because it can detect more than one outlier.

Ordinary one-way ANOVA and Tukey's multiple comparisons were performed to determine whether CLC knockdown significantly altered relative fluorescence intensity of E-cadherin-GFP (for both *shg*::E-cad-GFP and *ubi*::E-cad-GFP) at cell borders and the intensity/size of Notch-YFP puncta. This measure not only allowed comparison between CLC knockdown and the control, but also allowed comparison between the two different UAS-Clc-RNAi lines, v106632 and v22318 to determine if they each result in a similar phenotype.

The severity of retinal disorganisation in *ey*GAL4 UAS-Clc-RNAi (v106632 or v22318)/ *ubi*::E-cad-GFP pupal eye discs in comparison to *ey*GAL4/ *ubi*::E-cad-GFP pupal eyes, was quantified by calculating the coefficient of variation of distances between photoreceptor clusters per image. One-way ANOVA with multiple comparisons was used to determine whether CLC knockdown had a significant effect on the organisation of the retina and how similar the impact of v106632 and v22318 were.

To assess changes in cell morphology following CLC knockdown, cell properties of various cell types in each image were exported into an excel file. The coefficient of variation of each property per image was calculated and one-way ANOVA was used to determine whether CLC knockdown had a significant effect on the variation in cell size and shape, and how similar the impact of v106632 and v22318 were. To facilitate visualisation of the changes in cell morphology, radar charts were created: for each property the coefficients of variation in all images of each genotype were averaged (*ey*GAL4/ *ubi*::E-cad-GFP, *ey*GAL4 UAS-Clc-RNAi (v106632)/ *ubi*::E-cad-GFP and *ey*GAL4 UAS-Clc-RNAi (v22318)/ *ubi*::E-cad-GFP) to get an average measure of variation across all images.

One-way ANOVA and Tukey's multiple comparisons were used to analyse the area of adult eyes in the enhancer/suppressor screen. This approach allows the comparison between the two internal controls and the flies carrying both UAS-Clc-RNAi and the candidate mutation.

3. Results

3.1 CLC knockdown impairs morphogenesis of the *Drosophila* eye but not the wing or mesoderm

To investigate the function of CLC *in vivo*, CLC was knocked down in different tissues during development and adult flies were examined for a resulting phenotype. The UAS-GAL4 system was used to express two independent UAS-Clc-RNAi constructs in a tissue-specific manner during development to identify a physiological phenotype. Two different UAS-Clc-RNAi constructs were used to ensure that any phenotype that occurred as a result of the expression of the UAS construct was not due to off-target effects, but specifically due to CLC knockdown. If the same phenotype is seen in both RNAi lines, it can be concluded that this was specifically due to CLC knockdown. If a phenotype was only seen in one of the RNAi lines, this could be due to off-target effects. Flies expressing the GAL4 protein, but not the UAS-Clc-RNAi construct acted as a control because CLC expression remains unperturbed in the absence of the UAS sequence. Although GAL4 alone has been shown to cause developmental defects in the *Drosophila* eye when expressed under the control of the glass multiple reporter promoter (Kramer and Staveley, 2003), there was no obvious phenotype in the GAL4 only control in this experiment. CLC was knocked down in three tissues: the eye, the wing and the mesoderm, at different stages of development. For CLC knockdown in the eye, UAS-Clc-RNAi was expressed under the control of two tissue-specific drivers: *eyeless* (*ey*GAL4) and the glass multiple reporter (*GMR*GAL4), expressed throughout eye development or following the onset of differentiation in the third larval stage, respectively (Beronja et al., 2005; Hay et al., 1994). A rough eye phenotype in the adult fly resulted from expression of UAS-Clc-RNAi constructs in early, proliferative stages of eye development (*eyeless*), but not in later post-mitotic stages (*GMR*) (Figure 3.1A). As shown in Figure 3.1, the highly regular organisation and spacing of the ommatidia was lost in the adult eye where UAS-Clc-RNAi was expressed under the control of the *eyeless* promoter, but not *GMR*, demonstrating that CLC is required during early stages of eye development, but not later stages.

UAS-Clc-RNAi was also expressed in the wing during development, again using two different tissue-specific GAL4 drivers: *engrailed*GAL4, expressed in the posterior wing, and *MS1096*GAL4, expressed in the dorsal wing pouch of third instar larvae, however, this did not result in a significant phenotype (Figure 3.1B). Additionally, knockdown of CLC in all mesodermal cells throughout development does not produce any obvious phenotype or hinder fly viability (data not shown). As discussed above, it is worth noting that these phenotypes (or lack of) depend on the degree on CLC knockdown. These data support a significant but context-dependent developmental role of CLC *in vivo* and suggest that CLC is required for the morphogenesis of some tissues but is not necessary for the development of all tissues.
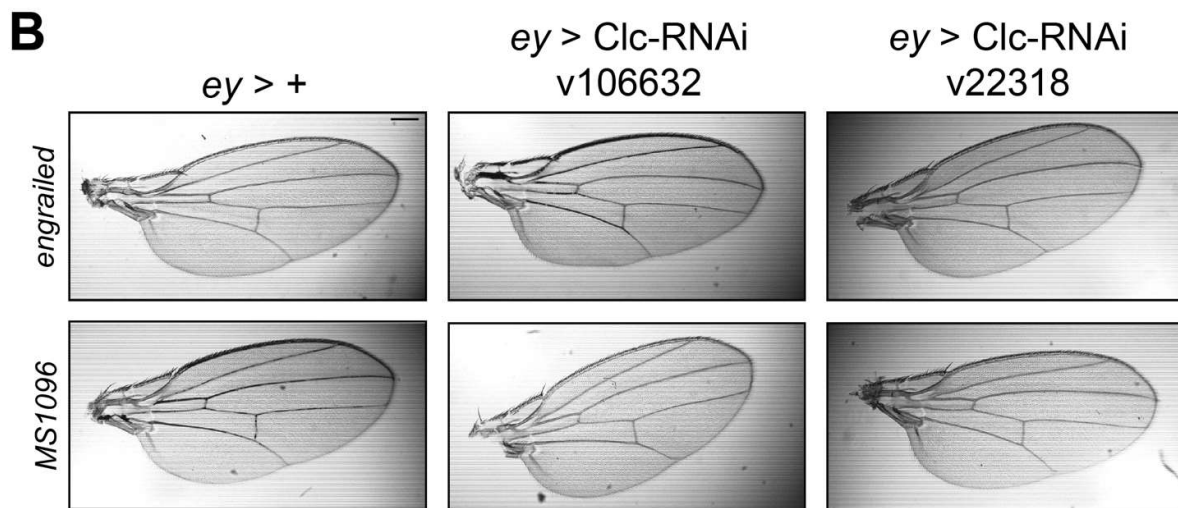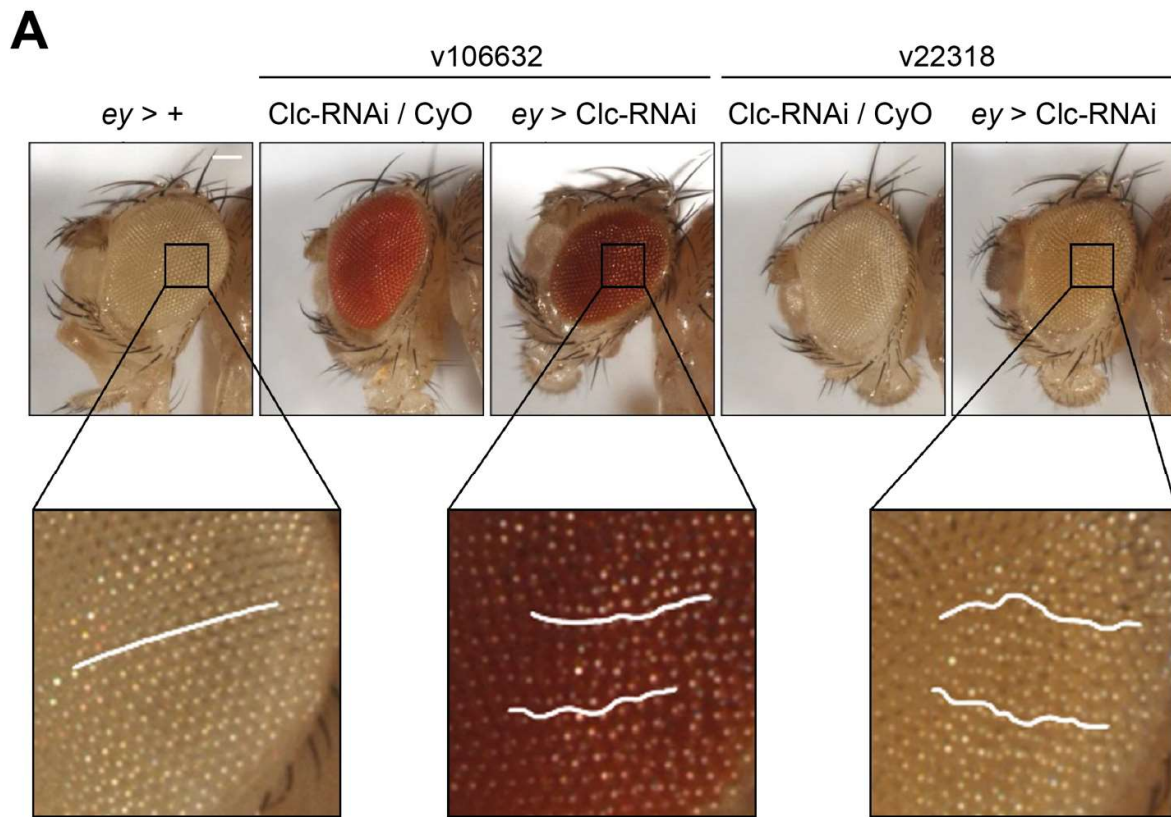
Figure 3.1: The effect of expressing UAS-Clc-RNAi in the adult *Drosophila* eye and wing during development. (A) The expression of two UAS-Clc-RNAi lines (v106632 and v22318) in the adult eye under the control of the *eyeless* promoter resulted in a rough eye phenotype. Scale bar - 100 µm. (B) Expression of UAS-Clc-RNAi in the wing under the control of two different GAL4 drivers, *en*GAL4 and *MS1096*GAL4. Scale bar - 100 µm.

Given a clear phenotype in the adult, the next step was to investigate its origins during development. Using the same system, the *Drosophila* eye was examined at pupal stages, specifically at 42% of pupal development (p.d.) (Grzeschik and Knust, 2005). At 42% p.d. the cells in the retina

are arranged into distinct hexagonal arrays called ommatidia and all excess cells have been removed by apoptosis. This stage was selected because disruption to the development of the eye would be apparent: at this point in development the cells in the retina are highly organised and precisely arranged so any alterations in cell number, organisation or shape can be quantified. Using confocal microscopy, the tissue architecture and cellular organization was examined, visualising cell outlines with E-cadherin-GFP. Several images were taken along the Z-plane of the retina and stacked together to form a projection. An average intensity projection that consists of several images each captured at a different focal plane provides a greater depth of field than one image alone.

The rough eye phenotype in the adult resulting from early CLC knockdown was also apparent in the pupal eye at 42% p.d. UAS-Clc-RNAi expressed under the control of the *eyeless* promoter resulted in a severely disorganised pupal retina: partial/full fusion of ommatidia, supernumerary and missing cells, a loss in the stereotypical hexagonal shape of the ommatidia, loss of planar cell polarity and in some cases stalled intercalation of cone cells (Figure 3.2A). To assess the severity of the rough eye phenotype in the pupal retina following early CLC knockdown, the distance between each photoreceptor cluster was measured and the coefficient of variation was calculated per image. This approach obtained the variability of distances between photoreceptor clusters. CLC knockdown at early stages of development resulted in a significant increase in the variation of the distance between photoreceptor clusters (Figure 3.2B). In contrast to the control, in which the ommatidia and therefore photoreceptor clusters are regularly spaced and highly organised, CLC knockdown resulted in a highly disorganised retina. This approach provided a robust measure of the tissue-level disorganisation of pupal retina following CLC knockdown.

Additionally, in pupal retinas expressing *ey*GAL4 UAS-ClcRNAi, ommatidia with the correct number of 4 cone cells typically also had 7 visible photoreceptors (R8 not visible) as in the control (although there was a highly infrequent occurrence of ommatidia with the correct number of cone cells that contained abnormal numbers of photoreceptors (Figure 3.2C, green asterisk)). In ommatidia with excess or missing cone cells, the number of photoreceptors was highly variable (Figure 3.2C). Ommatidia with 3 cone cells typically had fewer than 7 photoreceptors (Figure 3.2C, black asterisks), and there were some that had more than the expected 7 (Figure 3.2C, magenta asterisks). Ommatidia that failed to separate and had partially or completely fused also had varying numbers of photoreceptors (Figure 3.2C, blue asterisks). While some fused ommatidia contained exactly 14 photoreceptors, the number expected to be found in two separate ommatidia, some contained more or less than expected. There was no exact correlation between the number of cone cells and the number of photoreceptor cells across the CLC knockdown retina.

Together, this experiment shows that CLC is required in early stages of eye development, and that reducing its expression causes a significant disruption to the morphology of the retina.
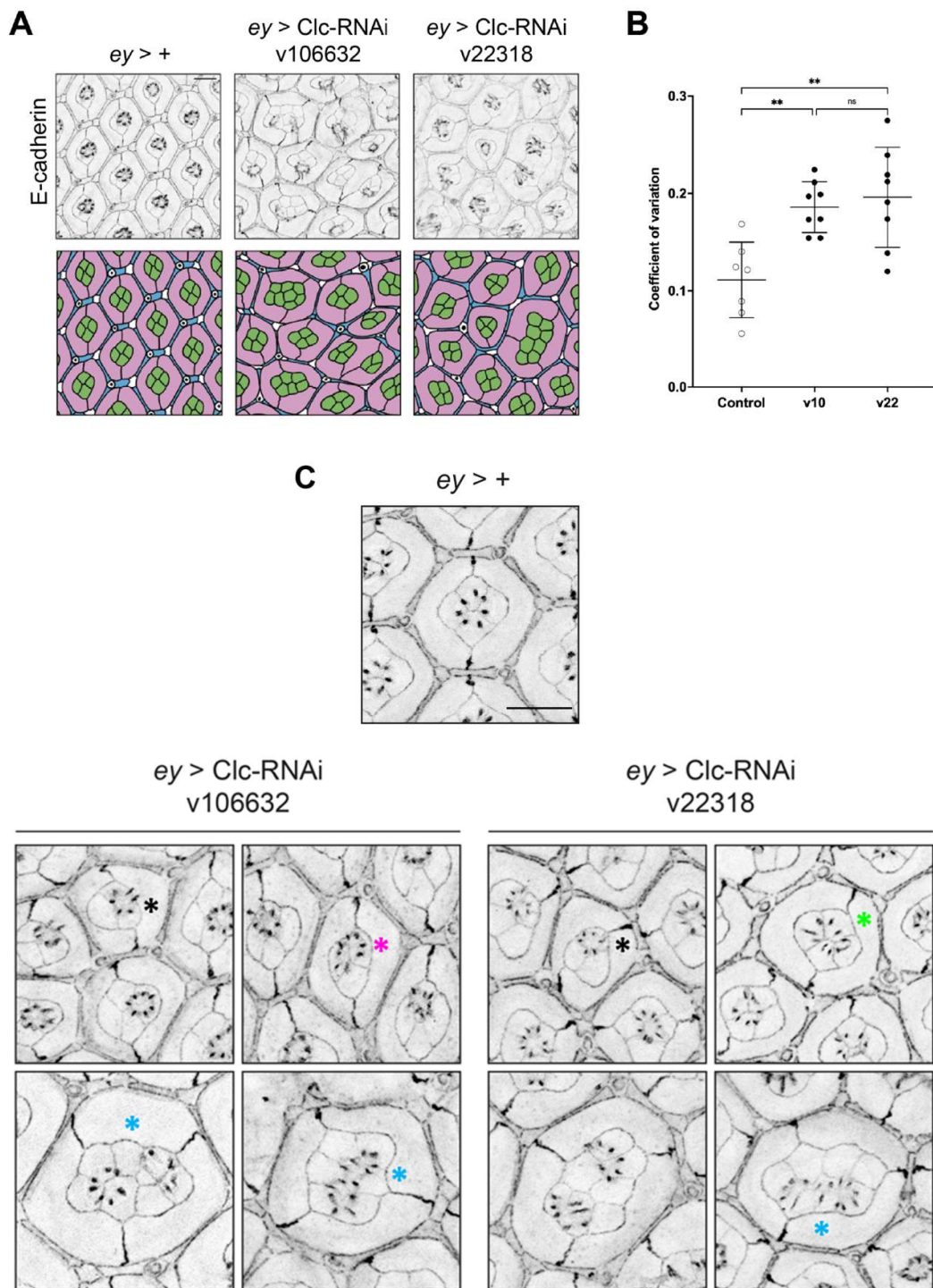
Figure 3.2: Two independent UAS-Clc-RNAi constructs (v103362 and v22318) expressed in all cells of the developing eye under the control of the *eyeless* promoter resulted in disorganisation of pupal retina at 42% p.d. (A) Pupal retinas expressing *ey*GAL4 UAS-Clc-RNAi at 42% p.d. with cell outlines visualised by E-cadherin-GFP. Primary cells – pink, secondary cells – blue, tertiary cells – white, bristle cells – white with black dot, cone cells – blue. Scale bar – 10 μm. (B) Disorganisation of pupal retina quantified by measuring the distance between central photoreceptor clusters and calculating the coefficient of variation

per image. ** - p < 0.005. (C) CLC knockdown at early stages of eye development resulted in aberrant numbers of cone cells and photoreceptors at 42% p.d. Scale bar – 10 μm.

3.2 CLC knockdown affects some cell types more than others

The next objective was to assess the impact of CLC knockdown in the pupal eye at the cellular level. Each cell type has different properties and is specified according to various developmental signalling pathways. Investigating this phenotype at the cellular level provides valuable information about the requirement for CLC in different cell types. Some cell types appeared more affected by Clc-RNAi than others. For example, from a qualitative assessment secondary interommatidial significantly varied in size and shape, while cone cells (although varying in number) exhibited relatively normal morphology. In order to classify the cells and measure their properties, I developed an Interactive Cell Classification MATLAB script. The cell borders in an image of the pupal retina were traced using the Tissue Analyzer plugin in Fiji to generate an image that just contains cell outlines. The code allows the user to interactively select different regions (cells) in the segmented image and then extract the properties of each region (Table 3.1). By selecting one cell type at a time, the user is able to measure the properties in a cell type-specific manner. As the retina is composed of multiple cell types, each with their differing properties, this provides valuable information on the effect of CLC knockdown in different cells, rather than across the whole tissue.

| Property	Description	Significance
Area	Measures the number of pixels in the region.	The area provides information on the size of the cells.
Eccentricity	Ratio of the distance between the foci of the ellipse and its major axis length i.e. how 'long' a cell is.	The eccentricity provides valuable information about changes in the shape of longer cells e.g. secondary cells.
Circularity	Roundness of objects.	The circularity provides information about changes in the roundness of cells.
Equivalent Diameter	Diameter of a circle with the same area as the region.	This measures changes in cell size.
Convex Hull	The smallest polygon that can contain the region.	These measures were not analysed individually, but they are important for calculating the solidity of the cell.
Convex Area	The area of the convex hull of the region.	
Solidity	Proportion of the pixels in the convex hull that are also in the	The solidity provides information about changes in cell shape.

	region i.e. the ratio of the area over the convex area.	
Perimeter	Distance around the boundary of the region.	The perimeter provides information about changes in cell size.
Mean Intensity	Mean of all the intensity values in the region.	This measures the intensity of all the pixels inside the cell and can be used to measure expression levels of fluorescent proteins in the cytoplasm e.g. NRE::EGFP (Notch signalling reporter).
Border Intensity	Average intensity of pixels within the border of the region.	This measures the intensity of all the pixels in the border of the cell and can be used to measure expression levels of fluorescent proteins in the cell membranes e.g. E-cad-GFP.

Table 3.1: Table to show properties of cells measured by Interactive Cell Classification Algorithm. These properties were selected because they provide information about cell size, shape and levels of cytoplasmic proteins (see Mean Intensity) in a cell type-specific manner.

Using this code to determine significant changes in cell morphology in a cell-type specific manner provided insight on the requirements of CLC in different cells. Once all the properties of each cell type in the eye had been measured, the variation in these properties following CLC knockdown was examined. In each image, the coefficient of variation was calculated for each property and this was compared to control pupal eye discs that did not express UAS-Clc-RNAi (Figures 3.3 – 3.6). CLC knockdown did perturb cell morphology in the retina, but the severity and properties affected varied between cell types. Primary cells exhibited increased variation in both cell size and shape, however, UAS-Clc-RNAi v22318 did not affect the cell size as significantly (Figure 3.3). The significantly increased variation in the eccentricity, circularity and solidity of these cells seen in both v106632 and v22318 shows that CLC knockdown impairs primary cell morphology. CLC knockdown in secondary cells resulted in severe perturbation of cell morphology (Figure 3.4). The coefficient of variation for every property measured was significantly increased, particularly the eccentricity. Secondary cells in a wild-type retina are typically long, thin cells with a little variation in their eccentricity, but following CLC knockdown, the regular rectangular shape of these cells drastically varied. While some secondary cells maintained their typical morphology, some more than halved in length, and lost their rectangular shape. Naturally, this increased variation in the cell shape was concurrent with increased variation in properties measuring cell size: perimeter, area and diameter. In contrast, CLC knockdown in the tertiary cells that neighbour secondary cells resulted in minor changes in cell morphology (Figure 3.5). While there was statistically significant variation in cell size and shape, the magnitude of this variation was much lower than primary and secondary cells

(Figure 3.7). The code was unable to differentiate between tertiary and bristle cells because the input images were binary images that only traced the borders of epithelia cells in the retina. As the morphology of these cell types is indistinguishable in wild type retinas, and in CLC knockdown retinas based on qualitative assessment of the images, the data from this experiment grouped the two cell types together. Lastly, CLC knockdown caused slight changes in the variation of the size of cone cells, but there was no significant change in any of the properties that measure cell shape (Figure 3.6). These cells maintained their regular shape, even in partially/fully fused ommatidia that contain abnormal numbers of cone cells. In comparison to all other cell types in the retina, cone cells were the least affected by CLC knockdown at early stages of development, while secondary cells exhibited the largest variation in cell shape and size (Figure 3.7). The radar charts in Figure 3.7 summarise the impact of CLC knockdown in each cell type, and the severity of the changes in variation of cell morphology. Note, the coefficient of variation for eccentricity in secondary cells in both the control and CLC knockdown is significantly lower than the other cells due to their typical elongated shape. Figure 3.7Bi highlights the impact of CLC knockdown on this property in secondary cells.

Primary cells

A Area

B Eccentricity

C Circularity

D Equivalent Diameter
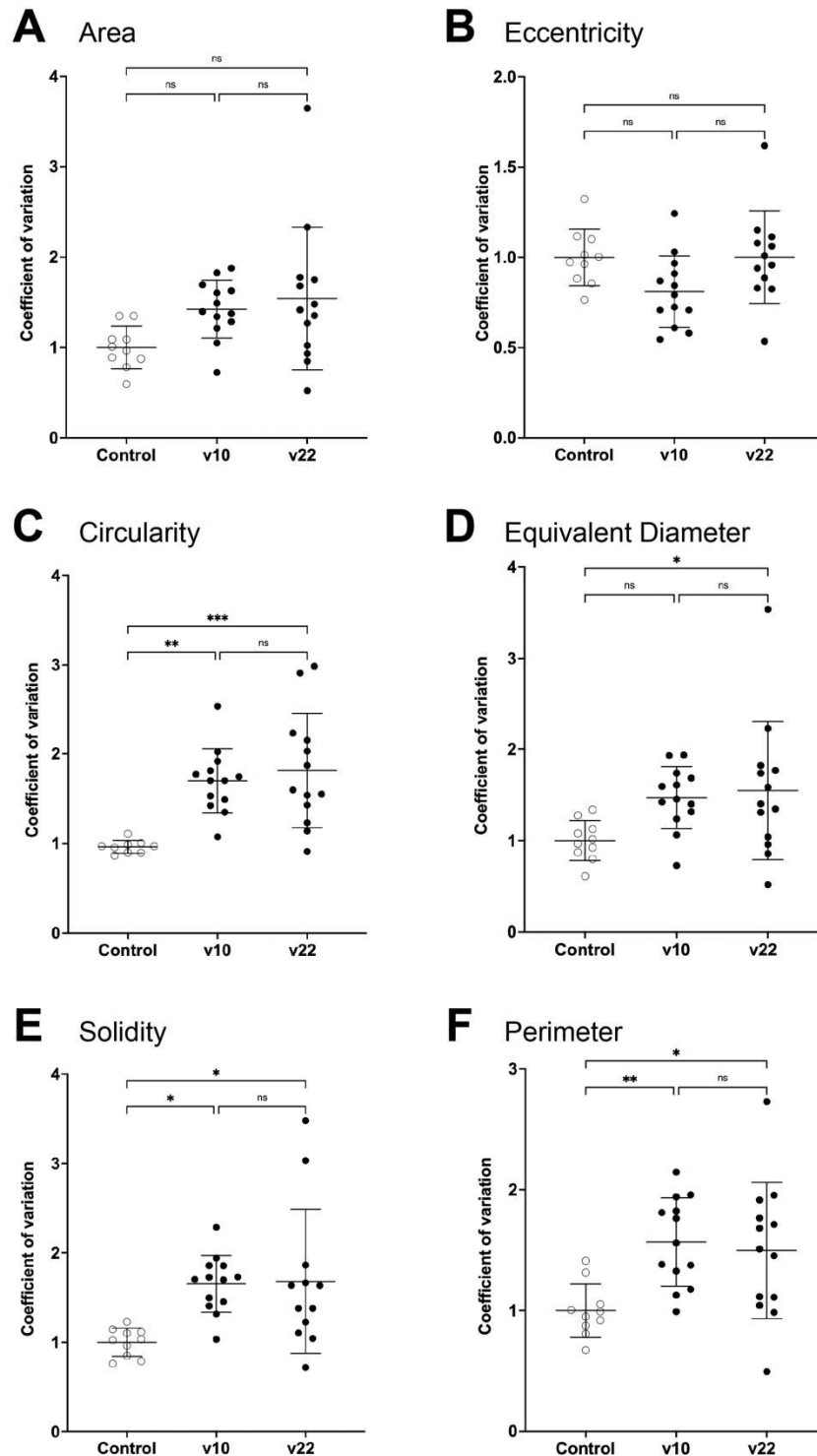
E Solidity

F Perimeter
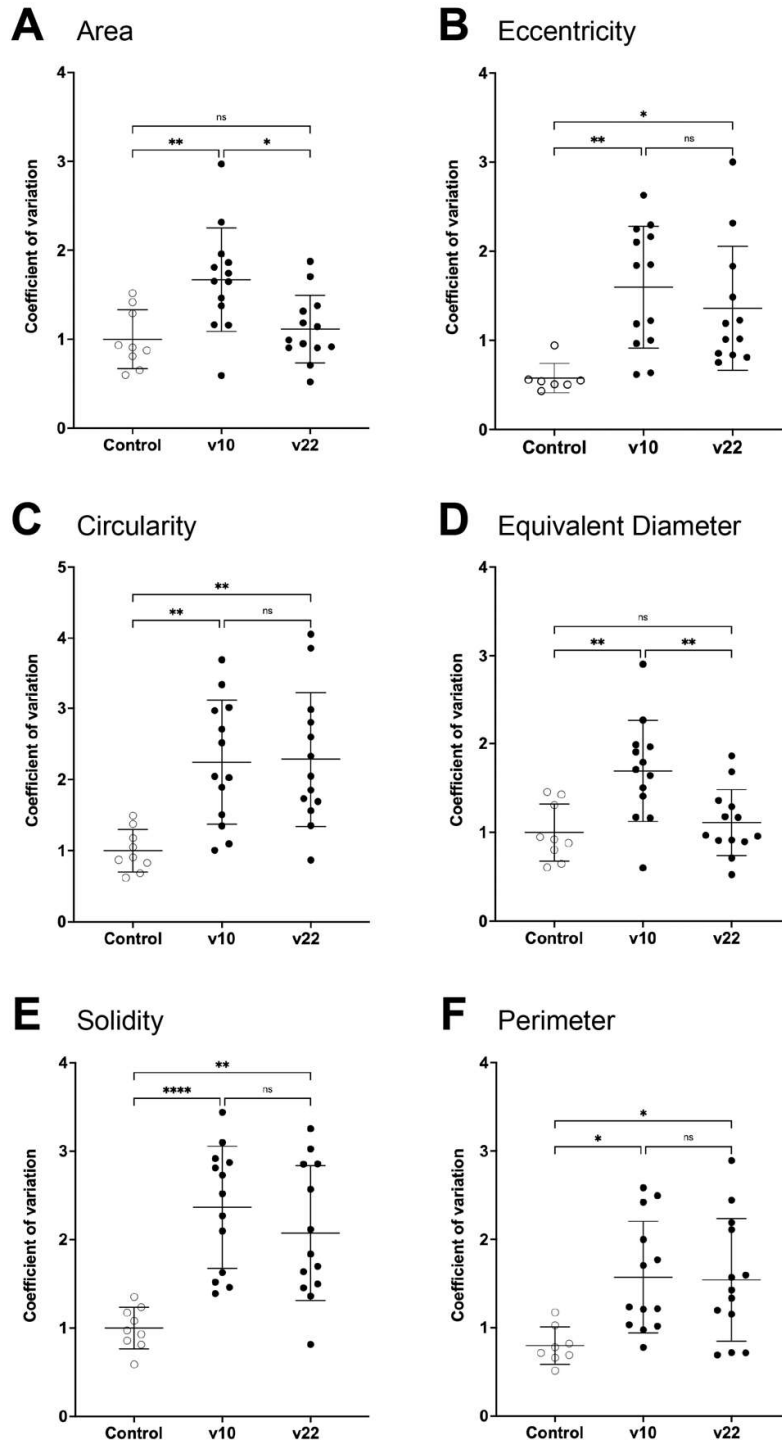
Figure 3.3: The effect of CLC knockdown during early stages of development on primary cell morphology at 42% p.d. quantified by calculating the coefficient of variation for each property per image. The (A) Area * p = 0.0108, ** p = 0.0052 (B) Eccentricity * p = 0.0325, ** p = 0.0041 (C) Circularity p ** < 0.0035 (D) Equivalent Diameter ** p < 0.006 (E) Solidity ** p = 0.0014, **** p < 0.0001 (F) Perimeter * p < 0.0235 were measured in *ey*GAL4 UAS-Clc-RNAi (v106632 or v22318)/ *ubi*::E-cad-GFP and *ey*GAL4 / *ubi*::E-cad-GFP (control) pupal eye discs.
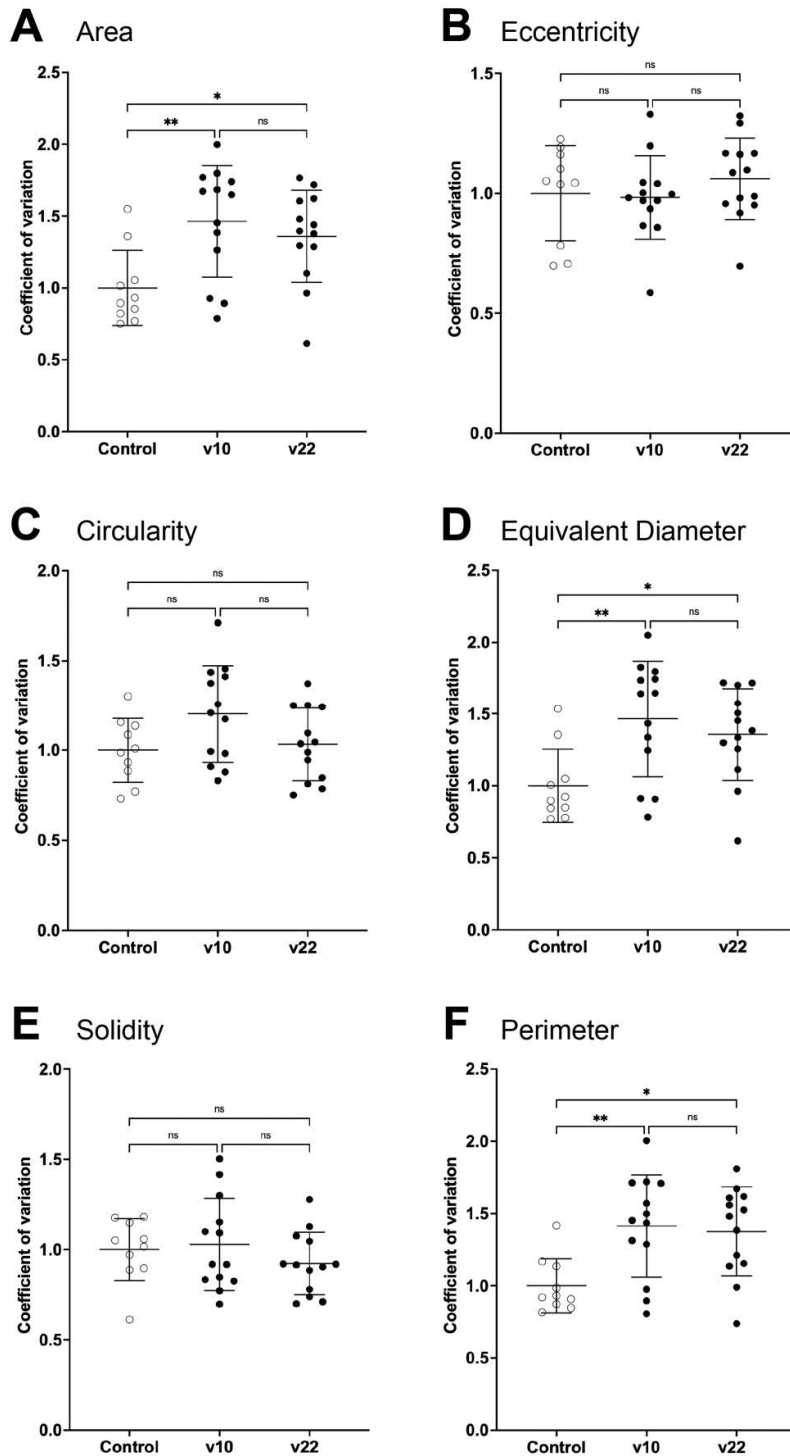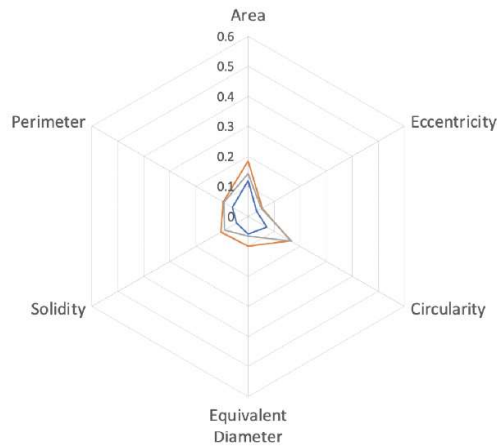
Secondary cells
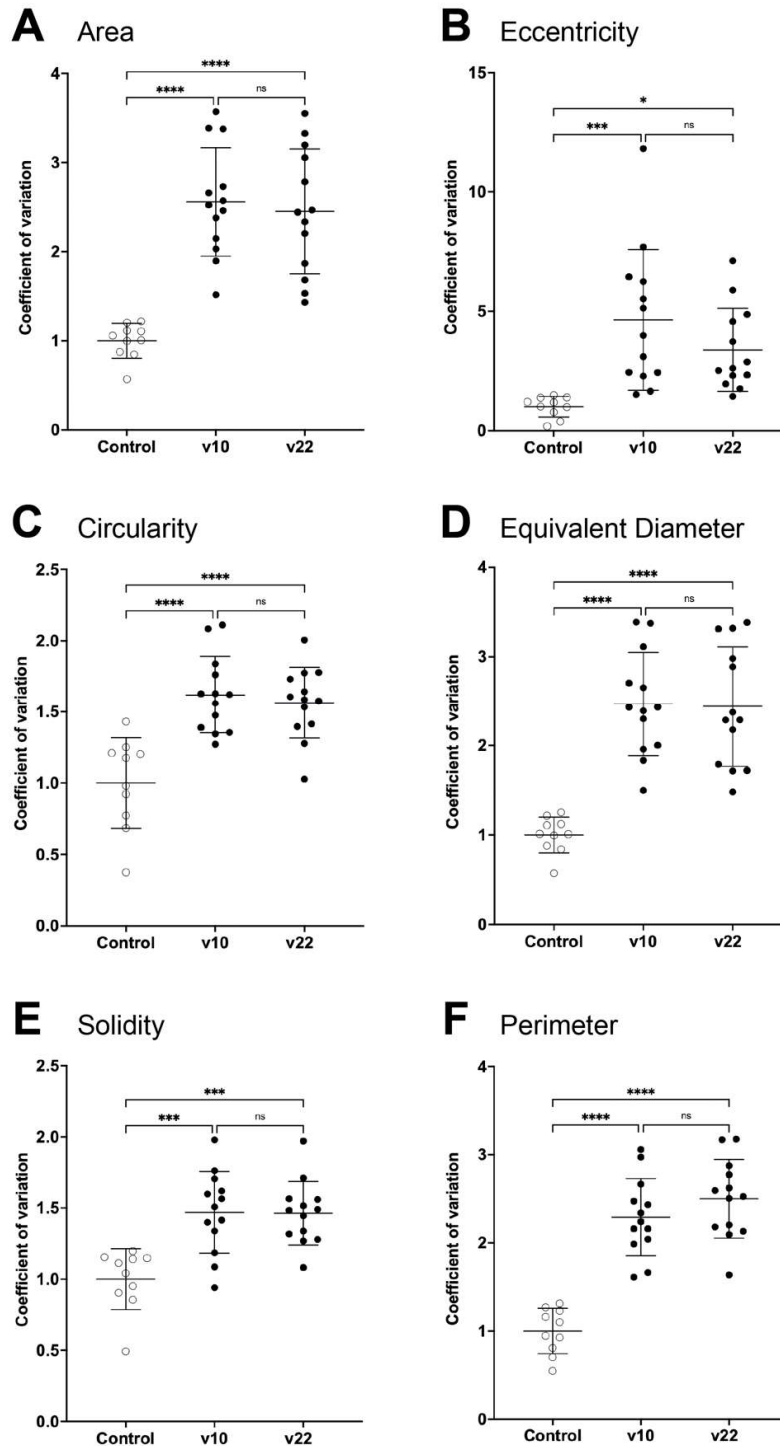
Figure 3.4: The effect of CLC knockdown during early stages of development on secondary cell morphology at 42% p.d. quantified by calculating the coefficient of variation for each property per image. The (A) Area **** p < 0.0001 (B) Eccentricity * p = 0.0268, *** p = 0.0006 (C) Circularity **** p < 0.0001 (D) Equivalent Diameter **** p < 0.0001 (E) Solidity *** p = 0.0002 (F) Perimeter **** p < 0.0001 were measured in *ey*GAL4 UAS-Clc-RNAi (v106632 or v22318)/ *ubi*::E-cad-GFP and *ey*GAL4 / *ubi*::E-cad-GFP (control) pupal eye discs.

Figure 3.5: The effect of CLC knockdown during early stages of development on tertiary cell morphology at 42% p.d. quantified by calculating the coefficient of variation for each property per image. The (A) Area (B) Eccentricity (C) Circularity ** p = 0.0018, *** p = 0.0003 (D) Equivalent Diameter * p = 0.0417 (E) Solidity * p < 0.014 (F) Perimeter * p = 0.0221, ** p = 0.0083 were measured in *ey*GAL4 UAS-Clc-RNAi (v106632 or v22318)/ *ubi*::E-cad-GFP and *ey*GAL4 / *ubi*::E-cad-GFP (control) pupal eye discs.
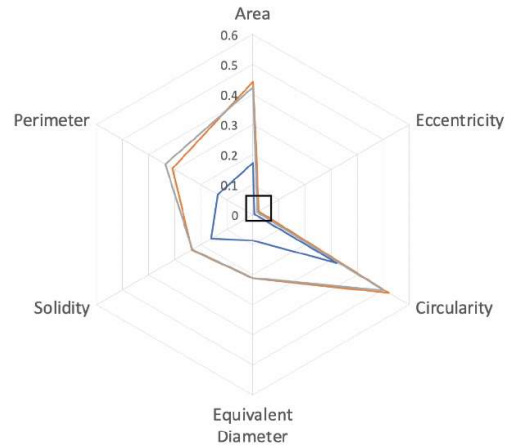
Cone cells

Figure 3.6: The effect of CLC knockdown during early stages of development on cone cell morphology at 42% p.d. quantified by calculating the coefficient of variation for each property per image. The A) Area * p = 0.0391, ** p = 0.0063 (B) Eccentricity (C) Circularity (D) Equivalent Diameter * p = 0.0443, ** p = 0.0067 (E) Solidity (F) Perimeter * p = 0.0144, ** p = 0.0067 were measured in *ey*GAL4 UAS-Clc-RNAi (v106632 or v22318)/ *ubi*::E-cad-GFP and *ey*GAL4 / *ubi*::E-cad-GFP (control) pupal eye discs.
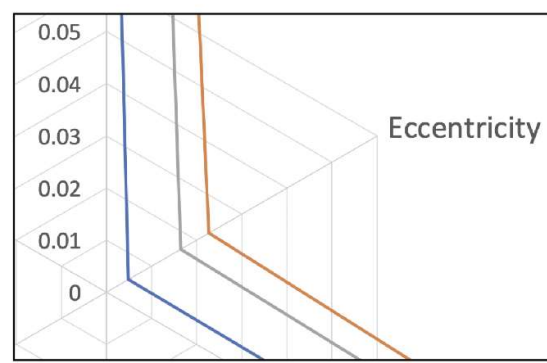
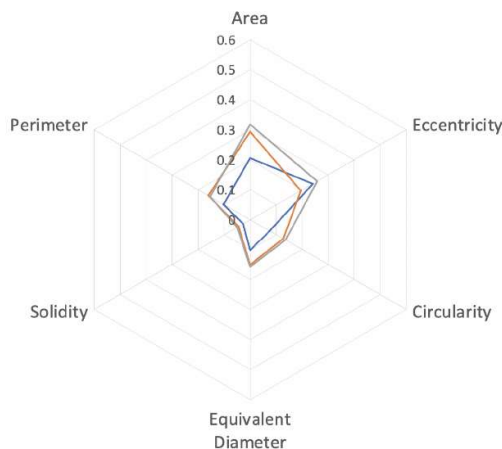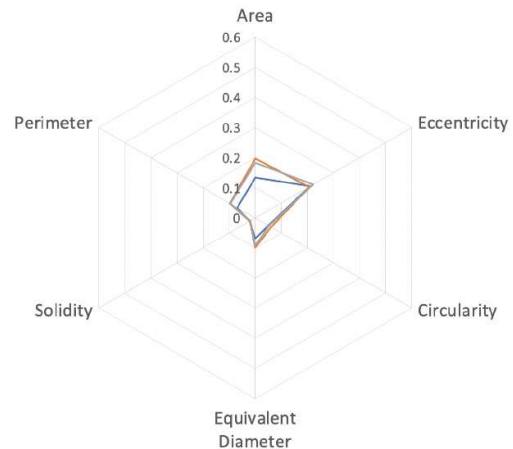**Figure 3.7:** The effect of CLC knockdown during early stages of development on (A) primary, (B) secondary, (C) tertiary and (D) cone cells. (Bii) Eccentricity of secondary cells. Graphs display the mean coefficient of variation for each property e.g. the coefficient of variation calculated per image for circularity was averaged for control, V106632 and V22318 to give an overall measure of variation. Blue lines indicate the control (*ey*GAL4/ *ubi*::E-cad-GFP), orange lines indicate *ey*GAL4 UAS-Clc-RNAi (v106632)/ *ubi*::E-cad-GFP and grey lines indicate *ey*GAL4 UAS-Clc-RNAi (v22318)/ *ubi*::E-cad-GFP.

As well as their morphology remaining largely unaffected by CLC knockdown, the soap bubble-like conformation of cone cells is maintained in flies expressing UAS-Clc-RNAi, even in ommatidia with abnormal numbers of cone cells (Figure 3.8). Regardless of the number of cone cells in the ommatidia in *ey*GAL4 UAS-Clc-RNAi pupal retinas, their conformation still largely follows Plateau's rules: the clusters of cone cells still formed the correct number of junctional interfaces and intersection points in a manner that minimises their surface area (the number of intersection points N(I) and junctional interfaces N(J) are N(I) = $N - 2$ and N(J) = $N - 3$, N = number of bubbles/cone cells). For example, cone cell clusters with 8 cells have 5 junctional interfaces and 6 intersection points (Figure 3.8, white asterisk); clusters with 5 cells have 2 junctional interfaces and 3 intersection points (Figure 3.8, magenta asterisk); clusters with 3 cells have 0 junctional interfaces and instead intersect at a single point (Figure 3.8, green asterisk).

The data acquired from the Interactive Cell Classification algorithm shows that the context-dependent requirement for CLC in different tissues (Figure 3.1), also extends to the cellular level. Although all cell types were affected by CLC knockdown, the properties and severity of the changes differed between cell types significantly.

3.3 CLC knockdown affects the localisation/trafficking of some proteins but not others

In order to understand why the cell types in the pupal retina were differentially affected by CLC knockdown, I decided to investigate the localisation of several key proteins that are involved in cell signalling and rearrangement during development in pupal retinas expressing *ey*GAL4 UAS-Clc-RNAi.

Figures 3.7 and 3.8 show that the morphology and soap-bubble-like conformation, respectively, of the cone cell quartet is not perturbed by CLC knockdown. As discussed in section 1.5.6, cone cell morphology is primarily determined by the adhesion molecule, N-cadherin, that is localised to the borders that connect the cone cell quartet. N-cadherin localisation is not impacted by CLC knockdown in ommatidia both with normal and abnormal numbers of cone cells (Figure 3.8). This data shows that the N-cadherin-dependent morphology and conformation of cone cells is not reliant on CLC during development. In comparison to secondary cells which are significantly affected by CLC knockdown, this data confirms that the cells in the developing *Drosophila* eye have a differential requirement for CLC during development, and each have distinct mechanisms at the protein level for maintaining their topology.
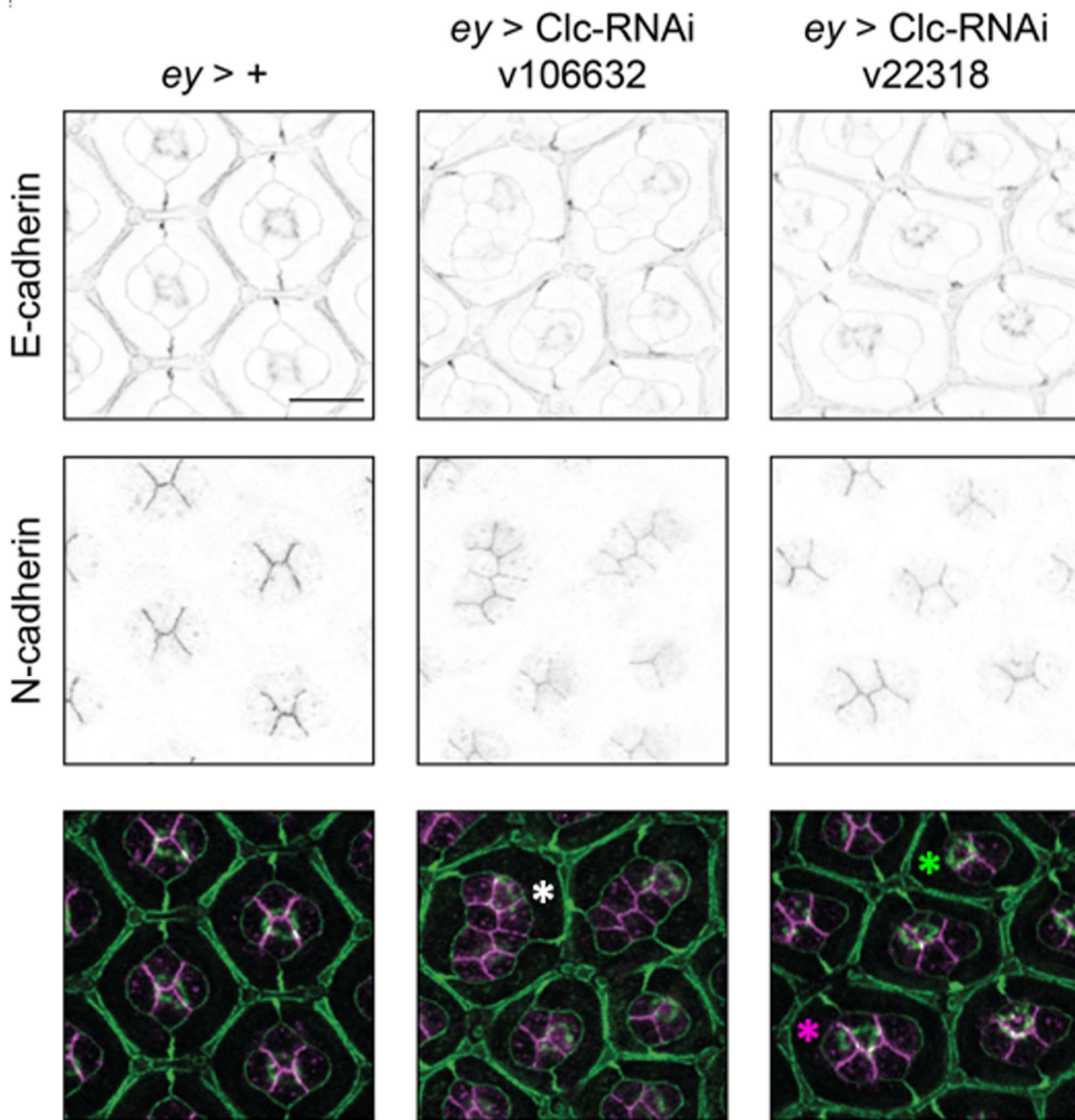
Figure 3.8: Two independent UAS-Clc-RNAi constructs (v103362 and v22318) expressed in all cells of the developing eye under the control of the *eyeless* promoter. Confocal image of pupal retinas expressing *ey*GAL4 UAS-Clc-RNAi at 42% p.d. with cell outlines visualised by E-cadherin-GFP (green) and N-cadherin localisation at cone cell junctions (magenta). Scale bar – 10 μm.

Next, I examined the localisation and levels of E-cadherin because it is expressed in all epithelial cells in the retina and is the major component of the adherens junctions that connect them. The fluorescence intensity of E-cadherin-GFP at cell borders in the pupal retina was measured using in-house MATLAB scripts. Neither E-cadherin-GFP expressed under the control of its endogenous promoter (*shg*) or an independent promoter (*ubi*) resulted in any changes in the average fluorescence intensity of all cell borders, and therefore any changes in protein levels, as a result of CLC knockdown at early stages of development (Figure 3.9A). However, analysing the borders of

individual cell types using the Interactive Cell Classification algorithm revealed there is a reduction in the relative fluorescence intensity of E-cadherin-GFP in cone cell borders, but not in primary or secondary cells (Figure 3.9B). This suggests that the reduction in fluorescence intensity of cone cell borders was masked when measuring all cells simultaneously. Additionally, as the fluorescence intensity of primary cells is unaffected, this raises the possibility that it is the cone-cone cell borders that are perturbed, rather than the primary-cone cell border. Further data specifically examining borders between specific cells (e.g. primary-primary, primary-cone, cone-cone etc) would provide more insight on this. Tertiary/bristle cells were excluded from this analysis: the level of E-cadherin in bristle cells is significantly higher than tertiary cells and the interactive code cannot distinguish between these two cell types because the cells are interactively selected from a binary image of the cell outlines.
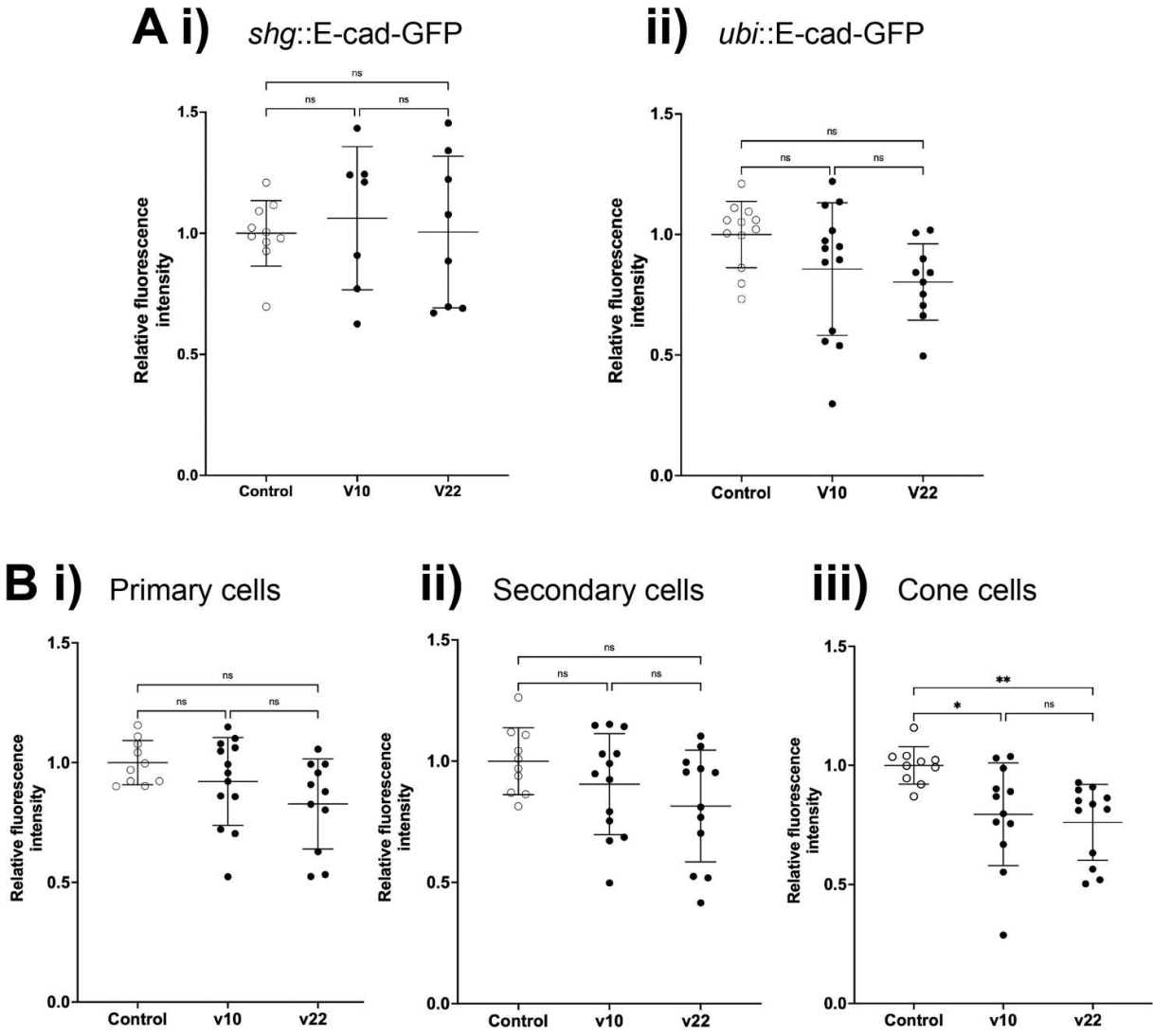
Figure 3.9: The levels of E-cadherin-GFP when measured in all cell borders in unaffected by CLC knockdown, but when measured on in individual cell types, there is a reduction in the relative fluorescence intensity of cone cells. (A) The levels of E-cadherin protein at all cell

Next, I investigated the localisation of Notch in the pupal retina because of its role in controlling adhesion molecule expression and cell fate determination in the developing retina. The volume and intensity of Notch-YFP puncta were quantitively analysed using the 3D Object Counter plugin in Fiji. While the volume of the puncta was unaffected by CLC knockdown, the intensity of the Notch puncta increased (Figure 3.10A). Furthermore, CLC resulted in abnormal distribution of the Notch puncta throughout the retina, however this was variable between eye discs. In some images, the puncta exhibited increased intensity but remained localised in secondary cells, as in the control. In other eye discs, the Notch puncta appeared in primary and cone cells (Figure 3.10B).
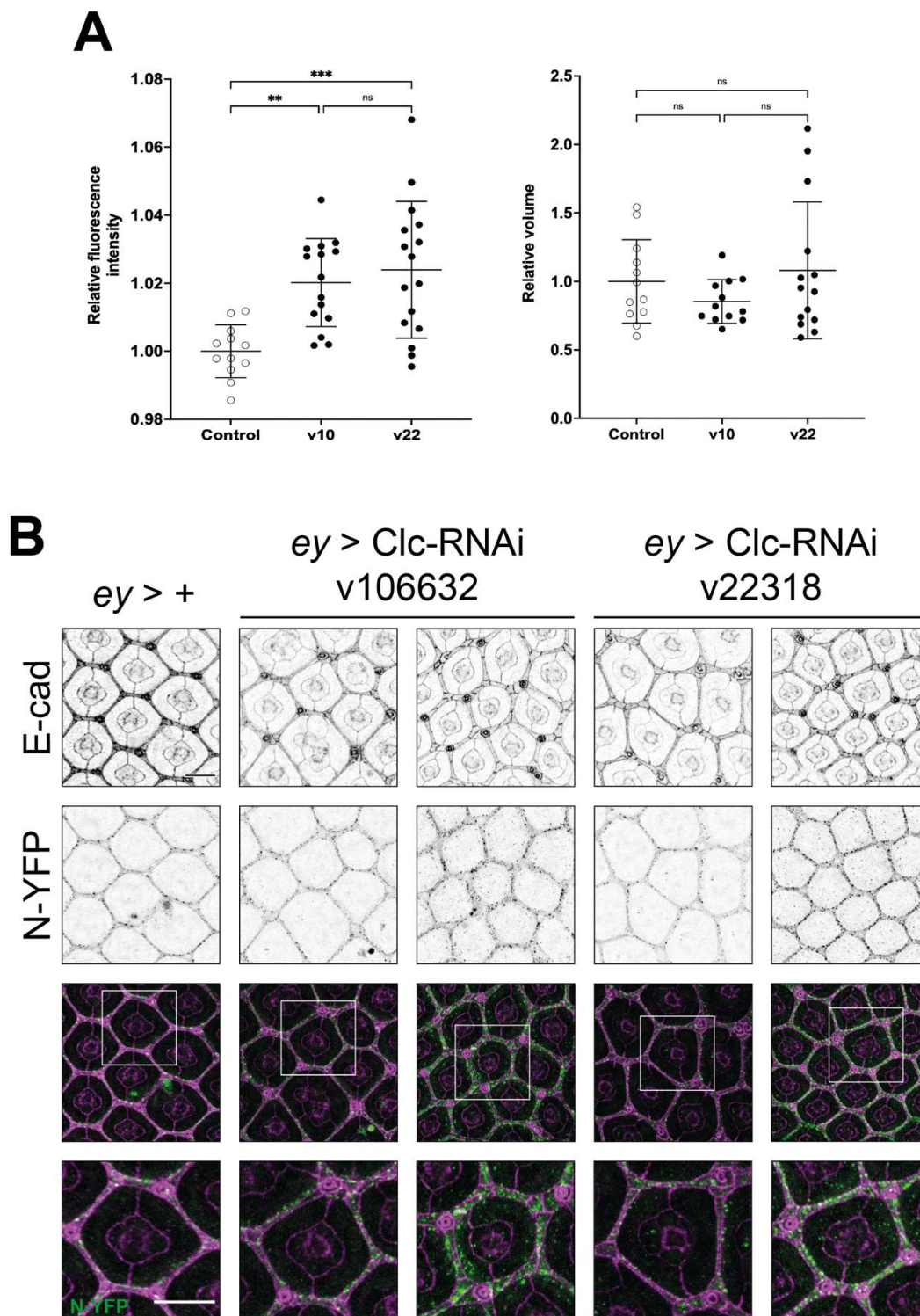
Figure 3.10: The intensity, but not the volume, of Notch-YFP puncta increased following CLC knockdown in pupal retinas at 42% p.d.. (A) The relative intensity and volume of Notch-YFP puncta in pupal retinas expressing *ey*GAL4 / N-YFP or *ey*GAL4 UAS-Clc-RNAi (v106632 or v22318). ** p = 0.0036, *** p = 0.0005. (B) Representative images Notch localisation (green) of pupal retinas expressing *ey*GAL4 / N-YFP or *ey*GAL4 UAS-Clc-RNAi (v106632 or v22318) / N-YFP with cell outlines visualised E-cadherin (magenta). Scale bars – 10 μm.

In contrast, a Notch-signalling reporter (NRE::EGFP) showed that following CLC knockdown, there was no change in downstream Notch signalling (Figure 3.11A). The intensity of NRE::EGFP in the cytoplasm of anterior/posterior cone cells, equatorial/polar cone cells, anterior primary cells and posterior primary cells was measured. These cells were grouped as such because NRE::EGFP is differentially expressed in primary cells and cone cells in wild-type retinas (Figure 3.11B). While the relative fluorescence intensity of NRE::EGFP was not affected by CLC knockdown, the localisation in cone cells was highly variable. In a wild-type retina, Notch is expressed in the polar and equatorial cone cells, but not the anterior and posterior cone cells, a pattern that is highly stereotyped in wild-type retinas (Figure 3.11B). Notably, this pattern is not recapitulated in the N-YFP puncta analysis, however, the localisation of Notch signalling visualised by NRE::EGFP may not necessarily reflect the location of the extracellular domain of the Notch receptor. Following CLC knockdown, this expression pattern is maintained in ommatidia containing the correct number of 4 cone cells (Figure 3.11B, black asterisks), however, in ommatidia with more or less than 4, the position and number of cone cells expressing Notch is seemingly random (Figure 3.11B, white asterisks). This is the case in both ommatidia that have failed to separate (more than 2 primary cells, more than 6 secondary cells etc) and in those that just have additional/missing cone cells. To elaborate, two ommatidia that have failed to separate and have 8 or more cone cells and more than 2 primary cells, do not necessarily have 4 Notch-expressing cells and 4 that do not express Notch.
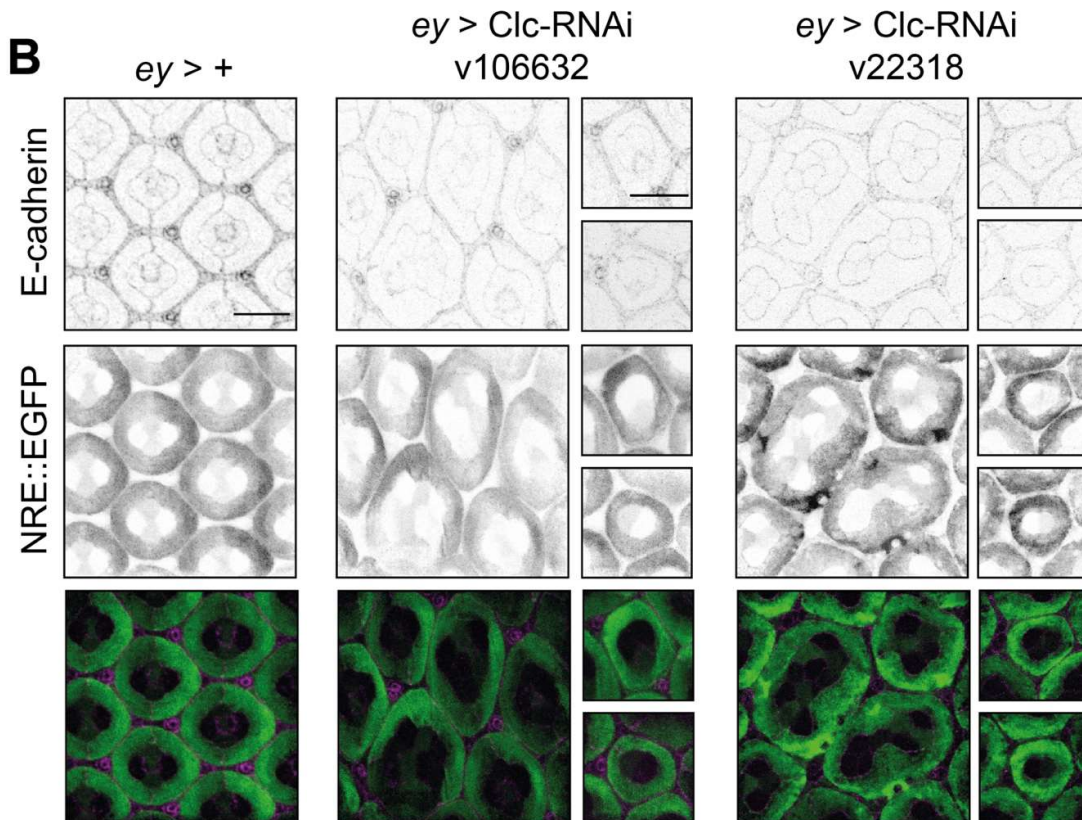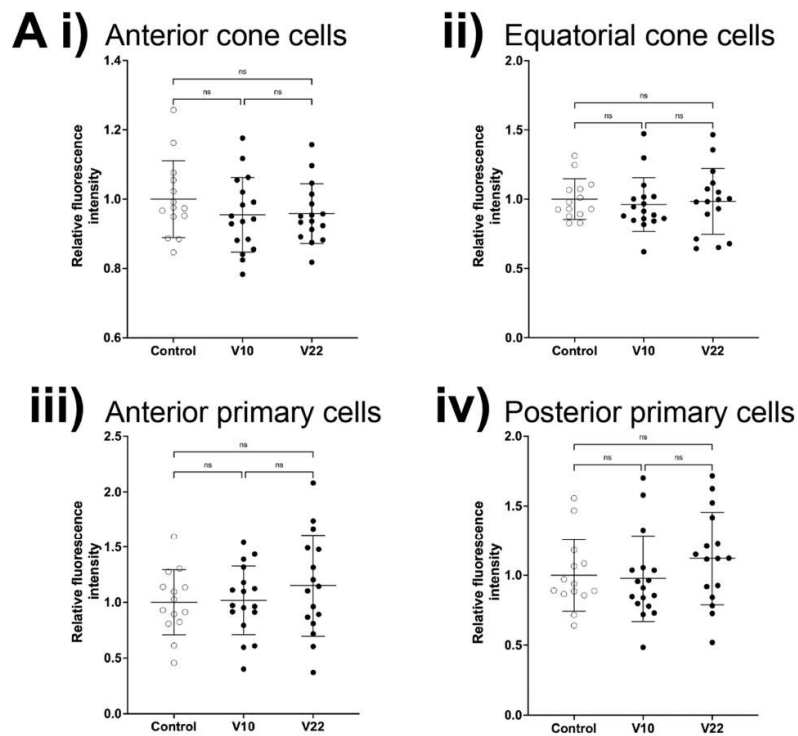
Figure 3.11: Notch signalling is unaffected in multiple cell types in pupal retinas expressing *ey*GAL4 UAS-Clc-RNAi (v106632 or v22318) compared to the control that expresses *ey*GAL4 only. (A) Relative fluorescence intensity of Notch signalling reporter, NRE::EGFP, in (i) anterior cone cells, (ii) equatorial cone cells, (iii) anterior primary cells and (iv) posterior primary cells. (B) Representative images of Notch signalling (green) in pupal retinas

Lastly, I examined the localisation of actin in the *Drosophila* pupal eye, the cytoskeletal protein that provides additional support during endocytosis in conditions refractory to membrane bending e.g. in membranes sustaining higher tension (Aghamohammadzadeh and Ayscough, 2009). CLC knockdown at early stages of development results in the abnormal localisation of actin in the *Drosophila* pupal retina at 42% p.d. (Figure 3.12). In pupal retinas expressing *ey*GAL4 UAS-Clc-RNAi (v106632 or v22318), actin accumulates in the interommatidial and cone cells (Figure 3.12, white asterisks), whereas in retinas expressing *ey*GAL4 alone, actin is only visible in the primary cells. The distribution of the actin also appears to be significantly more diffuse than that of E-cadherin. As these images are a projection of images captured at different focal planes, and therefore have a greater depth of field, the diffuse appearance of the actin staining may be exaggerated, especially in a rough eye phenotype. To ensure this is not an artefact, images than focus on a specific focal plane may mitigate this.
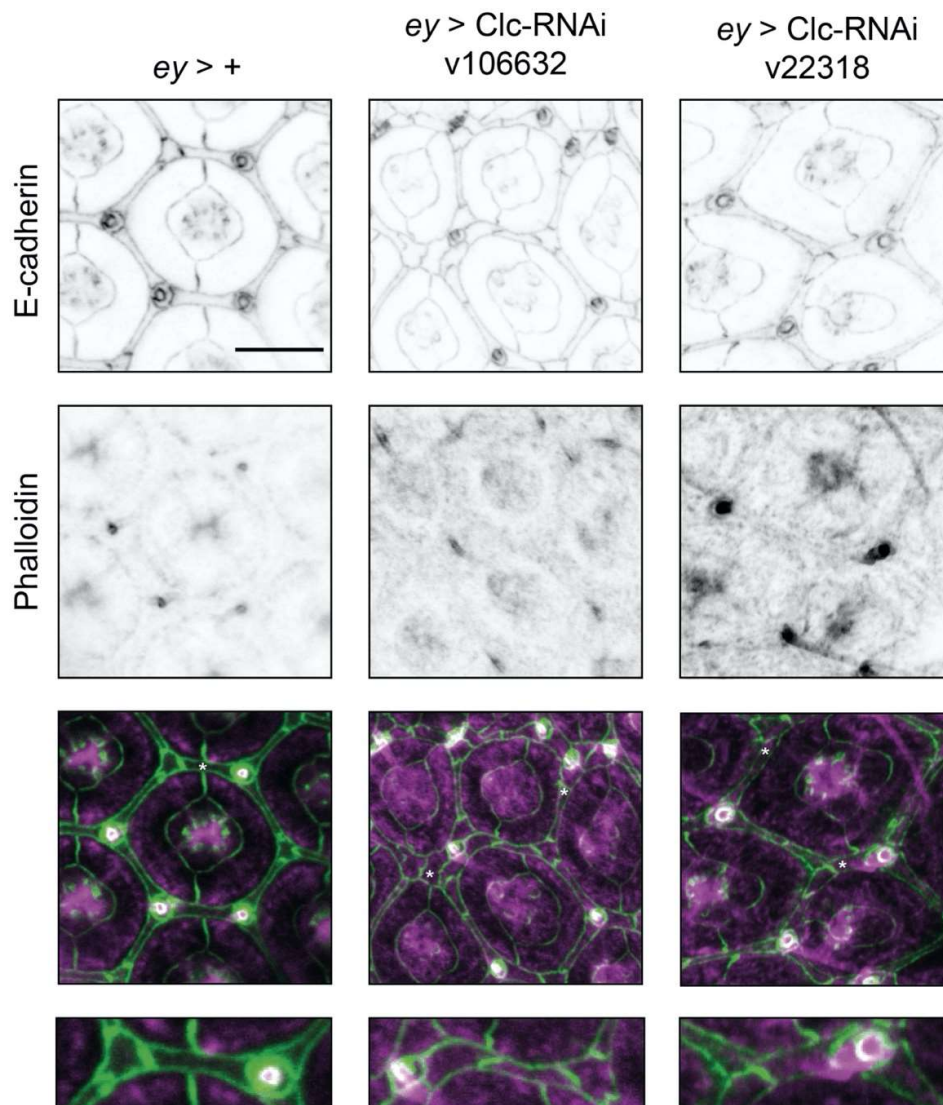
Figure 3.12: Two independent UAS-Clc-RNAi constructs (v103362 and v22318) expressed in all cells of the developing eye under the control of the *eyeless* promoter. Confocal image of pupal retinas expressing *ey*GAL4 UAS-Clc-RNAi at 42% p.d. with cell outlines visualised by E-cadherin-GFP (green) and actin localisation visualised by Phalloidin (magenta). Scale bar – 10 μm.

3.4 Novel genetic interactions with CLC

In order to identify other proteins dependent on CLC, I carried out a genetic enhancer/suppressor screen. By screening for enhancement or suppression of a CLC phenotype in flies expressing *ey*GAL4 UAS-Clc-RNAi (v106632 or v22318) in the presence and absence of an additional mutation it is possible to identify novel genetic interactions. A range of fly lines that express recessive mutations in proteins that are known to have key roles in *Drosophila* eye morphogenesis and adult tissue homeostasis were crossed with *ey*GAL4 UAS-Clc-RNAi (v106632 or v22318) and *ey*GAL4 / CyO *twi*GFP flies as an external control (table in section 2.1.4.4). The eyes of the resulting adult progeny were examined to identify enhancement or suppression of the CLC knockdown phenotype.

It is difficult to quantify whether the rough eye phenotype itself is enhanced or suppressed in these images, in part due to the variation in the severity of the rough eye in flies expressing *ey*GAL4 UAS-Clc-RNAi in the eye even in the absence of an additional mutation. Instead, I measured the area of the eyes in the adult progeny of each cross: flies expressing *ey*GAL4 UAS-Clc-RNAi (Clc-RNAi/+), flies expressing one copy of a candidate mutation (*n/+*, where *n* is the name of the mutation), and flies expressing both (Clc-RNAi/*n*). The area of the eyes in these flies was normalised to an external control that expressed neither the UAS-Clc-RNAi construct or the candidate mutation. Expression of UAS-Clc-RNAi under the control of the *eyeless* promoter consistently produced a rough eye in the adult fly that is significantly reduced in size compared the external control (Figure 3.13). Representative images of the eyes of the progeny from each cross are displayed in Figures 3.14 - 3.19.

The cross between flies expressing *ey*GAL4 UAS-Clc-RNAi and a loss of function mutation in Numb resulted in a suppression of the reduction eye size associated with CLC knockdown. The area of the eyes in the *numb[1]/+* internal control that did not express *ey*GAL4 UAS-Clc-RNAi was comparable to the external control, showing that the presence of one copy of this mutation does not affect eye size. This mutation in the presence of Clc-RNAi rescued the reduction in eye size seen in Clc-RNAi/+ progeny to a size indistinguishable from the internal and external controls (Figure 3.13A): there was no significant difference in the area of the eyes in Clc-RNAi/*numb[1]* and *numb[1]*/+ progeny. This change was also observed in the progeny produced from the cross between flies expressing *ey*GAL4 UAS-Clc-RNAi and a mutation in *shotgun*, the gene encoding *Drosophila* E-cadherin (Figure 3.13B). The reduction in the size of the eye in Clc-RNAi/+ progeny was rescued by the presence of the *shotgun* mutation. The eye size of the *shg[2]*/+ internal control was also comparable to the external control, showing that one copy of this mutation does not affect the area of the eye.

Similarly, the reduced eye size of flies expressing *ey*GAL4 UAS-Clc-RNAi was rescued in the presence of a loss of function Notch mutation (Figure 3.12C). In contrast to the *numb[1]*/+ and *shg[2]*/+

internal controls however, the eyes of N^{55e11}/+ flies were smaller than those of the external control (although not as significantly as the Clc-RNAi/+ progeny), showing that one copy of this mutation is able to perturb eye morphogenesis. Additionally, the eye size of Clc-RNAi/N^{55e11} was not restored to the size of the external control, but to the size of the N^{55e11}/+ eyes. This finding was not observed in flies expressing the v22318 UAS-Clc-RNAi construct however, only in the v106632 line. This mutation when crossed with the v22318 line also failed to produce more than one fly that expressed N^{55e11}/ CyO (the internal control), indicating that the v22318 line may have off-target effects.

There was no statistically significant difference between the eye size of flies expressing *ey*GAL4 UAS-Clc-RNAi alone and in the presence of a loss of function mutation in Hibris, however visual inspection of the data suggests there is a partial suppression of the reduced eye size phenotype of Clc-RNAi/+ progeny (Figure 3.13D). The size of the adult eye in the flies carrying both the RNAi and the Hibris mutation generally fall between the average size of the eyes in the internal control and the flies expressing *ey*GAL4 UAS-Clc-RNAi alone. However, similar to the cross between flies expressing *ey*GAL4 UAS-Clc-RNAi and a Notch mutation, the v22318 RNAi line did not produce the same results as the v106632 line. Furthermore, this cross failed to produce any flies expressing both the RNAi and the Hibris mutation, further suggesting the v22318 Clc-RNAi line produces off-target lethal effects.

Next, there were no statistically significant changes in eye size seen when crossing flies expressing *ey*GAL4 UAS-Clc-RNAi to flies carrying a loss of function mutation in the protein, Flamingo, a member of the GPCR family that is important in planar cell polarity (Figure 3.13E). Similarly, crossing CLC knockdown flies with flies expressing a mutation in Zipper (Myosin-II) did not yield any robust changes in eye size (Figure 3.13F). While the eyes of the Clc-RNAi(v106632)/*zip[2]* progeny were significantly larger than eyes of Clc-RNAi/+ progeny, this was not observed in the v22318 line, along with the expected reduced eye size of CLC knockdown flies. Lastly, progeny produced from crossing *ey*GAL4 UAS-Clc-RNAi and a loss of function mutation in EGFR did not result in any significant changes in eye size, either in the Clc-RNAi/+ or the Clc-RNAi/EGFR^{F2} progeny (Figure 3.13G). Together, these data support a novel interaction between CLC and Notch, Numb and E-cadherin. There may also be an interaction between CLC and Hibris, and CLC and Zipper, but given the differences in the v10 and v22 Clc-RNAi lines and the lack of statistically significant data, respectively, it is difficult to draw any robust conclusions. There is also the possibility that an interaction is with an unknown mutation on the tested chromosome, and so it would be ideal to confirm the interaction using a second independent allele.
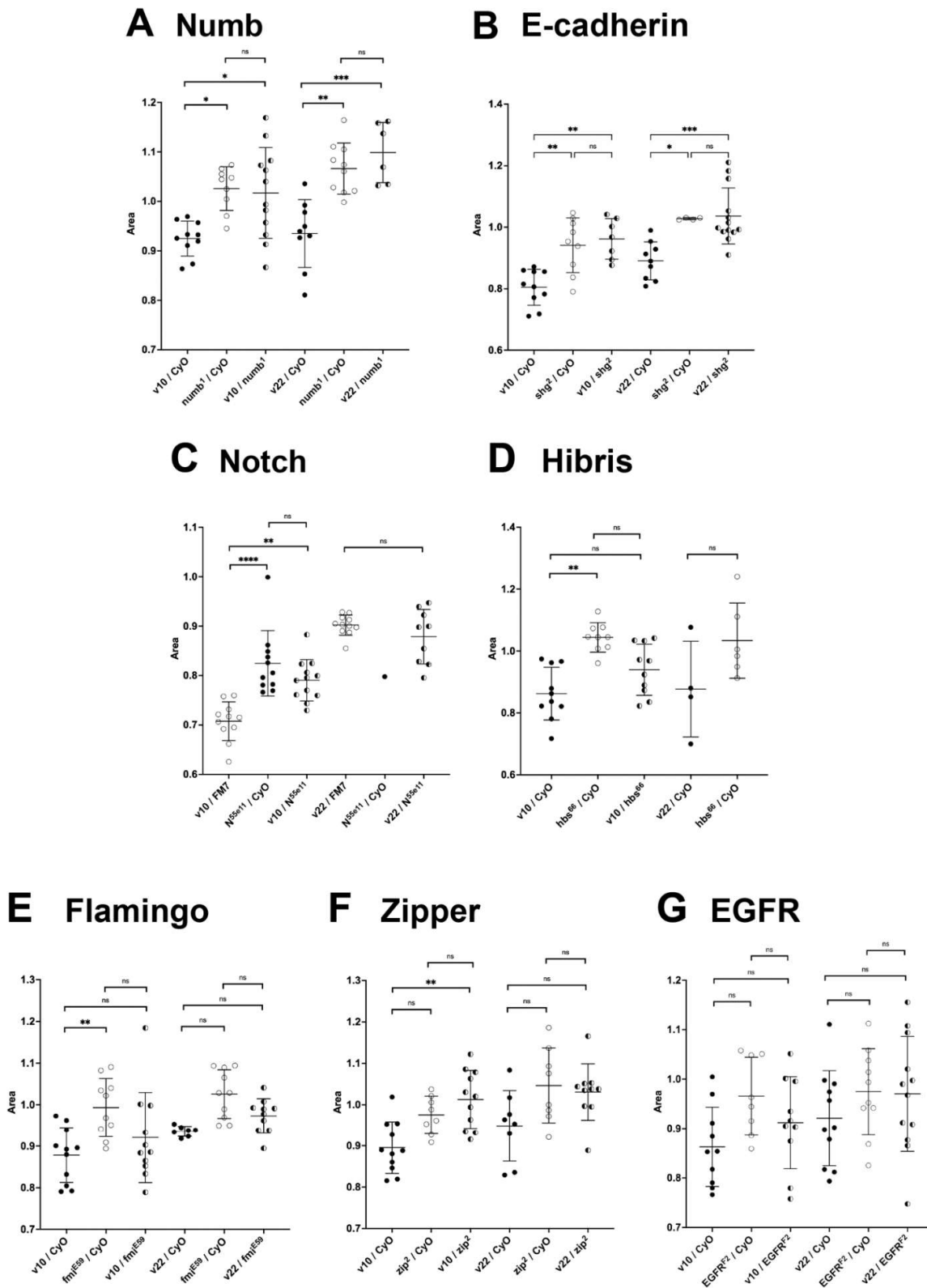
Figure 3.13: An enhancer suppressor screen between flies expressing *ey*GAL4 UAS-Clc-RNAi and flies carrying recessive mutations in proteins that are involved in eye morphogenesis. The area of adult eyes for Clc-RNAi+, *n*+ and Clc-RNAi+ *n*+ flies was normalised to the average size of the adult eyes of an external control that did not express the RNAi or candidate mutation.
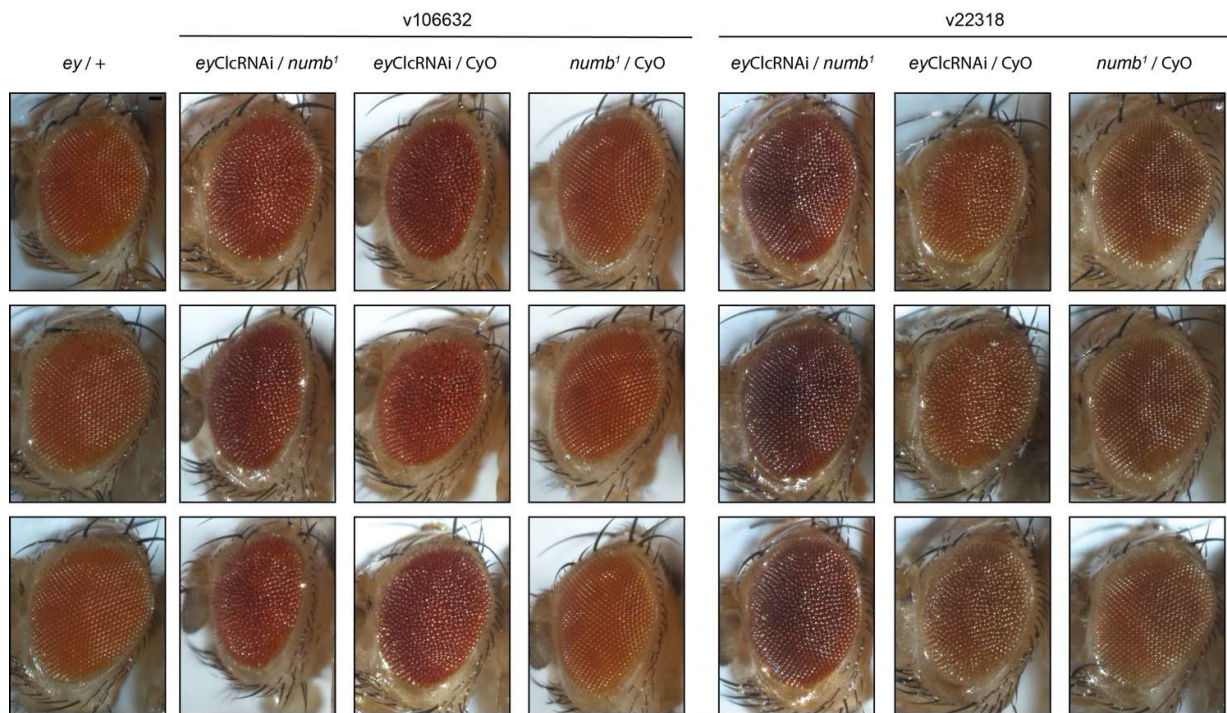
Figure 3.14: Representative images of the progeny of a cross between flies expressing *ey*GAL4 UAS-Clc-RNAi (v106632 or v22318) / CyO *act*GFP (or *ey*GAL4 / CyO twiGFP as a control) and flies expressing *numb¹* / CyO *twi*GFP. Scale bar – 100 μm.
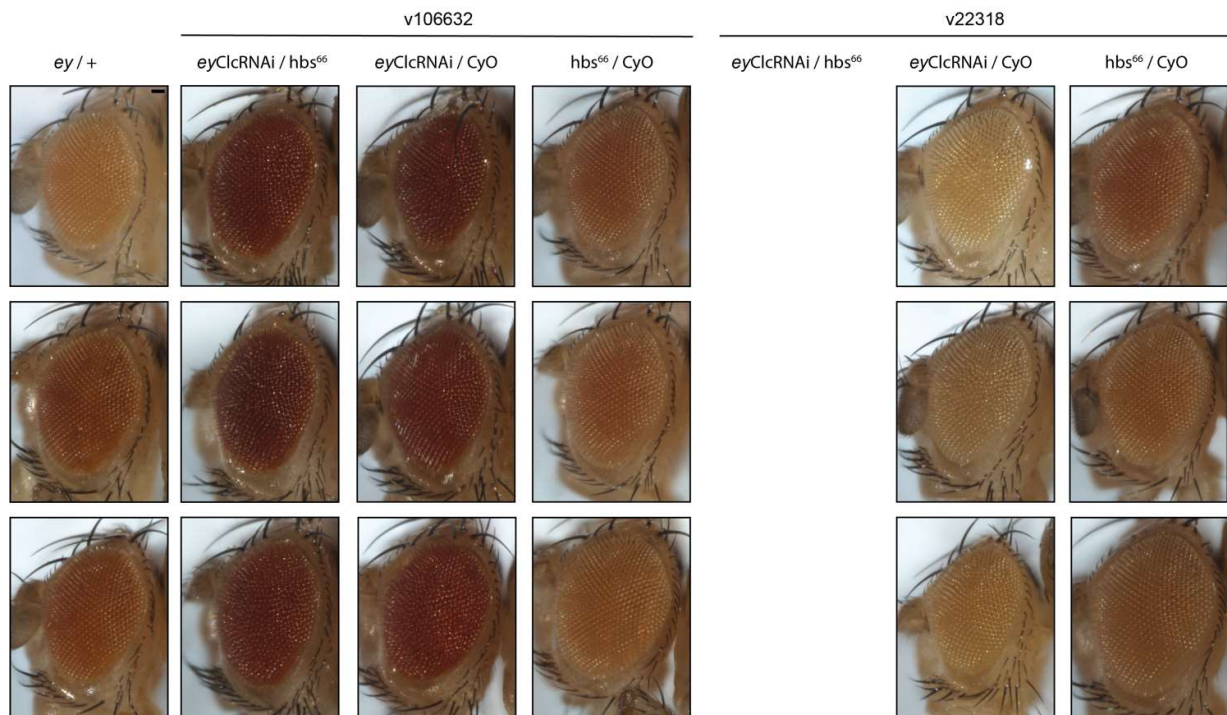
Figure 3.15: Representative images of the progeny of a cross between flies expressing *ey*GAL4 UAS-Clc-RNAi (v106632 or v22318) / CyO *act*GFP (or *ey*GAL4 / CyO twiGFP as a control) and flies expressing *hbs⁶⁶*/ CyO. Note: no *ey*GAL4 UAS-Clc-RNAi (v22318) / *hbs66* progeny were produced from this cross. Scale bar – 100 μm.
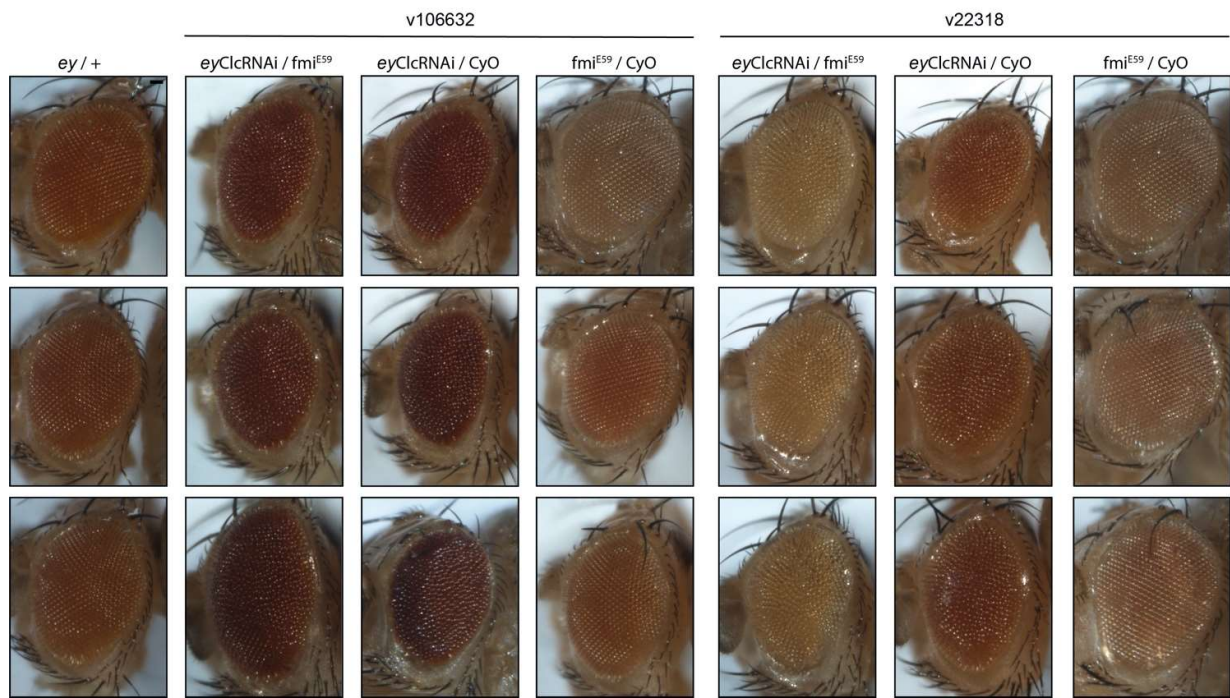
Figure 3.16: Representative images of the progeny of a cross between flies expressing *ey*GAL4 UAS-Clc-RNAi (v106632 or v22318) / CyO *act*GFP (or *ey*GAL4 / CyO twiGFP as a control) and flies expressing *fmi^E59^*/ CyO *act*GFP. Scale bar – 100 μm.

Figure 3.17: Representative images of the progeny of a cross between flies expressing *ey*GAL4 UAS-Clc-RNAi (v106632 or v22318) / CyO *act*GFP (or *ey*GAL4 / CyO *twi*GFP as a control) and flies expressing *zip^2^* / CyO *twi*GFP. Scale bar – 100 μm.

Figure 3.18: Representative images of the progeny of a cross between flies expressing *ey*GAL4 UAS-Clc-RNAi (v106632 or v22318) / CyO *act*GFP (or *ey*GAL4 / CyO twiGFP as a control) and flies expressing *shg²* / CyO *twi*GFP. Scale bar – 100 μm.
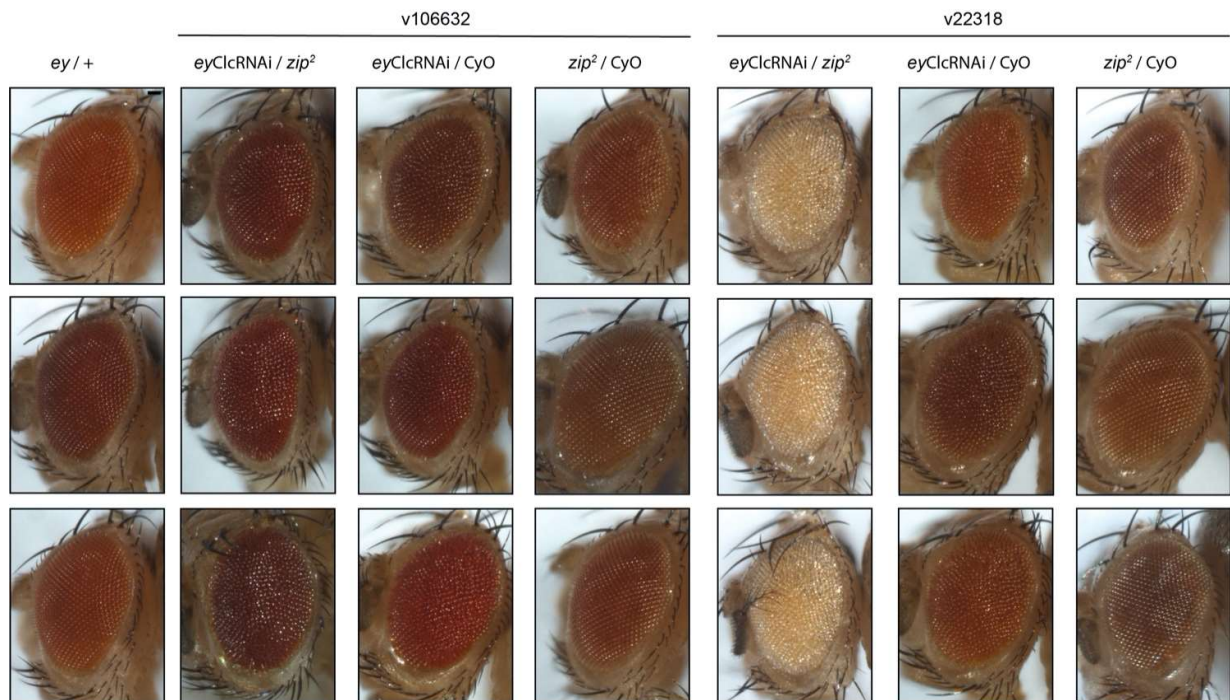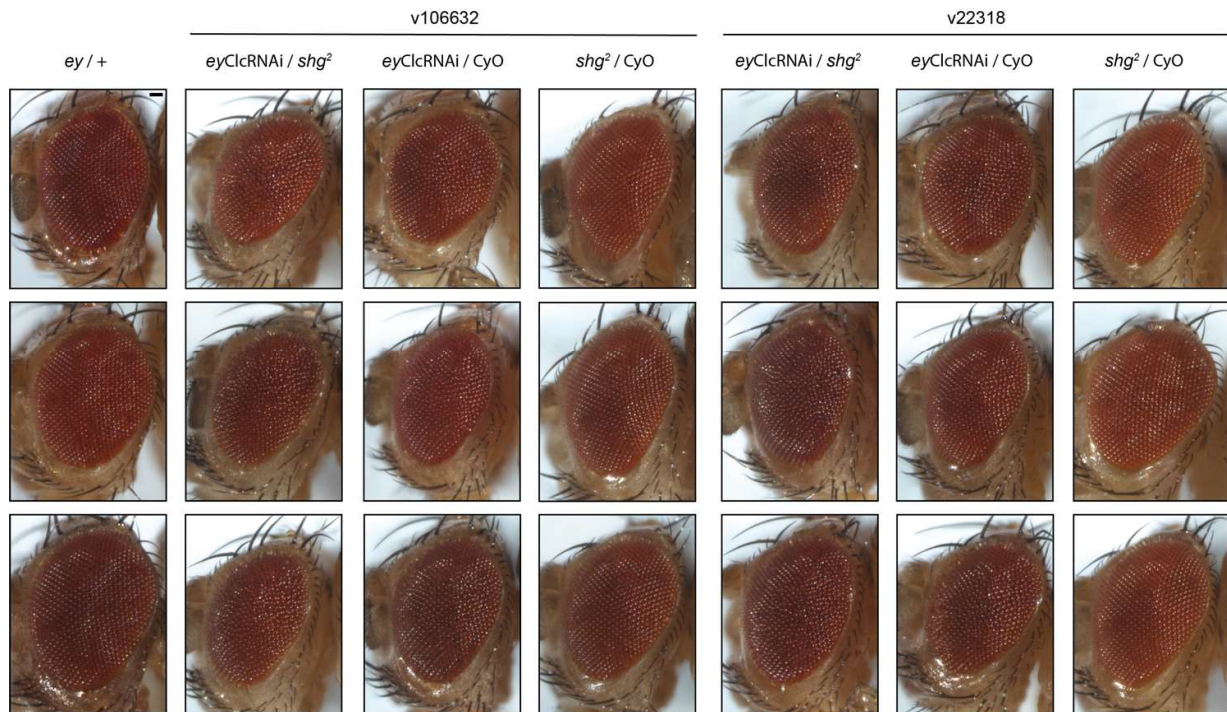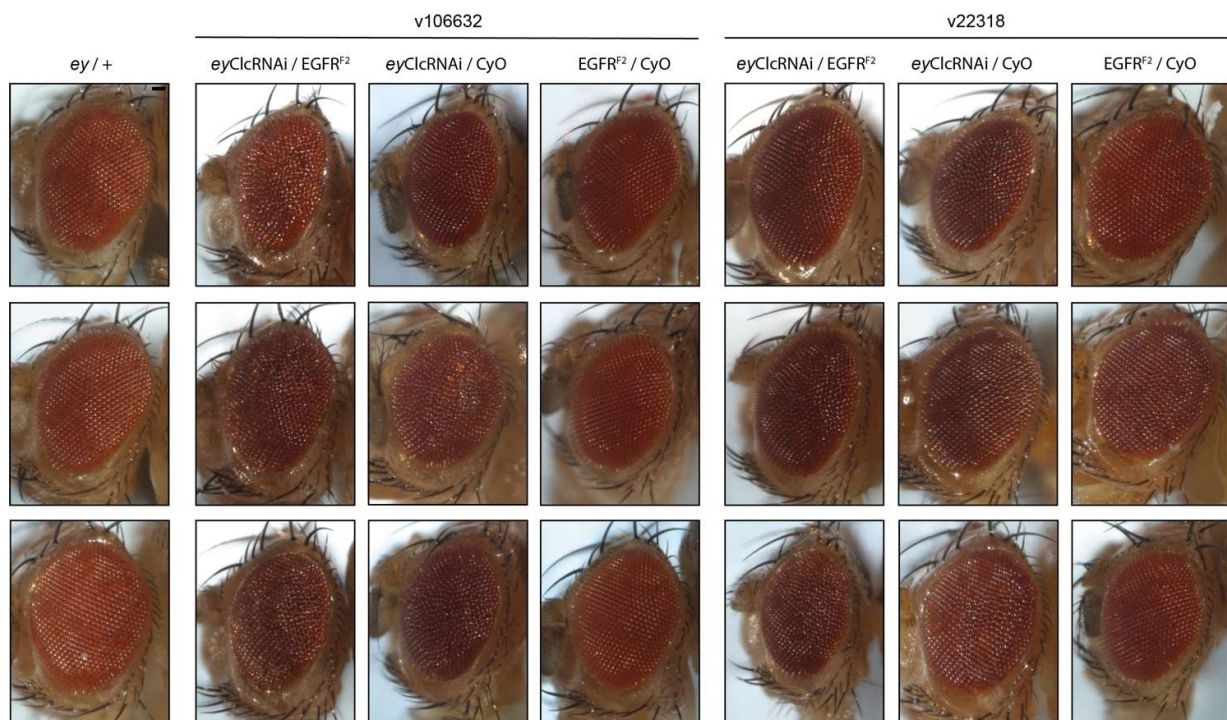

Figure 3.19: Representative images of the progeny of a cross between flies expressing *ey*GAL4 UAS-Clc-RNAi (v106632 or v22318) / CyO *act*GFP (or *ey*GAL4 / CyO twiGFP as a control) and flies expressing *EGFR^{F2}* / CyO. Scale bar – 100 μm.

4. Discussion

4.1 Research question/aim

This project aimed to investigate the role of the clathrin light chain *in vivo*, particularly during development. Early research indicated that CLC is not necessary for endocytosis to occur, however, further investigations revealed that this is not the case. While CLC is not required for universal endocytosis, it is indispensable in certain circumstances e.g. for the uptake of specific cargo or when the cell membrane sustains high tension. The exact mechanism behind this context-dependent function of CLC remains unclear, but studies show that CLC enhances the bending capacity of the membrane, alters the mechanical properties of the clathrin lattice, and interacts with the actin cytoskeleton during endocytosis, as well as with other important components of the endocytic machinery. Ultimately, the literature concludes that the requirement for CLC is reliant on how permissive the conditions for endocytosis are: when the polymerisation of the clathrin lattice alone is insufficient for membrane curvature generation to proceed unhindered, CLC is required. Most of the current research has investigated CLC using *in vitro* and cell culture systems. Although these studies have begun to elucidate the function of CLC, the role of CLC during development in a living organism has not been explored. Given that the requirement for CLC, at least in part, depends on the mechanical properties of the membrane, it is vital to study this protein *in vivo* in order to gain a holistic understanding of its function during development, in an environment where cells are continuously exposed to fluctuating mechanical surroundings.

In this project, a loss of function approach was used to assess the requirement for CLC in a developing organism, in order to overcome the limitations of studying this using *in vitro* systems. Based on observations of tissue survival and patterning, this work suggests that *in vivo* CLC is not required for universal endocytosis, in line with the current literature, but is required for development of specific tissues and cells in *Drosophila melanogaster*. This work has characterised the impact of CLC knockdown on a tissue, cellular and preliminarily protein level in the *Drosophila* eye. However, further data that examines the extent of CLC knockdown in these tissues would be required to be certain that any normal patterning, e.g. in the wing, is not as a result of poor knockdown, and can in fact develop in the absence of CLC.

4.2 Clathrin light chain may be required in some but not all tissues

During development, cells exist in a highly dynamic environment: the cells in a developing tissue are rearranged, they are exposed to a variety of signalling cues, and cell-cell contacts are modified. These dynamic surroundings result in the morphogenesis of tissues that exhibit a wide range of properties that suit each to its function. For example, the sheet of simple epithelial cells that make up much of the *Drosophila* wing disc each share very similar properties with their neighbours. In contrast, the epithelial cells in the *Drosophila* eye do not exist as a simple sheet, but as a complex and highly organised structure in which the cells have distinct characteristics from their neighbours. This difference occurs because the cells were specified according to different developmental signalling pathways and exposed to different mechanical environments. As a result, it is likely that the *Drosophila* eye and wing exhibit very different characteristics on a tissue level, despite both

63

consisting of epithelial cells, although the tension across these two tissues has not been directly compared. This highlights the importance of investigating CLC in different tissues, because the properties of cells such as polarity, membrane rigidity and endocytic cargo, are a major contributing factor to the requirement of CLC.

To determine whether CLC is necessary for the development of specific tissues, the expression of CLC was reduced at different stages of development. Several tissue-specific GAL4 drivers were used to drive expression of UAS-ClcRNAi constructs in the developing eye, wing and mesoderm. However, further data is needed to determine the success of CLC knockdown in these tissues. For example, a Western blot to measure the level of CLC in the wing would be an ideal control to ensure that, for example, the lack of phenotype is not due to incomplete knockdown. Additionally, given that the target sequences of these RNAi lines overlap and that they have the same off-target, Aurora A, further work would be required to rule out that the phenotypes produced in this project are not as a result of off-target Aurora A knockdown.

CLC knockdown in the mesoderm did not hinder fly viability or produce an obvious phenotype (data not shown). Additionally, CLC knockdown did not perturb the development of the wing (Figure 3.1). In contrast to the wing and mesoderm, reduced CLC expression in the *Drosophila* eye from early stages of development using two different RNAi lines resulted in a rough eye phenotype: the ommatidia that make up the compound eye lose their highly stereotypical arrangement in the retina and exhibit severe disorganisation. These data provide evidence that the context-dependent requirement for CLC is evident in a developing organism and that CLC is indispensable for normal eye morphogenesis (Figure 3.1). This raises the question of what properties of the *Drosophila* eye tissue deem CLC indispensable for its development, but not other tissues. Furthermore, the rough eye phenotype resulting from CLC knockdown from embryonic stages is apparent in the adult, showing that this has a long-lasting impact through the course of eye morphogenesis that the tissue is unable to compensate for. As discussed, the *Drosophila* eye and wing are both composed of epithelial cells, but with very distinct properties. What properties in the eye make it susceptible to disfiguration in the absence of CLC? It is clear from the literature that both increased membrane tension/rigidity and the uptake of specific cargo render cells reliant on CLC. As discussed in the introduction, Euler's theorem states that curved structures made up of hexagonal units are not energetically favourable. The retina of the *Drosophila* eye is also comprised of hexagonally shaped functional units, ommatidia, and forms a curved cup-like shape. Euler's theorem also draws an interesting parallel with the structure of the clathrin lattice itself: like the compound *Drosophila* eye, it is a structure composed of hexagons. Therefore, when the clathrin lattice is curved, it exists in an energetically unfavourable manner. To overcome this, pentagons are incorporated into the lattice as curvature is generated. As the *Drosophila* retina doesn't contain any pentagons to facilitate curvature generation, this tissue may sustain higher mechanical stress when compared to a tissue such as the *Drosophila* wing, a sheet of simple epithelia.

In the eye, the combination of external forces during development e.g. during ommatidial rotation, and a possibly intrinsic propensity to exist under higher tension due to its curvature and hexagonal lattice structure, may render this tissue more susceptible to deformation in the absence of CLC, a protein that facilitates endocytosis in cells under mechanical stress by enhancing the properties of

the clathrin lattice/through its interaction with the actin cytoskeleton. The wing and mesoderm do not share this curved structure made up of hexagonal units, and so this may explain the discrepancy in the requirement for CLC. Currently the tension sustained in these tissues has not yet been directly compared at different stages of development, so this is an important avenue to explore.

4.3 CLC knockdown results in severe disorganisation of the pupal retina

The phenotype in the adult that resulted from early CLC knockdown led to the *Drosophila* eye being the primary system in this project to study CLC during development. The developing epithelial tissue in the eye of *Drosophila melanogaster* is a powerful system to study development, due to its high amenability to genetic manipulation and quantitative imaging techniques. Furthermore, the eye is not required for survival, making it an ideal system to study and to perturb fundamental biological processes in a living organism without lethality. The strong phenotype in the adult showed that CLC is required for the morphogenesis of the tissue at early stages of development because the UAS-Clc-RNAi constructs were expressed under the control of a promoter which is expressed from embryonic stages, *eyeless*. The next step was to investigate this phenotype at earlier developmental stages. At 42% pupal development (p.d.), all cell types in the eye have been specified and differentiated. The excess cells have been eliminated via apoptosis and the remaining cells are arranged into the stereotypical lattice of hexagonal ommatidia. At this stage, any perturbations in cell morphology, number and arrangement are obvious and so this was suitable for investigating the rough eye phenotype earlier in development. Before the cells have settled into this organised lattice, these properties are highly variable and difficult to measure. Figure 3.2 shows that the rough eye phenotype in the adult is apparent in the pupal retina at 42% p.d. and allows one to investigate the impact of CLC knockdown at the cellular level.

The disorganisation of the pupal retina following CLC knockdown was quantified by measuring the variation in the distance between photoreceptor clusters that mark the centre of each ommatidium. This approach, rather than measuring the absolute distance between PRC clusters provides a quantitative measure of the tissue level disorganisation. The two independent Clc-RNAi lines both exhibited significant retinal disorganisation, highlighting the importance of CLC at the tissue level during development. This data shows that early knockdown of CLC has long-lasting impacts throughout development. This project has investigated the phenotype at pupal and adult stages, however, examining the impact of CLC knockdown at earlier stages may shed more light on what CLC is required for during morphogenesis. Similarly, it may be worth examining the rough eye phenotype in adult flies and observing whether it stays the same or becomes more severe with age.

4.4 Differential requirement for CLC between cell types in the Drosophila eye

Early CLC knockdown did not just have a significant impact on a tissue-wide level, but it also had a variable effect on the different cell types within the retina. Some cell types were more affected by CLC knockdown than others and exhibited striking changes in morphology and number. The morphology of secondary pigment cells for example, was significantly affected by CLC knockdown in

the pupal retina: they exhibited increased variation in their shape and size (Figure 3.4). In contrast, the morphology of cone cells was largely unaffected (Figure 3.6). Although CLC knockdown resulted in an abnormal number of cone cells in numerous ommatidia, their morphology remained unperturbed. These data highlight that although all epithelial cells in the pupal retina are affected by CLC knockdown, the extent and nature of the changes differs between cell types. As previously discussed, each of these cell types have distinct physical properties and functions, due to each being specified by different developmental signalling pathways. In parallel to the differential requirement of CLC in different tissues, this raises the question of which of these properties make one cell type in the retina more prone to deformation as a result of CLC knockdown than another? In order to understand why some cell types are affected more than others, I investigated the effect of CLC knockdown on the localisation of proteins that are known to determine the morphology, structure and organisation cells in the *Drosophila* retina.

Initially, I analysed the localisation and levels of E-cadherin in the pupal retina because it is expressed in every cell type and is indispensable for development and adult tissue homeostasis. The relative fluorescence intensity of E-cadherin-GFP correlates to the level of E-cadherin at the cell borders. An in-house MATLAB script revealed that the total relative fluorescence intensity of E-cadherin-GFP in the pupal retina, whether expressed under its endogenous promoter, *shg*, or an independent promoter, *ubi*, was not affected by CLC knockdown. However, the Interactive Cell Classification algorithm allows the user to analyse individual cell types. This on the other hand, showed that CLC knockdown actually results in decreased fluorescence intensity of E-cadherin-GFP at cone cell borders, but not in any other cell types. However, in the average intensity projections that were used to analyse these eye discs, the cone cell borders directly overlap with the E-cadherin-expressing photoreceptor cells that lie directly below them. This may have had an impact on the fluorescence intensity measured at the pixels in the borders of these cells. In CLC knockdown retinas the photoreceptors are often more disorganised/spread out/differ in number and so potentially occupy more or less pixels in the cell borders. Further analysis of z stacks in the absence of photoreceptors would be needed to determine whether the levels of E-cadherin at cone cell borders are affected by CLC knockdown. This data shows that E-cadherin localisation in the *Drosophila* eye is not dependent on CLC. Additionally, the levels of E-cadherin at the cell borders (excluding cone cells) is unaffected by CLC knockdown. Therefore, the perturbed morphology of retinal cells as a result of CLC knockdown is unlikely to be due to aberrant E-cadherin trafficking and localisation.

Next, I analysed the effect of CLC knockdown on a range of proteins in individual cell types. Secondary pigment cells are likely to be under increased cortical tension (due to enriched myosin-II expression) and are more prone to deformation in response to ablation of neighbouring cells (Blackie et al., 2020). Furthermore, the clathrin light chain has been shown to drive recruitment of myosin-VI to CCPs when the plasma membrane is under tension (Biancospino et al., 2019). This could make these cells more reliant on CLC to overcome the increased membrane tension during endocytosis. Conversely, despite primary cells displaying a similar, although less severe, variation in their properties to secondary cells, there is no evidence of increased myosin expression or higher cortical tension in primary cells. If secondary cells are under higher cortical tension relative to primary cells, a deformation in their shape and size would likely have a knock-on effect on the

morphology of the adjacent primary cells: the alteration in their morphology may simply be a consequence of the deformation seen in the more rigid secondary cells that surround them.

As discussed in the introduction, in cells sustaining high membrane tension the clathrin lattice alone is unable to deform the membrane during endocytosis, and so they depend on actin to counteract this (Aghamohammadzadeh and Ayscough, 2009). Actin indirectly interacts with the clathrin light chain via a protein called Hip1R to facilitate CCP formation (Boulant et al., 2011). When this interaction is disrupted in cells sustaining high membrane tension, CCP formation is stalled and actin accumulates in the cytoplasm (Poupon et al., 2008). This led me to investigate the effect of CLC knockdown on the localisation of actin in the developing *Drosophila* eye. CLC knockdown results in the aberrant accumulation of actin in secondary cells (Figure 3.12). Given that these cells may be under increased tension relative to other cells in the retina, and are affected significantly by CLC knockdown, secondary cells may rely on the interaction between CLC, Hip1R and actin during endocytosis. This data suggests that the intrinsic property of increased cortical tension in secondary cells renders them reliant on CLC in contrast to other cells in the eye that do not share this property.

Cone cell morphology remained largely unaffected by CLC knockdown, and displayed no changes in their circularity, solidity or eccentricity (Figure 3.6). Unlike other cell types in the *Drosophila* retina, the morphology of cone cells is dictated by the expression of N-cadherin in the junctions that connect these cells together. The localisation of N-cadherin in the cone cell clusters following CLC knockdown was normal (Fig 3.8). This suggests that the N-cadherin-mediated packing of cone cells is not dependent on CLC. The arrangement of cone cells follows Plateau's rules: in each ommatidium the cone cells are packed together in a configuration which minimises their surface area (Hayashi and Carthew, 2004). At 42% pupal development, they do not intersect at a single point 4-way vertex, but instead there is a central junctional interface between the polar and equatorial cone cells (Figure 1.9, white arrow) and at either side, two intersection points that connect three cells together (Figure 1.9, black arrows). The cone cells form this conformation during pupal stages in a process called intercalation. They progress from an immature 4-way vertex arrangement to the mature configuration (Hayashi and Carthew, 2004). As well their morphology remaining unperturbed, CLC knockdown did not significantly affect the ability of cone cells to adopt this stable soap bubble-like packing. Despite some ommatidia having supernumerary or missing cone cells, they still formed the correct number of junctional interfaces and intersection points as a soap bubble cluster (Figure 3.8). This has been previously observed in rough eye clusters in *Drosophila* retinas at a similar stage (Hayashi and Carthew, 2004). However, there was a small number of cone cell clusters that did not complete cone cell intercalation and were stalled at the 4-way vertex (data not shown). The number of cone cells and the process of intercalation are carefully controlled by various signalling pathways during development. Notably, Notch plays a vital role in the programmed cell death that removes excess cells in the developing eye disc (Cagan and Ready, 1989). Additionally, cone cell intercalation is dependent on the expression of the cell adhesion proteins Roughest and Hibris to be tightly controlled by differential Notch signalling within the cone cell quartet (Blackie et al., 2019). Consistent with the literature, this suggests that there may be role for CLC beyond providing additional mechanical support in cells sustaining high membrane tension, but that there are specific signalling pathways and proteins that rely on CLC to

establish correct tissue patterning and remodelling *in vivo*.

4.5 CLC knockdown results in aberrant Notch endocytosis

To determine whether Notch signalling was disrupted by CLC knockdown, I analysed the localisation and levels of Notch-YFP in the pupal retina. At early pupal stages, the ligand that binds to the Notch receptor, Delta, is normally transcribed in anterior and posterior cone cells, where it activates Notch signalling in primary cells (Bao, 2014). A fluorescent Notch signalling reporter, NRE::EGFP, confirmed this expression pattern in the pupal retina (Figure 3.11). At 42% p.d. in a wild-type retina, after patterning has been established, Notch puncta are localised to secondary cells in the form of puncta, and primary cells display more slightly more diffuse Notch staining (Figure 3.10). Once again, this is consistent with the literature: once programmed cell death has eliminated excess IOCs in the retina, the Notch receptor in IOCs and primary cells is endocytosed from the membrane and packaged into intracellular vesicles (Peralta et al., 2009; Reiter et al., 1996). CLC knockdown resulted in the aberrant localisation and an increase in the intensity of N-YFP puncta at 42% p.d. (Figure 3.10). The puncta were localised not just in secondary and primary cells, but they also accumulated in cone cells. Furthermore, while the volume of Notch-YFP puncta was unaffected, the intensity significantly increased as result of CLC knockdown. Notably, the aberrant localisation of the Notch puncta was variable between eye discs: some did not display bright puncta accumulating in primary and cone cells. It is possible this is a result of incomplete knockdown of CLC in some flies. The mislocalisation of the Notch-ECD has also been observed in the retinas of *Chc^4* mutant flies at the same stage. In pupal retinas that expressed *Chc^4,* Notch was localised at primary-secondary cell borders and primary-cone cell borders (Peralta et al., 2009), indicating that the endocytosis of Notch was disrupted. As shown in Figure 3.11, CLC knockdown did not alter the level of Notch signalling in multiple cell types in the pupal retina. However, in ommatidia containing more or less than 4 cone cells, the number and position of the cone cells expressing NRE::EGFP was unpredictable (Figure 3.11). Additionally, these ommatidia developed an abnormal number of photoreceptors (PRCS; wild type ommatidia have 7 visible PRCs), however, the number of cone cells in these ommatidia did not correlate to an exact number of PRCs: although ommatidia with missing cone cells tended to have less PRCs and ommatidia with supernumerary PRCs tended to have more, there were still ommatidia with three cone cells that had more than 7 PRCs, and ommatidia that failed to separate with fewer PRCs.

Along with being indispensable for the correct specification of photoreceptor cells early in eye morphogenesis, Notch and EGFR act antagonistically in the developing retina to induce and inhibit apoptosis, respectively, to eliminate excess cells (Cagan and Ready, 1989; Miller and Cagan, 1998; Kurada and White, 1999; Yu et al., 2002). It also is responsible for the induction of cone cells (Cagan and Ready, 1989; Flores et al., 2000; Parks, Annette L., and Marc A. Muskavitch., 1993). Therefore, the aberrant number of interommatidial, cone and photoreceptor cells may have arisen because of disruption to Notch endocytosis as a result of CLC knockdown. Furthermore, the intercalation defects seen in the cone cells of some ommatidia may be due to misregulation of Roughest and Hibris by Notch. Hibris mutants also display a rough eye phenotype (fused ommatidia, abnormal numbers of cone cells and IOCs) in pupal retinas similar to that caused by CLC

knockdown (Bao and Cagan, 2005).

This raises the question as to why Notch endocytosis is disrupted by CLC knockdown, when other proteins such as N-cadherin and E-cadherin are unaffected. A possible explanation is the unique mechanism behind Notch endocytosis. Upon ligand binding, the Notch receptor undergoes two sequential cleavage steps and the intracellular domain of the receptor is released into the signal-receiving cell where it regulates target gene expression. The bridge between the Notch receptor and its ligand requires a pulling force to be exerted on it for the first cleavage site to become exposed (Langridge and Struhl, 2017). If this force is not applied, the entire ligand-receptor bridge is endocytosed into the signal-receiving cell, and no active Notch signalling occurs. In comparison, E- and N-cadherin do not require this pulling force for endocytosis to occur. Given that CLC is able to enhance the stiffness of the clathrin lattice and provide mechanical additional support during endocytosis by interacting with actin, it may be that the endocytosis of Notch requires CLC to facilitate exerting the pulling force on the ligand-receptor bridge. Following CLC knockdown, Notch puncta may accumulate in the primary cells because without the additional support, the entire ligand-receptor bridge is internalised into the signal-receiving cells, as described by Langridge and Struhl (2017). Cone cells also exhibited an accumulation of actin following CLC knockdown (Fig 3.12). This supports the idea that as well as enhancing the properties of the clathrin lattice, CLC may provide additional support during Notch endocytosis through its indirect interaction with the actin cytoskeleton.

These data support the idea that the differential requirement for CLC in the different cell types in the *Drosophila* retina is because the morphology of these cells is determined by different mechanisms and signalling pathways. The properties of these cells and the proteins that determine their morphology may determine the cell's capacity to function in the absence of CLC. In the case of secondary cells, their higher tension may render them more reliant on CLC during endocytosis, consistent with the literature. Conversely, the morphology and conformation of cone cells appears to be independent of CLC. Rather, it is the number of cone cells that is affected by CLC knockdown, as is the case with photoreceptor cells. This suggests that while CLC is required in the developing cells of the retina, the conditions under which it is required may differ i.e. secondary cells sustaining high membrane vs specific signalling pathways such as Notch.

4.6 Novel genetic interactions with CLC

The next step in this project was to identify other candidates that are dependent on CLC during endocytosis. For this, an enhancer/suppressor screen was carried out. Flies expressing Clc-RNAi in the pupal eye were crossed with flies that carry mutations in proteins with important roles in eye development/structure. The progeny were screened to search for an enhancement or suppression of the rough eye phenotype. If there is no alteration in the severity of the phenotype it suggests that this protein does not rely on CLC during endocytosis. However, if the rough eye phenotype is enhanced or rescued by the presence of an additional mutation, this will indicate novel genetic interactions with CLC and provide information about the mechanism and function of CLC in endocytosis.

Crossing flies expressing *ey*GAL4 UAS-Clc-RNAi to flies carrying mutations in Numb, Notch and E-cadherin all gave rise to progeny that suppressed the phenotype associated with CLC knockdown alone: reduced eye size. In each of these crosses, the area of the adult eye in the Clc-RNAi+ *n*+ progeny was restored to the extent that they were not significantly different from the controls, which did not express the UAS-Clc-RNAi construct. The area of the eyes of the progeny that were produced from the cross between flies expressing *ey*GAL4 UAS-Clc-RNAi and a mutation in the cell adhesion protein, Hibris, suggested that the reduced eye size phenotype associated with CLC knockdown was partially suppressed. The eye size was not significantly different from either the Clc-RNAi+ flies, or the internal control, but was typically in between the two. The progeny that arose from a cross between flies expressing *ey*GAL4 UAS-Clc-RNAi and flies expressing a mutation in Zipper, the myosin heavy chain, appeared to give rise to a partial or even a full rescue. However, in this cross the Clc-RNAi+ flies did were not significantly smaller than those of the internal control, and so it difficult to draw any conclusions from this data. A visual inspection of the data would suggest the possibility of a partial rescue but no conclusive statements can be made due to the lack of a statistically significant difference in the eye size. In contrast, crossing *ey*GAL4 UAS-Clc-RNAi flies to flies expressing mutations in Flamingo and EGFR, did not result in either an enhancement or suppression of the CLC knockdown phenotype, indicating that the trafficking of these proteins is independent from CLC. While these data support this conclusion, the activity of these proteins may be unaffected by changes in dosage and trafficking defects, therefore raising the possibility that this approach could miss an interaction with CLC. An alternative approach such as using RT-qPCR to investigate expression levels or examining the levels/localisation of these proteins using fluorescent reporters may provide more insight, however, this method was suitable for a preliminary screen.

From the alterations in eye size alone, it is difficult to speculate on how these proteins are functioning together, however, the screen was successful in identifying novel candidates to investigate in future work. The Notch mutant-mediated suppression of the reduced eye size in CLC knockdown flies and the aberrant intensity and localisation of Notch puncta, together suggest a promising candidate to investigate in future work. The suppression of the reduced eye size in the Clc-RNAi+ *numb^1*+ flies further supports Notch as an interesting candidate to investigate because of the role of Numb in negatively regulating Notch the signalling pathway in eye morphogenesis. The potential partial rescue of reduced eye size in Clc-RNAi+ *hbs^66*+ flies may also indicate an interaction between CLC and Notch signalling: as discussed, differential Notch signalling controls the expression of Hibris in the *Drosophila* eye during morphogenesis (Bao and Cagan, 2005).

Despite the E-cadherin-GFP levels being unaffected by CLC knockdown (excluding cone cells), the suppression of the CLC knockdown-mediated reduced eye size in Clc-RNAi+ *shg^2*+ flies indicates that E-cadherin trafficking may in fact be in some way regulated by CLC. This may suggest that there is a compensatory mechanism at the transcriptional or translational level that ensures levels of E-cadherin are maintained. Together, the enhancer/suppressor identified some interesting candidates to be investigated in future work, and tie together the previous data that suggests Notch endocytosis is implicated following CLC knockdown.

This approach has the advantage of being a quick method to screen for novel genetic interactions using a straightforward crossing scheme and that using dominant markers allows for the selection

of internal controls. Furthermore, the use of two independent RNAi lines for CLC knockdown allows for validation of any phenotypes seen. However, the variation in the rough eye phenotype was difficult to score because the analysis at this point is qualitative. The severity of the adult rough eye is difficult to quantify, although a method for quantitative assessment of this phenotype using SEM imaging exists (Iyer et al., 2016). This could potentially be modified and applied to the images from this screen. Additionally, there could be a genetic interaction between CLC and one of the candidates that is missed due to a compensatory mechanism at a point in development before adulthood, and so some candidates could be missed.

4.7 Potential pitfalls in the project

This project heavily relies on the GAL4-UAS system to functionally deplete CLCs using RNAi, however, this method does not guarantee complete knockdown and can have off-target effects. To overcome this, two independent RNAi lines and appropriate controls were used to ensure any phenotypes observed were specifically due to CLC knockdown. Furthermore, this system will express these constructs early on in a living organism. This raises the possibility that compensatory mechanisms might set in, possibly masking the true impact of CLC knockdown at later stages. Despite these measures, there was variation in the phenotypes that resulted from CLC knockdown using these two RNAi lines, for example in the enhancer suppressor screen. To determine the extent of CLC knockdown, additional control experiments that can examine the level of protein in the tissue would be ideal e.g. Western blot. Ideally, two RNAi lines that target different regions of the same gene which do not share off-targets would be ideal, however for this project this was not possible. The RNAi lines both in fact target overlapping sequences and they share the off-target, Aurora A, which is involved in neuroblast self-renewal and mitosis. To mitigate the caveats of RNAi entirely, a loss of function CLC mutant line would be most ideal, however, this is currently unavailable. The data in this project therefore provides evidence that supports the tissue-specific context-dependent requirement for CLC during development, however, the above experiments would be vital to provide a more robust conclusion by ruling out insufficient CLC knockdown and off-target effects.

Fluorescence microscopy provides quantitative data on proteins of interest, such as expression levels/distribution, but comes with several disadvantages. Tissue photobleaching and possible limitations in resolution when tracking small particles are technical limitations associated with fluorescence microscopy. However, optimal microscope settings (e.g. adjusting laser power and signal-to-noise ratio to ensure quality image with minimal sample damage), proper training, and robust quantitative image analysis should reduce the impact of these factors.

4.7 Future work

So far, these data show that the CLC has an important role *in vivo* and that its depletion with RNAi results in aberrant tissue organization in the eye. It has highlighted several promising avenues for future work and has substantiated the previous findings that the requirement for CLC is context-dependent on the tissue, cellular (and maybe protein) level in a developing tissue. Future work would aim to characterise the function of CLC in the *Drosophila* eye further as it has shown to be a robust model system for this purpose.

This work has produced data that supports the idea that CLC is required for the morphogenesis of some tissue but not others. In order to gain a better understanding of which developing tissues require CLC and when, it would be ideal to examine the *Drosophila* eye, and other epithelial tissues, at earlier stages of development e.g. in the embryonic epidermis, larval eyes etc. The cell classification algorithm generated in this project can be applied to any segmented image and so would be useful for exploring the phenotype in these tissues at the cellular level.

This project has also shown that the requirement for CLC is variable between cell types and has begun to speculate on which characteristics render some cells more reliant on this protein for internalisation. Properties such as membrane tension and rigidity are a major contributing factor in the requirement for CLC, and so future work should investigate these characteristics on both a tissue and cellular level. Comparing the overall tension of different tissues, the eye vs the wing, and different cell types, secondary cells vs primary cells, would shed more light on the circumstances in which CLC is required and how it facilitates endocytosis *in vivo*. For example, using lasers to ablate cell membranes and then tracking the velocity of vertex displacement would be suitable for investigating membrane tension.

To continue the work from the enhancer/suppressor screen that aimed to identify proteins and signalling pathways dependent on CLC, there should be further investigation for candidates. It would be interesting to screen other proteins known to have a role in development and adult tissue homeostasis and that have been shown to interact with CLC e.g. Hip1/Hip1R, Spastin, Kurtz, Arp2 and Auxilin (https://thebiogrid.org/). It would also be ideal to have a more robust method of quantitatively assessing the enhancement or suppression of the rough eye phenotype similar to the work of Iyer et al., 2016, where SEM images of adult eyes could be used to quantify disorganisation of individual ommatidia. Alternatively, techniques such as RNA-seq could provide a high-throughput method of screening any changes in gene expression following CLC knockdown. These candidates could then be followed up by investigating the expression and localisation at various stages of development in the *Drosophila* eye.

Another aspect of future work to consider would be generating a tissue-specific CLC mutant using CRISPR/Cas9 technology. One way to do this would be to generate a line of flies that express mutant CLC clones using the FLP-FRT system. A gRNA targeting CLC could be expressed in the germline using a *nos* cassette plasmid. From there, stable heterozygous lines could be established and the mutation could be recombined onto a chromosome with an FRT site (Newsome et al., 2000). In the presence of *ey*FLP, for example, generate CLC mutant clones would be generated, surrounded by wild-type cells that could act as an internal control.

This would overcome the limitations of RNAi: incomplete knockdown of protein, potential off-target effects, the need to use two independent RNAi lines, controlling for UAS dosage etc. *Drosophila* provides a powerful genetic toolkit, and it is possible to generate a line that expresses clones of mutant and wild type cells, as an internal control, next to one another in the same tissue. Additionally, taking advantage of CRISPR/Cas9 to generate a line of *Drosophila* flies that express GFP-tagged AP-2, could enable tracking of CME dynamics *in vivo*. The common approach of investigating lifetimes of clathrin-coated structures is challenging in living organisms, but measuring the growth rates of such structures using fluorescence imaging has been validated in *Drosophila* (Ferguson et al., 2016). Analysing CME using live imaging would be invaluable in understanding the impact of not just CLC knockdown on endocytosis, but it would provide a much more in-depth understanding of the dynamics of this process in a developing tissue in real time.

4.7 Summary

Together, the data produced from this project shows that there is a differential requirement for CLC at the tissue, cellular and protein level in *Drosophila melanogaster.* This context-dependent requirement for CLCs in the different cell types of the retina is most likely due to intrinsic differences in their properties i.e. high versus low membrane tension (secondary cells) and that some cells rely on signalling pathways that require CLC (Notch). Furthermore, the enhancer suppressor screen has identified candidates that may genetically interact with CLC and so has provided potential avenues for future research. This project has highlighted the importance of investigating the role of CLC in the developing tissues of a living organism. The combination of a dynamic, mechanically fluctuating environment and the range of developmental signalling pathways that the cells are exposed clearly plays a vital role in determining whether certain cells rely on CLC. This is an exciting area of research and future work will shed light on the highly dynamic regulation of the fundamental process of clathrin-mediated endocytosis during development.

5. Acknowledgements

discussions in relation to my work at our regular lab meetings, as well as the kind words of support and friendship from you all throughout my time in the department.

In particular, Dr Miguel Ramirez of the Bulgakova lab was someone I consistently received fantastic support and guidance from and I'd like to thank for him for his continual time and encouragement. I am also eternally grateful for everyone in my student cohort. I'm incredibly thankful for the brilliant friendships developed and the support we gave each other over the last couple of years.

Additionally, a massive thank you to the Light Microscopy Facility and Fly Facility at the University of Sheffield. To Kath, Darren, and Nick – I can't thank you enough for all your invaluable advice and help during this project.

Last but not least, I'd like to thank my friends and family. Your never-ending patience, kindness and support is what got me where I am. I don't know where I'd be without you all.

6. References

Agajanian, M.J., Walker, M.P., Axtman, A.D., Ruela-de-Sousa, R.R., Serafin, D.S., Rabinowitz, A.D., Graham, D.M., Ryan, M.B., Tamir, T., Nakamichi, Y., Gammons, M.V., Bennett, J.M., Couñago, R.M., Drewry, D.H., Elkins, J.M., Gileadi, C., Gileadi, O., Godoi, P.H., Kapadia, N., Müller, S., Santiago, A.S., Sorrell, F.J., Wells, C.I., Fedorov, O., Willson, T.M., Zuercher, W.J., Major, M.B., 2019. WNT Activates the AAK1 Kinase to Promote Clathrin-Mediated Endocytosis of LRP6 and Establish a Negative Feedback Loop. Cell Rep. 26, 79-93.e8. https://doi.org/10.1016/j.celrep.2018.12.023

Aghamohammadzadeh, S., Ayscough, K.R., 2009. Differential requirements for actin during yeast and mammalian endocytosis. Nat. Cell Biol. 11, 1039–1042. https://doi.org/10.1038/ncb1918

Avinoam, O., Schorb, M., Beese, C.J., Briggs, J.A.G., Kaksonen, M., 2015. Endocytic sites mature by continuous bending and remodeling of the clathrin coat. Science 348, 1369–1372. https://doi.org/10.1126/science.aaa9555

Baker, N.E., Yu, S.-Y., 1997. Proneural function of neurogenic genes in the developing Drosophila eye. Curr. Biol. 7, 122–132. https://doi.org/10.1016/S0960-9822(06)00056-X

Bao, S., 2014. Notch Controls Cell Adhesion in the Drosophila Eye. PLoS Genet. 10, e1004087. https://doi.org/10.1371/journal.pgen.1004087

Bao, S., Cagan, R., 2005. Preferential adhesion mediated by Hibris and Roughest regulates morphogenesis and patterning in the Drosophila eye. Dev. Cell 8, 925–935. https://doi.org/10.1016/j.devcel.2005.03.011

Baschieri, F., Porshneva, K., Montagnac, G., 2020. Frustrated clathrin-mediated endocytosis – causes and possible functions. J. Cell Sci. 133. https://doi.org/10.1242/jcs.240861

Baumann, O., 2004. Spatial pattern of nonmuscle myosin-II distribution during the development of the Drosophila compound eye and implications for retinal morphogenesis. Dev. Biol. 269, 519–533. https://doi.org/10.1016/j.ydbio.2004.01.047

Beronja, S., Laprise, P., Papoulas, O., Pellikka, M., Sisson, J., Tepass, U., 2005. Essential function of Drosophila Sec6 in apical exocytosis of epithelial photoreceptor cells. J. Cell Biol. 169, 635–646. https://doi.org/10.1083/jcb.200410081

Blackie, L., Walther, R.F., Staddon, M.F., Banerjee, S., Pichaud, F., 2020. Cell-type specific mechanical response and myosin dynamics during retinal lens development in Drosophila. Mol. Biol. Cell mbc.E19-09-0523. https://doi.org/10.1091/mbc.E19-09-0523

Bonazzi, M., Vasudevan, L., Mallet, A., Sachse, M., Sartori, A., Prevost, M.-C., Roberts, A., Taner, S.B., Wilbur, J.D., Brodsky, F.M., Cossart, P., 2011. Clathrin phosphorylation is required for actin recruitment at sites of bacterial adhesion and internalization. J. Cell Biol. 195, 525–536. https://doi.org/10.1083/jcb.201105152

Boulant, S., Kural, C., Zeeh, J.-C., Ubelmann, F., Kirchhausen, T., 2011. Actin dynamics counteract membrane tension during clathrin-mediated endocytosis. Nat. Cell Biol. 13, 1124–1131. https://doi.org/10.1038/ncb2307

Bucher, D., Frey, F., Sochacki, K.A., Kummer, S., Bergeest, J.-P., Godinez, W.J., Kräusslich, H.-G., Rohr, K., Taraska, J.W., Schwarz, U.S., Boulant, S., 2018. Clathrin-adaptor ratio and membrane tension regulate the flat-to-curved transition of the clathrin coat during endocytosis. Nat. Commun. 9. https://doi.org/10.1038/s41467-018-03533-0

Burke, P., Schooler, K., Wiley, H.S., 2001. Regulation of Epidermal Growth Factor Receptor Signaling by Endocytosis and Intracellular Trafficking. Mol. Biol. Cell 12, 1897–1910.

Cagan, R., 2003. The signals that drive kidney development: a view from the fly eye. Curr. Opin. Nephrol. Hypertens. 12, 11–17. https://doi.org/10.1097/00041552-200301000-00003

Cagan, R.L., Ready, D.F., 1989. Notch is required for successive cell decisions in the developing Drosophila retina. Genes Dev. 3, 1099–1112. https://doi.org/10.1101/gad.3.8.1099

Carthew, R.W., 2007. Pattern formation in the Drosophila eye. Curr. Opin. Genet. Dev. 17, 309–313. https://doi.org/10.1016/j.gde.2007.05.001

Chan, C.-C., Epstein, D., Hiesinger, P.R., 2011. Intracellular Trafficking in Drosophila Visual System Development: A Basis for Pattern Formation Through Simple Mechanisms. Dev. Neurobiol. 71, 1227–1245. https://doi.org/10.1002/dneu.20940

Chen, C.-Y., Brodsky, F.M., 2005. Huntingtin-interacting Protein 1 (Hip1) and Hip1-related Protein (Hip1R) Bind the Conserved Sequence of Clathrin Light Chains and Thereby Influence Clathrin Assembly in Vitro and Actin Distribution in Vivo. J. Biol. Chem. 280, 6109–6117. https://doi.org/10.1074/jbc.M408454200

Cossart, P., Helenius, A., 2014. Endocytosis of Viruses and Bacteria. Cold Spring Harb. Perspect. Biol. 6, a016972. https://doi.org/10.1101/cshperspect.a016972

Dai, J., Ting-Beall, H.P., Sheetz, M.P., 1997. The Secretion-coupled Endocytosis Correlates with Membrane Tension Changes in RBL 2H3 Cells. J. Gen. Physiol. 110, 1–10.

Dannhauser, P.N., Platen, M., Böning, H., Ungewickell, H., Schaap, I.A.T., Ungewickell, E.J., 2015. Effect of Clathrin Light Chains on the Stiffness of Clathrin Lattices and Membrane Budding. Traffic 16, 519–533. https://doi.org/10.1111/tra.12263

Dannhauser, P.N., Ungewickell, E.J., 2012. Reconstitution of clathrin-coated bud and vesicle formation with minimal components. Nat. Cell Biol. 14, 634–639. https://doi.org/10.1038/ncb2478

den Otter, W.K., Briels, W.J., 2011. The generation of curved clathrin coats from flat plaques. Traffic Cph. Den. 12, 1407–1416. https://doi.org/10.1111/j.1600-0854.2011.01241.x

Doroquez, D.B., Rebay, I., 2006. Signal integration during development: mechanisms of EGFR and Notch pathway function and cross-talk. Crit. Rev. Biochem. Mol. Biol. 41, 339–385. https://doi.org/10.1080/10409230600914344

Fan, B., Zhu, L., Chang, X., Zhou, J., Guo, R., Zhao, Y., Shi, D., Niu, B., Gu, J., Yu, Z., Song, T., Luo, C., Ma, Z., Bai, J., Zhou, B., Ding, S., He, K., Li, B., 2019. Mortalin restricts porcine epidemic diarrhea virus entry by downregulating clathrin-mediated endocytosis. Vet. Microbiol. 239, 108455. https://doi.org/10.1016/j.vetmic.2019.108455

Ferguson, J.P., Willy, N.M., Heidotting, S.P., Huber, S.D., Webber, M.J., Kural, C., 2016. Deciphering dynamics of clathrin-mediated endocytosis in a living organismDeciphering dynamics of clathrin-mediated endocytosis in a multicellular organism. J. Cell Biol. 214, 347–358. https://doi.org/10.1083/jcb.201604128

Ferreira, F., Foley, M., Cooke, A., Cunningham, M., Smith, G., Woolley, R., Henderson, G., Kelly, E., Mundell, S., Smythe, E., 2012. Endocytosis of G protein-coupled receptors is regulated by clathrin light chain phosphorylation. Curr. Biol. CB 22, 1361–1370. https://doi.org/10.1016/j.cub.2012.05.034

Flores, G.V., Duan, H., Yan, H., Nagaraj, R., Fu, W., Zou, Y., Noll, M., Banerjee, U., 2000. Combinatorial signaling in the specification of unique cell fates. Cell 75–85.

Frankfort, B.J., Mardon, G., 2002. R8 development in the Drosophila eye: a paradigm for neural selection and differentiation. Dev. Camb. Engl. 129, 1295–1306.

Freeman, M., 1996. Reiterative Use of the EGF Receptor Triggers Differentiation of All Cell Types in the Drosophila Eye. Cell 87, 651–660. https://doi.org/10.1016/S0092-8674(00)81385-9

Gaiano, N., Fishell, G., 2002. The role of notch in promoting glial and neural stem cell fates. Annu. Rev. Neurosci. 25, 471–490. https://doi.org/10.1146/annurev.neuro.25.030702.130823

Greenwood, S., Struhl, G., 1999. Progression of the morphogenetic furrow in the Drosophila eye: the roles of Hedgehog, Decapentaplegic and the Raf pathway. Dev. Camb. Engl. 126, 5795–5808.

Greig, J., Bulgakova, N.A., 2019. E-cadherin endocytosis is modulated by p120-catenin through the opposing actions of RhoA and Arf1. bioRxiv 477760. https://doi.org/10.1101/477760

Grzeschik, N.A., Knust, E., 2005. IrreC/rst-mediated cell sorting during Drosophila pupal eye development depends on proper localisation of DE-cadherin. Development 132, 2035–2045. https://doi.org/10.1242/dev.01800

Guo, M., Jan, L.Y., Jan, Y.N., 1996. Control of daughter cell fates during asymmetric division: interaction of Numb and Notch. Neuron 17, 27–41. https://doi.org/10.1016/s0896-6273(00)80278-0

Harding, C., Heuser, J., Stahl, P., 1983. Receptor-mediated endocytosis of transferrin and recycling of the transferrin receptor in rat reticulocytes. J. Cell Biol. 97, 329–339. https://doi.org/10.1083/jcb.97.2.329

Hay, B.A., Wolff, T., Rubin, G.M., 1994. Expression of baculovirus P35 prevents cell death in Drosophila. Development 120, 2121–2129.

Hayashi, T., Carthew, R.W., 2004. Surface mechanics mediate pattern formation in the developing retina. Nature 431, 647–652. https://doi.org/10.1038/nature02952

Heuser, J., 1980. Three-dimensional visualization of coated vesicle formation in fibroblasts. J. Cell Biol. 84, 560–583. https://doi.org/10.1083/jcb.84.3.560

Hinrichsen, L., Harborth, J., Andrees, L., Weber, K., Ungewickell, E.J., 2003. Effect of clathrin heavy chain- and alpha-adaptin-specific small inhibitory RNAs on endocytic accessory proteins and receptor trafficking in HeLa cells. J. Biol. Chem. 278, 45160–45170. https://doi.org/10.1074/jbc.M307290200

Houalla, T., Shi, L., van Meyel, D.J., Rao, Y., 2010. Rab-mediated vesicular transport is required for neuronal positioning in the developing Drosophila visual system. Mol. Brain 3, 19. https://doi.org/10.1186/1756-6606-3-19

Hsiung, F., Moses, K., 2002. Retinal development in Drosophila: specifying the first neuron. Hum. Mol. Genet. 11, 1207–1214. https://doi.org/10.1093/hmg/11.10.1207

Huang, F., Khvorova, A., Marshall, W., Sorkin, A., 2004. Analysis of clathrin-mediated endocytosis of epidermal growth factor receptor by RNA interference. J. Biol. Chem. 279, 16657–16661. https://doi.org/10.1074/jbc.C400046200

Ichinose, J., Murata, M., Yanagida, T., Sako, Y., 2004. EGF signalling amplification induced by dynamic clustering of EGFR. Biochem. Biophys. Res. Commun. 324, 1143–1149. https://doi.org/10.1016/j.bbrc.2004.09.173

Iyer, J., Wang, Q., Le, T., Pizzo, L., Grönke, S., Ambegaokar, S.S., Imai, Y., Srivastava, A., Troisí, B.L., Mardon, G., Artero, R., 2016. Quantitative assessment of eye phenotypes for functional genetic studies using Drosophila melanogaster. G3: Genes, Genomes, Genetics, 6(5), 1427-1437.

Joseph, B.B., Wang, Y., Edeen, P., Lažetić, V., Grant, B.D., Fay, D.S., 2020. Control of clathrin-mediated endocytosis by NIMA family kinases. PLoS Genet. 16. https://doi.org/10.1371/journal.pgen.1008633

Kaksonen, M., Roux, A., 2018. Mechanisms of clathrin-mediated endocytosis. Nat. Rev. Mol. Cell Biol. 19, 313–326. https://doi.org/10.1038/nrm.2017.132

Kim, B., Park, Y.S., Sung, J.S., Lee, J.W., Lee, S.B., Kim, Y.H., 2020. Clathrin-mediated EGFR endocytosis as a potential therapeutic strategy for overcoming primary resistance of EGFR TKI in wild-type EGFR non-small cell lung cancer. Cancer Med. https://doi.org/10.1002/cam4.3635

Kirchhausen, T., 1993. Coated pits and coated vesicles — sorting it all out. Curr. Opin. Struct. Biol. 3, 182–188. https://doi.org/10.1016/S0959-440X(05)80150-2

Kirchhausen, T., Harrison, S.C., 1981. Protein organization in clathrin trimers. Cell 23, 755–761. https://doi.org/10.1016/0092-8674(81)90439-6

Koca, Y., Housden, B.E., Gault, W.J., Bray, S.J., Mlodzik, M., 2019. Notch signaling coordinates ommatidial rotation in the Drosophila eye via transcriptional regulation of the EGF-Receptor ligand Argos. Sci. Rep. 9, 18628. https://doi.org/10.1038/s41598-019-55203-w

Kramer, J.M., Staveley, B.E., 2003. GAL4 causes developmental defects and apoptosis when expressed in the developing eye of Drosophila melanogaster. Genet. Mol. Res. GMR 2, 43–47.

Kurada, P., White, K., 1998. Ras Promotes Cell Survival in Drosophila by Downregulating hid Expression. Cell 95, 319–329. https://doi.org/10.1016/S0092-8674(00)81764-X

Langridge, P., Struhl, G., 2017. Epsin-dependent ligand endocytosis activates Notch by force. Cell 171, 1383-1396.e12. https://doi.org/10.1016/j.cell.2017.10.048

Lecuit, T., Lenne, P.-F., 2007. Cell surface mechanics and the control of cell shape, tissue patterns and morphogenesis. Nat. Rev. Mol. Cell Biol. 8, 633–644. https://doi.org/10.1038/nrm2222

Li, Y., Liu, Hui, Wu, K., Liu, Hongbin, Huang, T., Chen, Z.-J., Zhao, S., Ma, J., Zhao, H., 2019. Melatonin promotes human oocyte maturation and early embryo development by enhancing clathrin-mediated endocytosis. J. Pineal Res. 67, e12601. https://doi.org/10.1111/jpi.12601

Maib, H., Ferreira, F., Vassilopoulos, S., Smythe, E., 2018. Cargo regulates clathrin-coated pit invagination via clathrin light chain phosphorylation. J. Cell Biol. 217, 4253–4266. https://doi.org/10.1083/jcb.201805005

Mettlen, M., Chen, P.-H., Srinivasan, S., Danuser, G., Schmid, S.L., 2018. Regulation of Clathrin-Mediated Endocytosis. Annu. Rev. Biochem. 87, 871–896. https://doi.org/10.1146/annurev-biochem-062917-012644

Midorikawa, R., Yamamoto-Hino, M., Awano, W., Hinohara, Y., Suzuki, E., Ueda, R., Goto, S., 2010. Autophagy-Dependent Rhodopsin Degradation Prevents Retinal Degeneration in Drosophila. J. Neurosci. 30, 10703–10719. https://doi.org/10.1523/JNEUROSCI.2061-10.2010

Miller, D.T., Cagan, R.L., 1998. Local induction of patterning and programmed cell death in the developing Drosophila retina. Dev. Camb. Engl. 125, 2327–2335.

Mitsunari, T., Nakatsu, F., Shioda, N., Love, P.E., Grinberg, A., Bonifacino, J.S., Ohno, H., 2005. Clathrin Adaptor AP-2 Is Essential for Early Embryonal Development. Mol. Cell. Biol. 25, 9318–9323. https://doi.org/10.1128/MCB.25.21.9318-9323.2005

Miura, G.I., Roignant, J.-Y., Wassef, M., Treisman, J.E., 2008. Myopic acts in the endocytic pathway to enhance signaling by the Drosophila EGF receptor. Dev. Camb. Engl. 135, 1913–1922. https://doi.org/10.1242/dev.017202

Nagaraj, R., Banerjee, U., 2007. Combinatorial signaling in the specification of primary pigment cells in the Drosophila eye. Development 134, 825–831. https://doi.org/10.1242/dev.02788

Newsome, T.P., Asling, B., Dickson, B.J., 2000. Analysis of Drosophila photoreceptor axon guidance in eye-specific mosaics. Dev. Camb. Engl. 127, 851–860.

Nusse, R., Clevers, H., 2017. Wnt/β-Catenin Signaling, Disease, and Emerging Therapeutic Modalities. Cell 169, 985–999. https://doi.org/10.1016/j.cell.2017.05.016

Overstreet, E., Fitch, E., Fischer, J.A., 2004. Fat facets and Liquid facets promote Delta endocytosis and Delta signaling in the signaling cells. Dev. Camb. Engl. 131, 5355–5366. https://doi.org/10.1242/dev.01434

Parks, A.L., Klueg, K.M., Stout, J.R., Muskavitch, M.A., 2000. Ligand endocytosis drives receptor dissociation and activation in the Notch pathway. Development 127, 1373–1385.

Parks, Annette L., and Marc A. Muskavitch., 1993. Cell Lineage and Fate Determination. Developmental biology.

Parody, T.R., Muskavitch, M.A., 1993. The pleiotropic function of Delta during postembryonic development of Drosophila melanogaster. Genetics 135, 527–539. https://doi.org/10.1093/genetics/135.2.527

Peralta, S., Gómez, Y., González-Gaitán, M.A., Moya, F., Vinós, J., 2009. Notch down-regulation by endocytosis is essential for pigment cell determination and survival in the Drosophila retina. Mech. Dev. 126, 256–269. https://doi.org/10.1016/j.mod.2008.10.011

Poupon, V., Girard, M., Legendre-Guillemin, V., Thomas, S., Bourbonniere, L., Philie, J., Bright, N.A., McPherson, P.S., 2008. Clathrin light chains function in mannose phosphate receptor trafficking via regulation of actin assembly. Proc. Natl. Acad. Sci. U. S. A. 105, 168–173. https://doi.org/10.1073/pnas.0707269105

Raucher, D., Sheetz, M.P., 1999. Membrane expansion increases endocytosis rate during mitosis. J. Cell Biol. 144, 497–506. https://doi.org/10.1083/jcb.144.3.497

Reiter, C., Schimansky, T., Nie, Z., Fischbach, K.F., 1996. Reorganization of membrane contacts prior to apoptosis in the Drosophila retina: the role of the IrreC-rst protein. Dev. Camb. Engl. 122, 1931–1940.

Reiter, L.T., Potocki, L., Chien, S., Gribskov, M., Bier, E., 2001. A systematic analysis of human disease-associated gene sequences in Drosophila melanogaster. Genome Res. 11, 1114–1125. https://doi.org/10.1101/gr.169101

Roote, J., Prokop, A., 2013. How to Design a Genetic Mating Scheme: A Basic Training Package for Drosophila Genetics. G3 GenesGenomesGenetics 3, 353–358. https://doi.org/10.1534/g3.112.004820

Saleem, M., Morlot, S., Hohendahl, A., Manzi, J., Lenz, M., Roux, A., 2015. A balance between membrane elasticity and polymerization energy sets the shape of spherical clathrin coats. Nat. Commun. 6, 6249. https://doi.org/10.1038/ncomms7249

Santolini, E., Puri, C., Salcini, A.E., Gagliani, M.C., Pelicci, P.G., Tacchetti, C., Di Fiore, P.P., 2000. Numb is an endocytic protein. J. Cell Biol. 151, 1345–1352. https://doi.org/10.1083/jcb.151.6.1345

Scott, B.L., Sochacki, K.A., Low-Nam, S.T., Bailey, E.M., Luu, Q., Hor, A., Dickey, A.M., Smith, S., Kerkvliet, J.G., Taraska, J.W., Hoppe, A.D., 2018. Membrane bending occurs at all stages of clathrin-coat assembly and defines endocytic dynamics. Nat. Commun. 9, 419. https://doi.org/10.1038/s41467-018-02818-8

Seugnet, L., Simpson, P., Haenlin, M., 1997. Requirement for dynamin during Notch signaling in Drosophila neurogenesis. Dev. Biol. 192, 585–598. https://doi.org/10.1006/dbio.1997.8723

Sheetz, M.P., Dai, J., 1996. Modulation of membrane dynamics and cell motility by membrane tension. Trends Cell Biol. 6, 85–89. https://doi.org/10.1016/0962-8924(96)80993-7

Shetty, K.M., Kurada, P., O'Tousa, J.E., 1998. Rab6 regulation of rhodopsin transport in Drosophila. J. Biol. Chem. 273, 20425–20430. https://doi.org/10.1074/jbc.273.32.20425

Shieh, J.C., Schaar, B.T., Srinivasan, K., Brodsky, F.M., McConnell, S.K., 2011. Endocytosis regulates cell soma translocation and the distribution of adhesion proteins in migrating neurons. PloS One 6, e17802. https://doi.org/10.1371/journal.pone.0017802

Shilo, B.Z., 2003. Signaling by the Drosophila epidermal growth factor receptor pathway during development. Exp. Cell Res. 284, 140–149. https://doi.org/10.1016/s0014-4827(02)00094-0

Tomlinson, A., 2012. The Origin of the Drosophila Subretinal Pigment Layer. J. Comp. Neurol. 520, 2676–2682. https://doi.org/10.1002/cne.23063

Treisman, J.E., 2013. Retinal differentiation in Drosophila. Wiley Interdiscip. Rev. Dev. Biol. 2, 545–557. https://doi.org/10.1002/wdev.100

Wu, S., Majeed, S.R., Evans, T.M., Camus, M.D., Wong, N.M.L., Schollmeier, Y., Park, M., Muppidi, J.R., Reboldi, A., Parham, P., Cyster, J.G., Brodsky, F.M., 2016. Clathrin light chains' role in selective endocytosis influences antibody isotype switching. Proc. Natl. Acad. Sci. U. S. A. 113, 9816–9821. https://doi.org/10.1073/pnas.1611189113

Yamaguchi, S., Desplan, C., Heisenberg, M., 2010. Contribution of photoreceptor subtypes to spectral wavelength preference in Drosophila. Proc. Natl. Acad. Sci. 107, 5634–5639. https://doi.org/10.1073/pnas.0809398107